
FEASIBILITY STUDY OF POSITIVE GAUGING SYSTEMS

PHASE II REPORT DESIGN AND ANALYSIS

Document No. 07582-6001-R000

CONTRACT NO. NAS9-6750

DECEMBER 1967

FACILITY FORM 802

N70-17431	(THRU)
117	1
(PAGES)	(CODE)
NASA-CR#65962	14
(NASA CR OR TMX OR AD NUMBER)	(CATEGORY)

TRW
SYSTEMS GROUP

NASA-CR-65962

FEASIBILITY STUDY OF
POSITIVE GAUGING SYSTEMS

PHASE II REPORT
DESIGN AND ANALYSIS

Document No. 07582-6001-R000

CONTRACT NO. NAS9-6750

DECEMBER 1967

TRW
SYSTEMS GROUP


Prepared for
NATIONAL AERONAUTICS AND SPACE ADMINISTRATION
MANNED SPACECRAFT CENTER
Houston, Texas

Prepared by:

B. Siegel
R. Rusch
R. Wolfrum
H. Lurie

S. Lieberman
M. Makowski
O. Fiet

Under the direction of


B. Siegel
Program Manager

Approved by


I. R. Jones, Manager
Nuclear Technology Department

ABSTRACT

This report describes the work performed during the second phase of the Feasibility Study of Positive Gauging Systems for NASA/Manned Spacecraft Center under Contract NAS9-6750.

The primary objective of the program was to demonstrate the feasibility of an advanced storable propellant-mass gauging system capable of operating independent of propellant location or gravity field. The program was divided into two phases. The first phase consisted of a systematic study of various possible gauging systems following by analysis to establish their potential capability and feasibility. As a result of the Phase I study, a Resonant Infrasonic Gauging System (RIGS) was selected for study in Phase II. The second phase, which is the subject of this report, consisted of a detailed investigation of this system and included the following major objectives:

- Perform feasibility tests of the RIGS gauging concept
- Analytically evaluate operational and integration problems for application of RIGS to the Apollo SPS tankage
- Complete a prototype RIGS gauge design and evaluate system performance

All objectives were successfully accomplished. The operating principle of the RIGS system was successfully demonstrated using subscale tankage and boilerplate hardware and components. During closed-loop operation of the system, the propellant volume was measured to an accuracy of ± 1 percent. These tests were performed with the tank in upright and inverted positions, thus demonstrating the ability of the RIGS to gauge propellants independent of the gravity field. All identifiable operational and integration problems for application of the RIGS system to the Apollo SPS tankage were analytically evaluated and each was satisfactorily resolved. Design of prototype hardware was carried out and indicated that a four-tank gauging system for the Apollo SPS applications would weigh 38 pounds and require about 28 watts of power. The results of this program have demonstrated the soundness of the RIGS concept and provide a firm basis for initiation of the engineering development phase of the RIGS system.

CONTENTS

	Page
1. INTRODUCTION AND SUMMARY	1-1
2. PRINCIPLE OF RIGS OPERATION	2-1
3. SYSTEM DESIGN	3-1
3.1 Sensor/Driver Assembly (SDA)	3-1
3.1.1 Driver Assembly	3-1
3.1.2 Resonant Element Assembly	3-9
3.1.3 Pressure Transducer	3-11
3.2 Data Processor	3-15
3.2.1 Control System	3-15
3.2.2 Display Electronics	3-19
3.3 RIGS Integration in Apollo SPS Tanks	3-20
3.3.1 Description of the Apollo SPS Tankage	3-22
3.3.2 Gauge Installation	3-22
3.3.3 Effect of Storage-to-Sump-Tank Transfer Line on RIGS	3-25
3.4 Material Compatibility	3-26
3.5 System Characteristics	3-26
3.5.1 System Weight	3-26
3.5.2 System Power Requirements	3-28
3.5.3 System Performance	3-28
4. SYSTEM ANALYSIS	4-1
4.1 Analysis of Error Sources	4-1
4.1.1 Wave Transmission Effects	4-1
4.1.2 Variable Ullage Gas Properties	4-8
4.1.3 Heat Transfer to the Ullage Gas	4-11
4.1.4 Acoustically Isolated Regions	4-12
4.2 Error Analysis of the RIGS System	4-12
4.2.1 System Error Sources	4-13
4.2.2 Measurement and Data Processing Errors	4-13
4.2.3 Total Error for RIGS System	4-15
4.3 Control System Analysis	4-15
4.3.1 System Simulation	4-15
4.3.2 Conclusions	4-32
4.4 RIGS Failure Mode and Reliability Analysis	4-32

CONTENTS (Continued)

	Page
5. FEASIBILITY DEMONSTRATION TEST PROGRAM	5-1
5.1 Introduction	5-1
5.2 Description of Test Hardware	5-1
5.3 Test Results	5-4
5.3.1 Initial Testing	5-4
5.3.2 Closed Loop Testing	5-7
5.3.3 Additional Testing	5-12
6. CONCLUSIONS	6-1
7. RECOMMENDATIONS	7-1
APPENDIX A — RHO PROPELLANT GAUGE	A-1

ILLUSTRATIONS

		Page
2-1	RIGS Schematic	2-1
2-2	System Mechanical Equivalent	2-2
2-3	RIGS Frequency Response	2-5
2-4	Generalized Response of a Resonant System	2-6
3-1	Prototype Resonant Infrasonic Gauge	3-2
3-2	Schematic of Electrodynamic Driver	3-6
3-3	Resonant Infrasonic Gauging System	3-8
3-4	Three Basic Diaphragm Configurations	3-12
3-5	Variable Reluctance Pressure Transducer	3-13
3-6	Variation of $K \cos \phi$ with Frequency	3-17
3-7	Control System Schematic	3-18
3-8	Display Electronics	3-21
3-9	Service Propulsion Propellant Feed System	3-23
3-10	Possible RIGS Installations in SPS Tankage	3-24
3-11	Inertial Damping Device	3-27
4-1	Submerged Gas Pocket	4-4
4-2	Transmission Through Liquid by a Compliant Bladder . .	4-4
4-3	Error Due to Signal Transmission Through Liquid as a Function of Empty Tank Frequency	4-7
4-4	Variation of Gamma with N_2O_4 Concentration and Temperature	4-9
4-5	Variation of Gamma with Aerozine-50 Vapor Composition and Temperature	4-10
4-6	Error Caused by Heat Transfer to the Ullage Gas	4-11
4-7	System Error Sources as a Function of Liquid Mass	4-14
4-8	RIGS Error as a Function of Liquid Volume	4-16

ILLUSTRATIONS (Continued)

		Page
4-9	Block Diagram (RIGS) of Zero-G Infrasonic Gauging System	4-17
4-10	Block Diagram of Driver Cavity and Propellant Tank Transfer Function	4-18
4-11a	Computer Traces of Zero-G Gauging System Response (Ullage Volume = 13 cu ft)	4-19
4-11b	Computer Traces of Zero-G Gauging System Response (Ullage Volume = 13 cu ft)	4-20
4-11c	Computer Traces of Zero-G Gauging System Response (Ullage Volume = 179.4 cu ft)	4-21
4-11d	Computer Traces of Zero-G Gauging System Response (Ullage Volume = 179.4 cu ft)	4-22
4-12a	Computer Traces of Zero-G Gauging System Response as Ullage Volume Varies	4-23
4-12b	Computer Traces of Zero-G Gauging System Response as Ullage Volume Varies	4-24
4-13	Block Diagram Based on DC Signal Implementation	4-25
4-14a	Computer Traces for Zero-G Gauging System Response to a 30-msec Pulse (Ullage Volume = 13 cu ft) . .	4-26
4-14b	Computer Traces of Zero-G Gauging System Response to a 30-msec Pulse (Ullage Volume = 179.4 cu ft)	4-27
4-15a	Computer Traces of Zero-G Gauging System Response to a Gaussian White Noise Input (Wideband); Ullage Volume = 179.4 cu ft	4-28
4-15b	Computer Traces of Zero-G Gauging System Response to a Gaussian White Noise Input (Wideband); Ullage Volume = 179.4 cu ft	4-29
4-15c	Computer Traces of Zero-G Gauging System Response to a Gaussian White Noise Input (Wideband); Ullage Volume = 13 cu ft	4-30
4-15d	Computer Traces of Zero-G Gauging System Response to a Gaussian White Noise Input (Wideband); Ullage Volume = 13 cu ft	4-31

ILLUSTRATIONS (Continued)

	Page
5-1 Feasibility Test Fixture	5-2
5-2 Feasibility Test Hardware	5-2
5-3 Feasibility Test Hardware	5-3
5-4 Feasibility Test Driver and Sensor Assembly	5-3
5-5a System Response at Constant Volume and Variable Frequency	5-5
5-5b System Response at Constant Volume and Variable Frequency	5-6
5-6 Amplitude Response for RIGS Feasibility Test	5-8
5-7 Feasibility Test, Closed Loop Control System	5-9
5-8 Closed-Loop System Response at Resonance	5-10
5-9 Performance of Feasibility Demonstration System	5-11
5-10 Inverted Tank Tests with Rubber Diaphragm	5-13
5-11 Performance of Feasibility Test System - Tank in Upright and Inverted Positions	5-14
A-1 Schematic Diagram of RHO Gauge.	A-2
A-2 Mass Attenuation Coefficients for the Elements H, He, O, N, and C	A-4
A-3 Mass Attenuation Coefficients for He, N ₂ O ₄ , and Aerozine-50	A-5
A-4 Gas Composition Test Hardware	A-7
A-5 X-Ray Attenuation Hardware	A-8
A-6 Measurement of Nitrogen Partial Pressure in a Helium-Nitrogen Gas Mixture (Total Pressure: 93 psia)	A-10
A-7 Measurement of Nitrogen-Oxygen Partial Pressure in a Helium, Nitrogen-Oxygen Gas Mixture (Total Pressure: 84 psia).	A-11
A-8 Experimental System For Measuring Gas Density	A-14
A-9 Beta Particle Attenuation Measurements of Argon Density	A-15
A-10 Count Rate Versus Argon Gas Density for Detector to Source Distance of 3 cm.	A-16

1. INTRODUCTION AND SUMMARY

The Feasibility Study of Positive Gauging Systems was divided into two phases. The first phase consisted of a systematic analysis of various possible gauging systems capable of operating under zero gravity. The results of this first phase are reported under separate cover. Over 50 separate concepts for gauging propellants were identified and the relative advantages, limitations, and characteristics of the systems were analytically evaluated. The results of these evaluations indicated that a Resonant Infrasonic Gauging System (RIGS) appeared to be the most promising concept for gauging the storable propellants, N_2O_4 and Aerozine-50, in the Apollo SPS tankage. This system was selected for further study in the second phase of the program.

The objectives of Phase II were to:

- Perform feasibility tests of the RIGS gauging concept
- Analytically evaluate operational and integration problems for application of RIGS to the Apollo SPS tankage
- Complete a prototype RIGS gauge design and evaluate system performance

Section 2 of this report presents a description of the operating principles of the RIGS system and a summary of the key mathematical derivations and relationships developed during Phase I. Section 3 presents a preliminary design of the RIGS system as applied to the SPS tankage. The design was carried out under the ground rule that no major modification of the tanks was permissible. The proposed design satisfies this requirement and the four-tank system weighs 38 pounds and requires only 28 watts of power. In Section 4, a discussion of error sources, system accuracy, control system stability, and reliability is presented. Section 5 describes the feasibility test program. The RIGS concept was successfully demonstrated in the laboratory using subscale tankage and boilerplate components. When operated with a closed-loop control system, the propellant volume was measured to within ± 1 percent with the tank in both upright and inverted positions. The results of this program verified the feasibility of the RIGS concept and provide a firm basis for initiation

of the engineering development phase of the RIGS system. The conclusions and recommendations are summarized in Sections 6 and 7, respectively.

As a result of the Phase I evaluations, a second system was also considered highly promising for zero-gravity propellant gauging. Exploratory development of this system, called the RHO gauge (or ρV gauge) is currently underway under AEC sponsorship, and a summary of the work to date is included as an appendix to this report.

2. PRINCIPLE OF RIGS OPERATION

In this section, the principle of operation of the RIGS gauging concept is presented. A detailed description of the RIGS design appears in Section 3.

In schematic form, Figure 2-1 shows the operating components of the RIGS system. Basically, the system consists of a driver piston

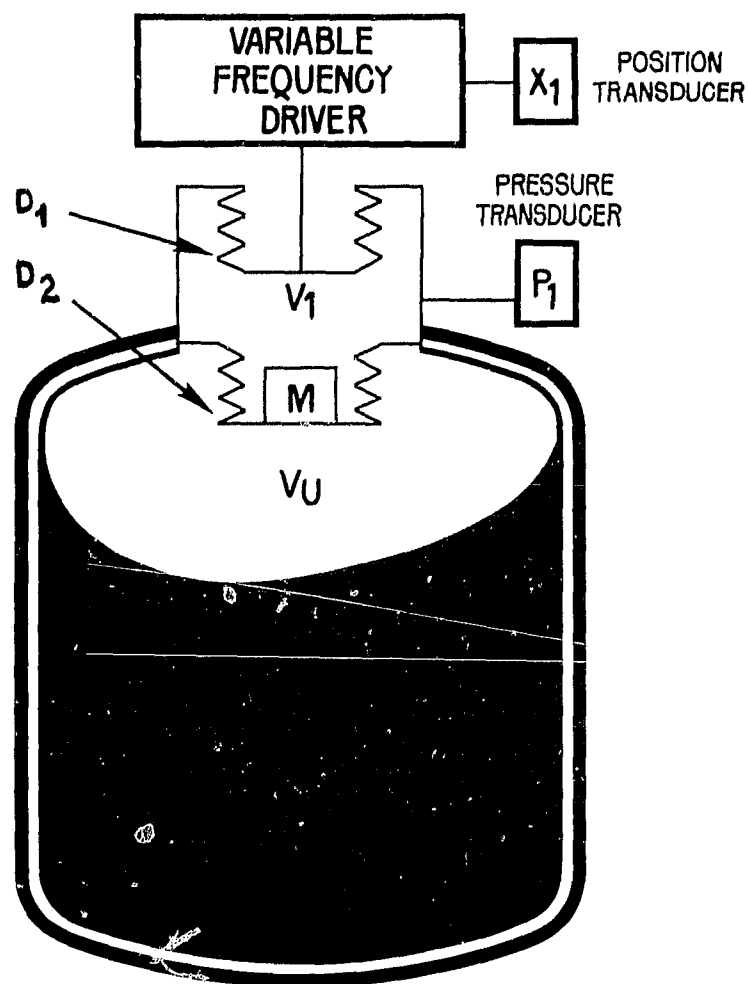


Figure 2-1. RIGS Schematic

(D_1), a follower piston or diaphragm (D_2), and a pressure transducer. Motion of the driver piston produces a volume displacement and causes the follower piston to move a corresponding distance, compressing the ullage. If the driver is moved slowly so that dynamic effects can be ignored, the pressure change in the ullage is simply:

$$\frac{\Delta P}{P} = -\gamma \frac{\Delta V}{(V_u + V_1)} \cong -\gamma \frac{\Delta V}{V_u} \text{ with } V_u \gg V_1 \quad (2.1)$$

where:

V_1 = volume between pistons

V_u = ullage volume

γ = ratio of specific heats

If, however, the driver piston is driven sinusoidally at increasing frequencies, the dynamic effects must be taken into account. The follower piston is a mass that is coupled to the driver and the ullage gas through two gas springs represented by the volume between the two pistons (V_1) and the ullage volume (V_u). The spring rates of the two volumes are (assuming an adiabatic process):

$$K_1 = \gamma \frac{P_1 A^2}{V_1} \quad K_u = \gamma \frac{P_u A^2}{V_u} \quad (2.2)$$

where:

A = area of follower piston

$P_1 = P_u$ = system static pressure

The mechanical equivalent of the system is shown in Figure 2-2.

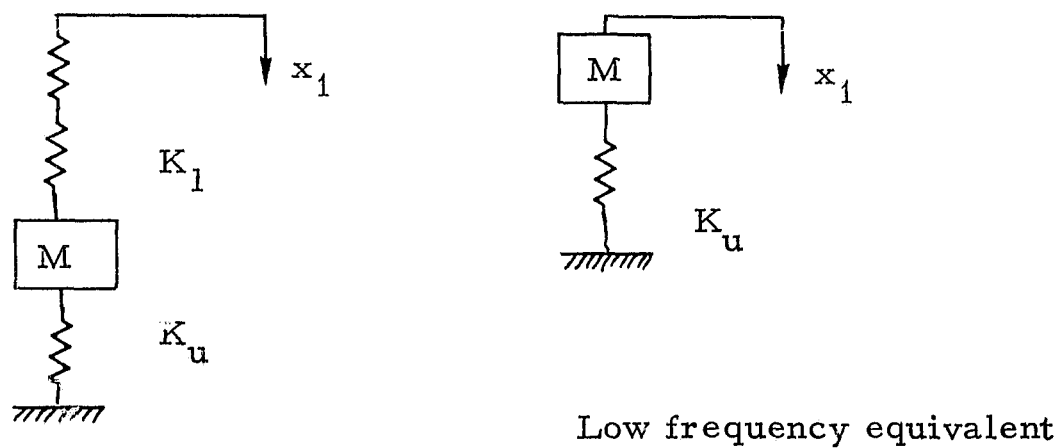


Figure 2-2. System Mechanical Equivalent

Since the ullage gas volume (V_u) is much larger than V_1 , the spring rate K_1 is appreciably greater than K_u , and at low frequencies the upper volume acts essentially as if it were a stiff rod imposing a motion on the mass M (Figure 2-2). The force which must be transmitted by K_1 to pro-

duce the motion of the mass is a function of the dynamic impedance of the mass and the ullage gas spring as shown below:

$$\begin{aligned}
 F_{\text{total}} &= \text{Force to accelerate mass} + \text{force to compress } K_u \\
 &= F_M + F_K \\
 F_{\text{total}} &= M \frac{d^2 x_1}{dt^2} + K_u x_1 = M \ddot{x}_1 + \frac{A^2 \gamma P_u}{V_u} x_1
 \end{aligned} \tag{2.3}$$

At some frequency, the force required to accelerate the mass will be balanced by the restoring force of the gas spring and the system will be in resonance (i. e. , in the absence of friction, the system will continue to oscillate without any additional applied force). At this condition,

$$M \ddot{x}_1 + \frac{A^2 \gamma P_u}{V_u} x_1 = 0 \tag{2.4}$$

Solving the equation for the resonant frequency

$$f_r = \frac{1}{2\pi} \sqrt{\frac{A^2 \gamma P_u}{M V_u}} \tag{2.5}$$

Thus, the resonant frequency is related to the magnitude of the ullage gas spring rate or the ullage volume. By knowing the mass and area of the follower piston, and the pressure and specific heat ratio of the ullage gas, one can determine ullage volume by measuring the resonant frequency.

This is the basis of the RIGS system. The force on the follower piston is determined by measuring the pressure in the cavity, V_1 . As the driver frequency is varied, the dynamic component of this pressure experiences a minimum and at this point, the driven piston mass is in resonance with the ullage gas cavity. It will be noted from Equation (2.4) that the direction of the force changes at this point, causing a 180° change in the phase of the pressure signal. This phase reversal simplifies the detection of the resonant frequency.

A complete derivation of the behavior of the RIGS system including the effects of friction, will be found in Appendix B-2 of Volume 1. Using Laplace transform notation, the resulting transfer function relating the pressure in the cavity, V_1 , and the displacement of the driver, x_1 , is:

$$\frac{P_1}{x_1} = \frac{\left(S^2 \frac{M}{A^2} \frac{V_u}{\gamma P} + S R \frac{V_u}{\gamma P} + 1 \right)}{\left(S^2 \frac{M}{A^2} \frac{V_1 V_u}{V_1 + V_u} + \frac{S R}{\gamma P} \frac{V_1 V_u}{V_1 + V_u} + 1 \right) (V_1 + V_u)} A \gamma P \quad (2.6)$$

where:

S = Laplace operator

R = frictional resistance to piston motion

$$\text{As } V_1 \ll V_u, \quad \frac{V_1 V_u}{V_1 + V_u} \cong V_1$$

then

$$\frac{P_1}{x_1} \cong \frac{\left(S^2 \frac{M V_u}{A^2 \gamma P} + \frac{S R V_u}{\gamma P} + 1 \right) A \gamma P}{\left(S^2 \frac{M V_1}{A^2 \gamma P} + \frac{S R V_1}{\gamma P} + 1 \right) V_u} \quad (2.7)$$

As will be noted, the system has two resonant frequencies. One appears in the numerator of the above equation corresponding to the resonance frequency of the follower piston mass with the ullage volume. The second appears in the denominator corresponding to the resonance of the follower piston mass with the volume V_1 . As the volume V_1 is very much smaller than V_u , its resonant frequency is appreciably higher and may be ignored. The system response as a function of driver frequency is shown in Figure 2-3.

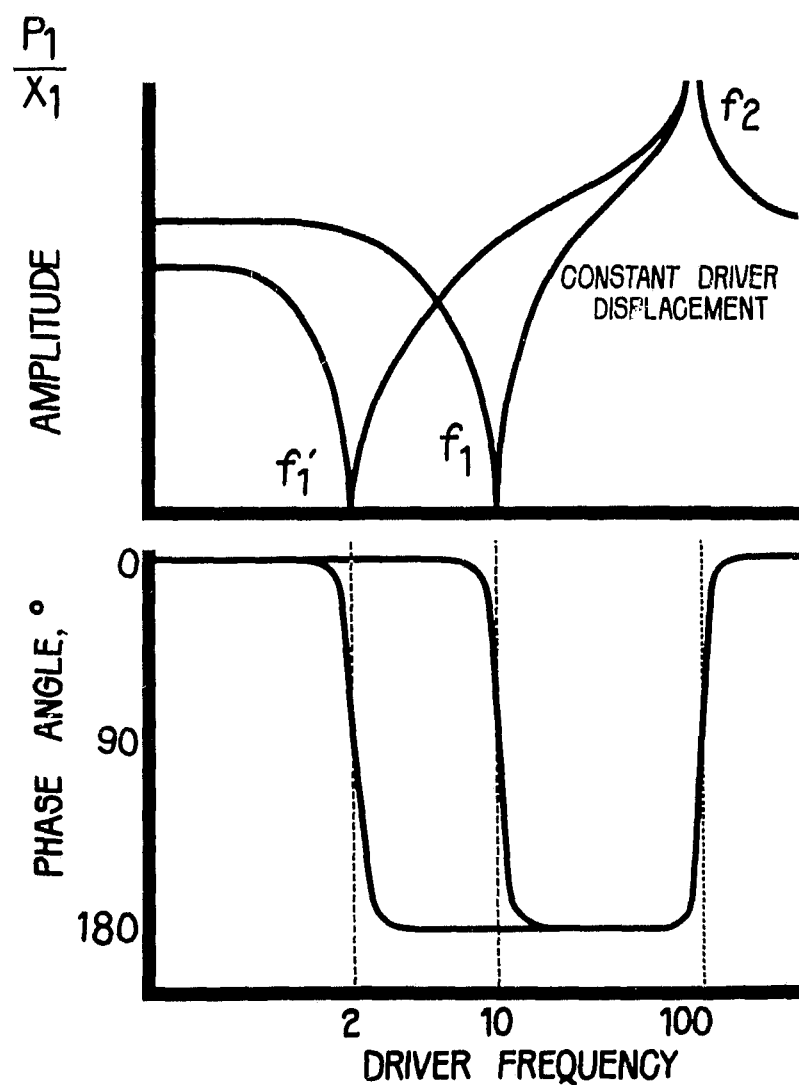
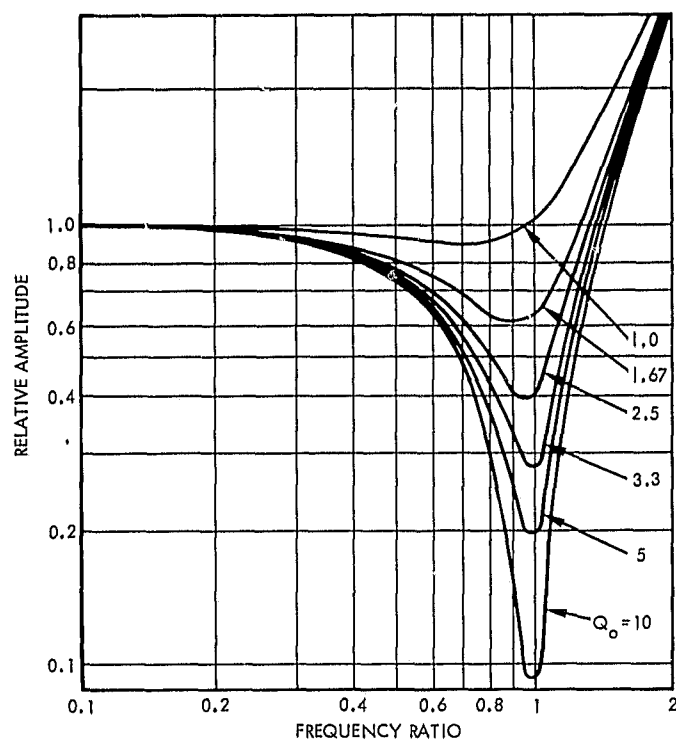


Figure 2-3. RIGS Frequency Response

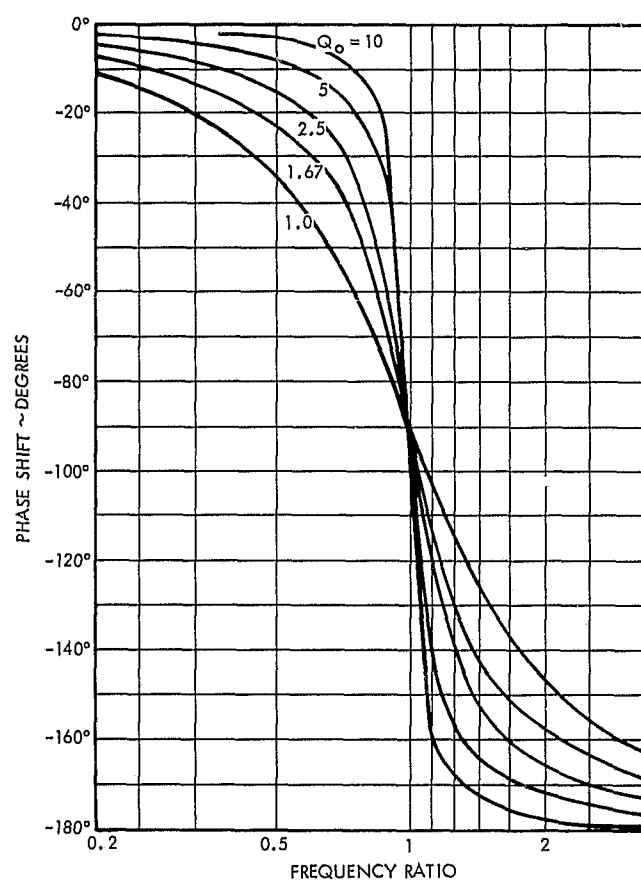
The sharpness of the resonance is determined by the amount of damping (friction) associated with the motion of the follower piston. A common figure of merit for this factor is Q_o , the ratio of the reactive power to the frictional power given by:

$$Q_o = \frac{2\pi f_r M}{R A^2} \quad (2.8)$$

The effect of Q_o upon the sharpness of the peak and phase angle change is shown in Figure 2-4. For ease of detection, therefore, the Q_o should be at least 5 and preferably higher.



a) Amplitude Response



b) Phase Shift

Figure 2-4. Generalized Response of a Resonant System

In actual operation, the driver piston is operated by a variable frequency driver. A pressure transducer measures the dynamic pressure above the follower piston. The electronics associated with the system uses the output of the pressure transducer to control and maintain the driver frequency at the point where the pressure is minimum and the phase shift is 90 degrees (the resonant frequency). The system is thus a null-seeking device and not subject to sensitivity changes or drift in the pressure transducer or electronics.

The resonant frequency, thus determined, is combined in the data processor with the propellant temperature, tank pressure, and the ratio of specific heats to provide an output proportional to the propellant mass. A detailed discussion of the data processor is presented in Section 3.

3. SYSTEM DESIGN

The RIGS system is broken down into two main subsystems; the sensor/driver subsystem which includes the driver assembly; the resonant element assembly, and the pressure transducer; and the data processor subsystem which includes the control system and display electronics. A detailed description of these components is given in Sections 3.1 and 3.2. Since the RIGS system was selected for integration into the Apollo SPS tankage, a description of these tanks, methods of incorporating the RIGS system into them, and material compatibility considerations are discussed in Sections 3.3 and 3.4. A summary of the system characteristics is given in Section 3.5.

3.1 SENSOR/DRIVER ASSEMBLY (SDA)

The proposed Sensor/Driver Assembly for the Apollo SPS tanks is shown in Figure 3-1. The driver piston is actually a metallic bellows powered by a variable-frequency electromagnetic driver. The follower piston (the resonant element) is supported by a flexible elastomeric diaphragm. A controlled amount of damping (friction) is provided for the follower piston by two teflon guide rings. A differential pressure transducer is used to measure the cavity pressure.

In order to keep liquid off the follower diaphragm and to facilitate operation with an unknown liquid orientation, an additional large-surface-area bladder serves to distribute the pressure pulse in the tank cavity. Additional components of the gauge also include a fill valve and a latching solenoid to prevent excessive vibration of the follower piston during the launch accelerations.

Typical operation of the assembly and components is described below.

3.1.1 Driver Assembly

The function of the driver assembly is to provide a sinusoidal volume variation in the cavity V_1 at a frequency controlled by the data processor. For the SPS tankage, the driver assembly must operate over a

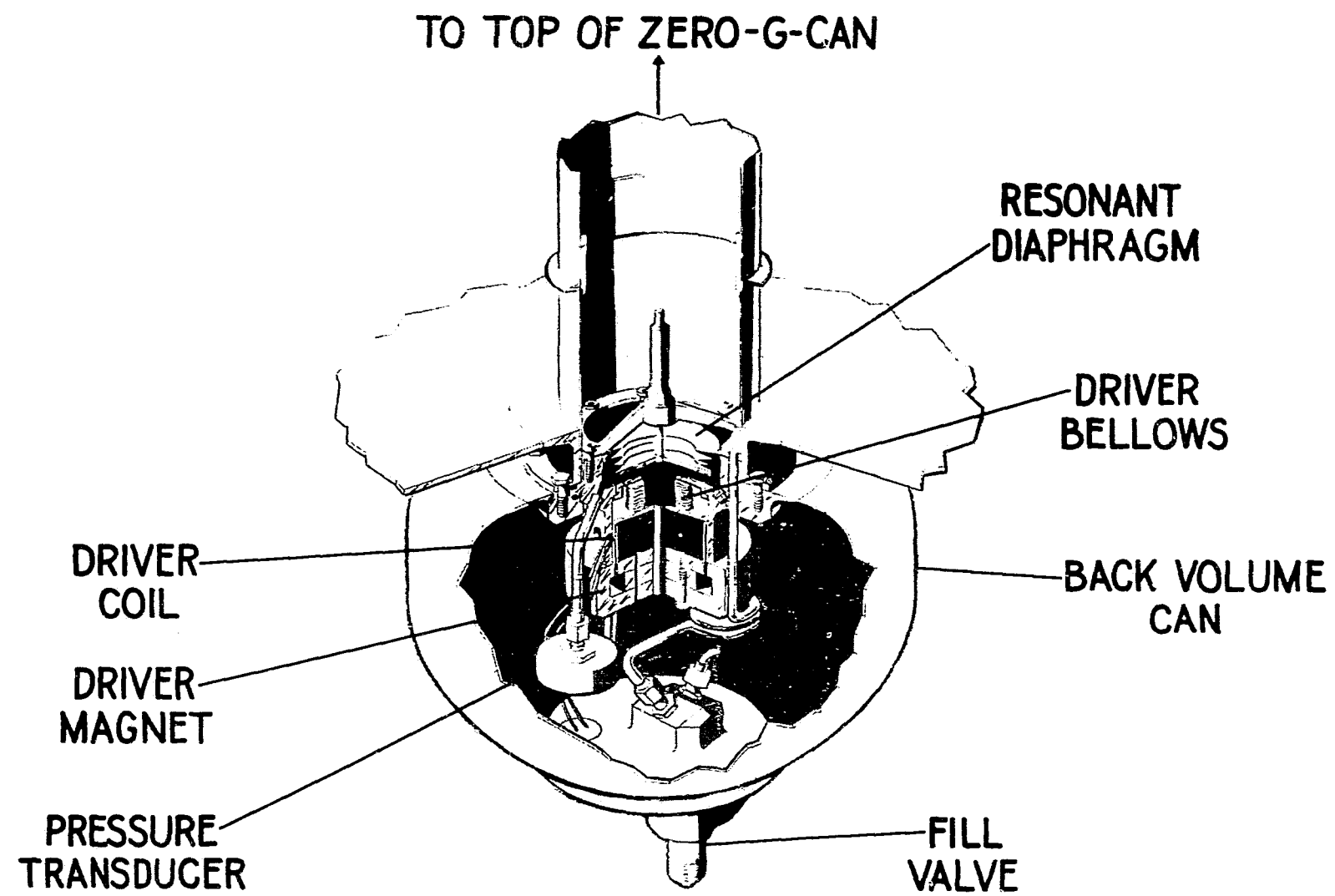


Figure 3-1. Prototype Resonant Infrasonic Gauge

frequency range of 0.5 to 3 cps while providing a 0.5 in³ volume displacement. The low frequency has been selected in order to limit the error from random liquid orientation, as discussed in Section 4.

3.1.1.1 Driver Selection

A number of different drive mechanisms were considered before the electromagnetic driver shown in Figure 3-1 was selected. Among those considered were:

- 1) Variable speed motor and cam
- 2) Variable speed motor and linkage
- 3) Piezoelectric crystal
- 4) Fluidic driver with fan
- 5) Electrodynamic driver

The first two schemes using variable-speed dc motors were eliminated because of the excessive harmonics present in the driver motion. As the motor operates against the gas spring of the enclosed volume behind the driver, its speed varies depending upon whether the motion is with or against the spring. This generates a large second harmonic component in the driver motion. A design which reduces this effect is no longer competitive with the electrodynamic driver in either weight or power requirements. The piezoelectric driver was found to be impractical for the relatively large volume displacement required. The fluidic approach, employing a proportional fluidic oscillator in series with a small fan, appeared promising but would require appreciably more development than an electromagnetic driver. Thus, the electrodynamic driver was selected for the RIGS application.

3.1.1.2 Driver Description

The electrodynamic driver selected is similar to a conventional loudspeaker driver. Motion is produced by passing current through a coil located in a fixed magnetic field which is produced by a permanent magnet assembly. A force is generated on the coil proportional to the

magnitude and direction of the current and the field. The coil is rigidly fixed to the driver piston and the current is fed to the coil from an electronic amplifier.

The force produced on the coil is:

$$F = B \ell I = B n \pi D I \quad (3.1)$$

where

F = force generated

B = flux density, weber/m²

I = current

ℓ = length of coil = $n \pi D = \frac{w \pi D}{D_w}$

n = number of turns

D = diameter of coil

w = width of magnet gap

D_w = wire diameter

3.1.1.3 Driver Design

Commercially available electrodynamic drivers are not optimum for the RIGS application. In general, cost and wide-range response are emphasized rather than weight and input power optimization. Therefore, a study of a driver specifically designed for this application was carried out. The design parameters were selected to correspond to the present state of the art in loudspeaker design and, thus, were quite conservative. The major difference from the commercial drivers was in the elimination of excess iron weight and an increase in the voice coil dimensions commensurate with the high force/low frequency requirements.

The design parameters selected are shown below. A gap flux density of 1.700 gauss was selected which is a factor of 6 lower than the theoretical saturation point for iron magnetic circuits. Round copper

wire was used for the voice coil design for conservatism, whereas square silver wire could reduce the power requirement by approximately 40 percent. Other assumptions made in the design were:

- Any cross section carrying the flux, B , must have an area equal to the gap cross sectional area. Since the actual flux density is a function of minimum area anywhere in the magnetic circuit, this is the lightest design.
- The coil is wound in two layers to bring both leads to the open end.
- The density of the magnet material is the same as that of the iron used.

A schematic of the driver is shown in Figure 3-2. The total driver weight (M_D), available force output (F), and coil power dissipation (W) were then solved for in terms of gap width (w), gap thickness (t), coil mean diameter (D), peak displacement (δ), wire diameter (D_w), and current (I). The following equations were obtained:

$$M_D = 4 \pi \rho w D \left[w + \delta + \frac{9}{8} t \right] \text{ pounds} \quad (3.2)$$

$$F = 3.58 \times 10^{-6} \frac{w D B I}{D_w} \text{ pounds} \quad (3.3)$$

$$W = \frac{8 I^2 \sigma D (w + 2 \delta)}{D_w^3} \text{ watts} \quad (3.4)$$

where ρ is the density of the magnet and σ is the resistivity of the coil wire.

A low spring rate metallic bellows serves to isolate the driver cavity from the enclosed volume behind the piston (the back volume). The actual displacement of the driver piston is then governed by the force applied to the coil working against the parallel spring rates of the bellows and the gas in the back volume. The spring rate contribution due to the driver cavity V_1 in series with the ullage gas volume is negligible because of the large relative size of this total volume. Due to the low frequency

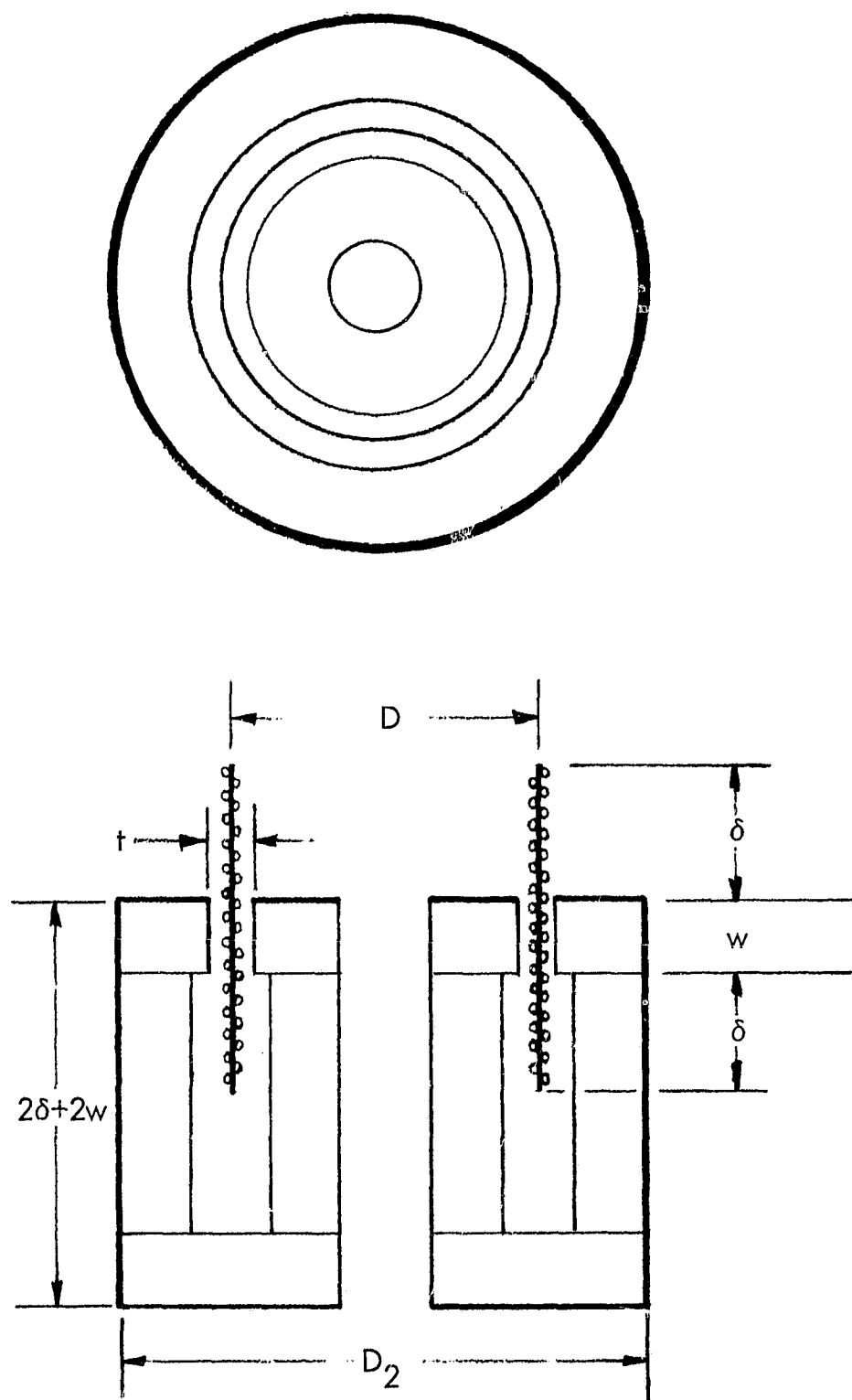


Figure 3-2. Schematic of Electrodynamic Driver

of the driver piston, the piston mass may also be neglected. Thus, the driver displacement is simply:

$$\Delta V = \frac{FA}{K_g + K_B} = \frac{F V_B A}{\gamma P A^2 + K_B V_B} \quad (3.5)$$

where:

ΔV = volume displacement

F = applied force

A = area of driver piston

K_g = back volume gas spring rate

K_B = bellows spring rate

V_B = back volume

As shown in Equation (3.5), for a given force the volume displacement is roughly proportional to the size of the back volume and this volume becomes one of the major driver design variables. In addition, the piston area is quite important. If the bellows spring rate is small compared to the gas spring rate, the volume displacement for a given force is inversely proportional to the piston area, thus favoring a long stroke. If the bellows spring rate is large, a short stroke is preferred.

A series of designs employing the above equations was carried out and typical results are shown in Table 3-1. For this study, the bellows spring rate was assumed to be 0.1 lb/in. The effect of the back volume is clearly seen in cases 1-5, and it is apparent that a back volume of approximately 300 cubic inches is required in order to minimize both the coil power and weight. On the basis of the study, the driver represented by case 6 and shown schematically in Figure 3-3, was selected. The pertinent design parameters are:

Stroke = ± 0.40 inch

Piston area = 0.625 inch^2

Back volume = 300 inch^3

Weight = 3.5 lb

Power required = 3.4 watts

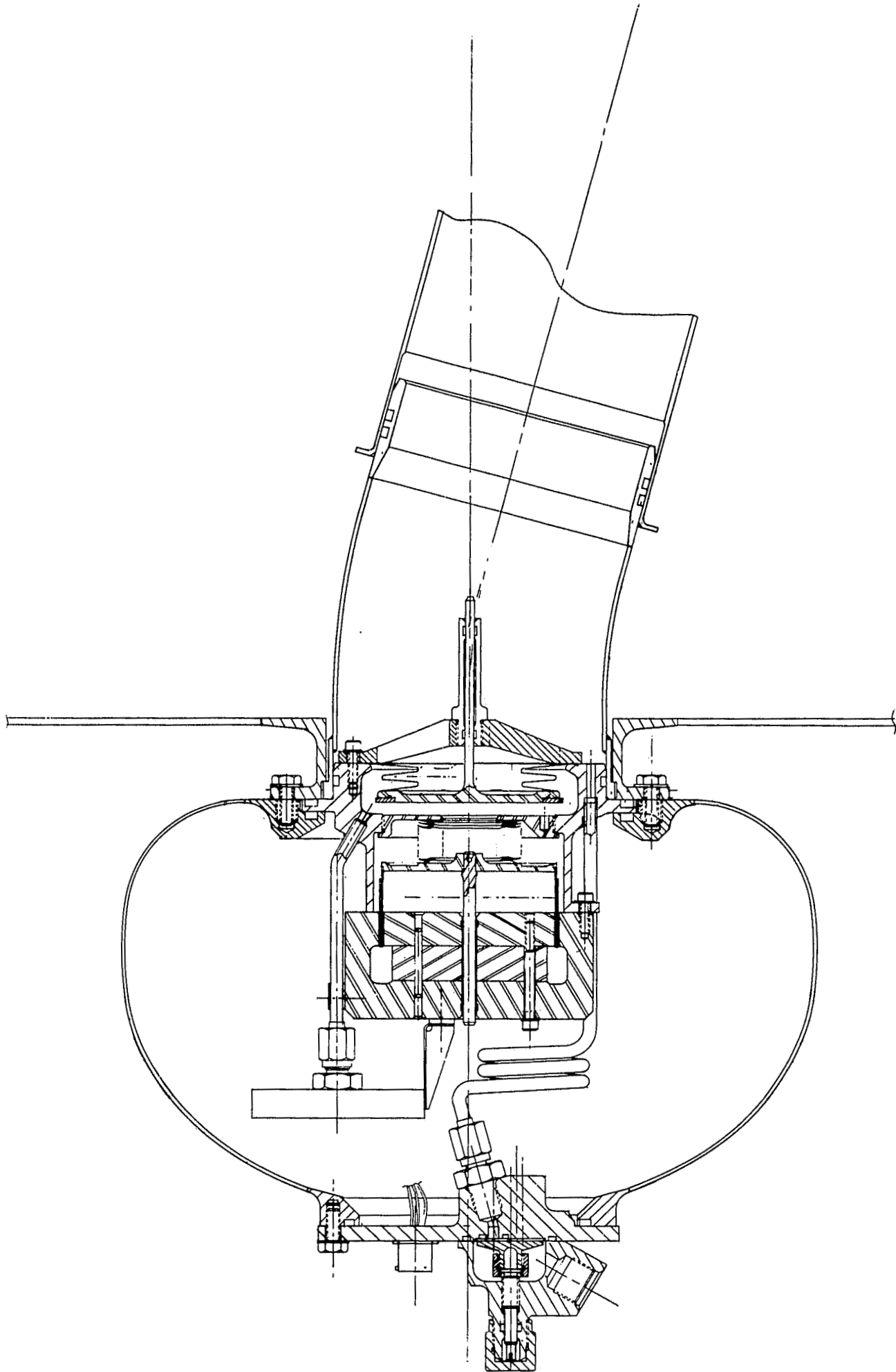


Figure 3-3. Resonant Infrasonic Gauging System

Table 3-1. Parametric Study of Electrodynamic Driver Designs

Case No.	Volume Displacement (\pm in ³)	Linear Displacement (in.)	Force (lb)	Back Volume (in ³)	Power (watts)	Weight (lb)
1	0.125	0.25	1.50	2.0	8.0	17.2
2	0.25	0.40	1.25	47.0	8.55	15.7
3	0.25	0.25	1.25	75.0	6.95	13.38
4	0.25	0.10	1.25	186.0	5.39	10.15
5	0.25	0.25	0.50	300.0	3.96	3.73
6	0.25	0.40	0.41	300.0	3.42	3.51
7	0.25	0.10	0.88	300.0	3.89	7.25

In all cases, the following design parameters are the same:

Current = 1.0 amp

Wire diameter = 0.016 inch (No. 26)

Gap thickness = 0.060 in.

3.1.2 Resonant Element Assembly

The key to the operation of the RIGS system is the resonant element, or follower piston. In order to achieve the benefits of the resonant type of system, it is necessary to have a fairly high value of Q_o (resonance figure of merit) and a well defined relationship between the measured frequency and the gas volume (or spring rate). This imposes severe restrictions on the design of the resonant element. Since the spring rate of the diaphragm adds directly to the gas spring rate, the resonant element spring rate must be small compared to that of the gas. The spring rate of the ullage gas, when the SPS tanks are empty, is:

$$K_{u_{\min}} = \frac{A^2 \gamma P}{V_{u_{MT}}} = \left(10^{-3} \frac{\text{lb}}{\text{in}^5}\right) (A)^2 \quad (3.6)$$

The diaphragm spring rate should be at least a factor of ten lower. The spring rate K_D for a flat diaphragm is:

$$K_D = \frac{4 E t^3}{(1 - \nu^2) A} \quad (3.7)$$

where:

E = modulus of elasticity

t = thickness

ν = Poisson's ratio

In order for K_D to be 0.1 of $K_{u_{min}}$

$$\frac{4 E t^3}{(1 - \nu^2) A^3} = 10^{-4} \text{ lb/in}^5$$

It is apparent that in order to achieve the required spring rate, a material such as an elastomer with a low modulus of elasticity is desired. Also, appreciable benefit can be derived from using thin diaphragms with large diameters. For example, for a 3-inch-diameter diaphragm made of nitroso rubber ($E = 1060$ psi and $\nu = 0.5$), Equation (3.7) can be used to determine the material thickness required to provide a spring rate equal to one-tenth of the empty tank gas spring rate. The resulting thickness is 0.019 inch, which represents a reasonable design value.

In order for the diaphragm to resonate at the desired frequency, additional mass must, however, be added. From Equation (2.5), the required mass for the empty SPS tank to resonate at 0.5 cps with a 3-inch diaphragm is:

$$M = \frac{A^2 \gamma P_u}{(2 \pi f_r)^2 V_u} = 1.84 \text{ lb}$$

where:

$$P_u = 180 \text{ psia}$$

$$V_u = 171 \text{ ft}^3$$

$$\gamma = 1.60$$

$$f_r = 0.5 \text{ cps}$$

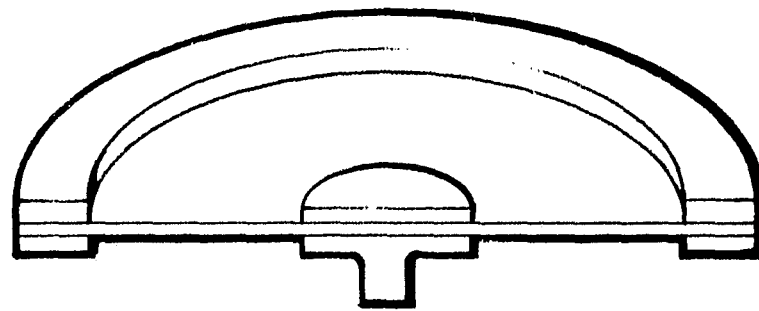
This mass is clearly excessive. Since the mass varies directly with the square of the diaphragm area and since large diameter diaphragms are required to achieve the required spring rate, other means of lowering the spring rate are required. The most promising technique appears to be the addition of convolutions to the diaphragm. Simple convolutions such as those shown in Figure 3-4 can reduce the spring rate by a factor of 4 or more. Even greater reductions are possible by going to multiple element designs such as shown in Figure 3-4c. Application of convoluted designs permits the use of diameters of 2 inches or less with corresponding reductions in the resonant mass.

For the prototype design shown in Figure 3-1, a multiple element design has been selected. However, some development testing will probably be required prior to the selection of the most satisfactory design.

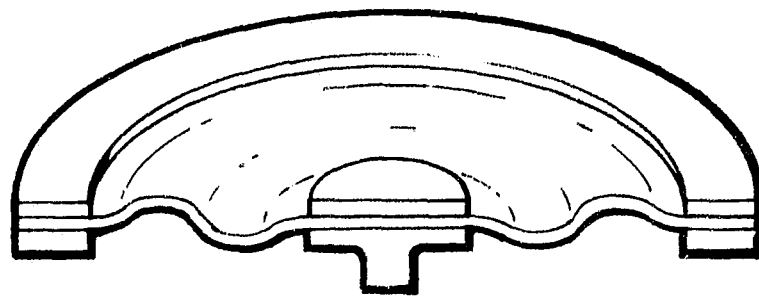
3.1.3 Pressure Transducer

The requirements for the pressure transducer are the ability to detect a sinusoidal pressure signal varying in frequency from 0.3 to 5 cps over a pressure range of 10^{-3} to 10^{-5} psi. Accurate linearity of the gauge is not required because of the resonant nature of the system. The gauge should also be capable of withstanding a 200 psi pressure differential without being damaged.

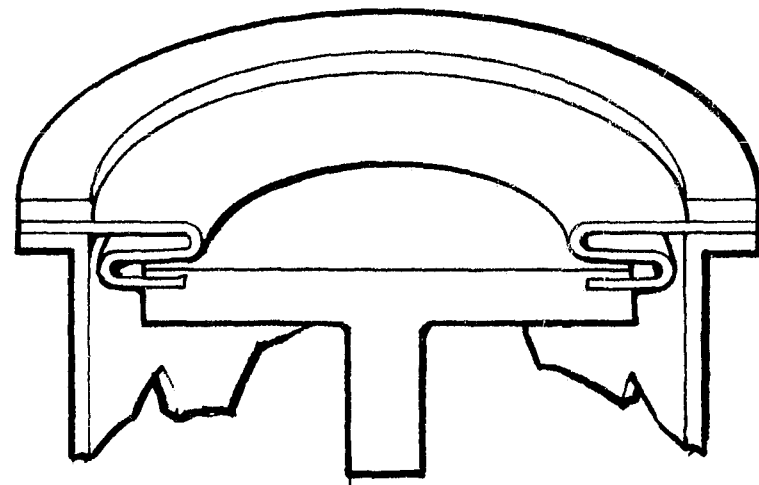
The principle of the transducer is shown in Figure 3-5. The basic element is a 2-inch-diameter, thin, metallic diaphragm encapsulated in an aluminum body. The enclosed volume behind the gauge is vented to the cavity by a porous plug which acts as a low pass acoustical filter. The static pressure on both sides of the diaphragm is thus balanced, and the diaphragm responds only to the sinusoidal pressure component. The



a) FLAT DIAPHRAGM



b) CONVOLUTED DIAPHRAGM



c) MULTIPLE CONVOLUTIONS

Figure 3-4. Three Basic Diaphragm Configurations

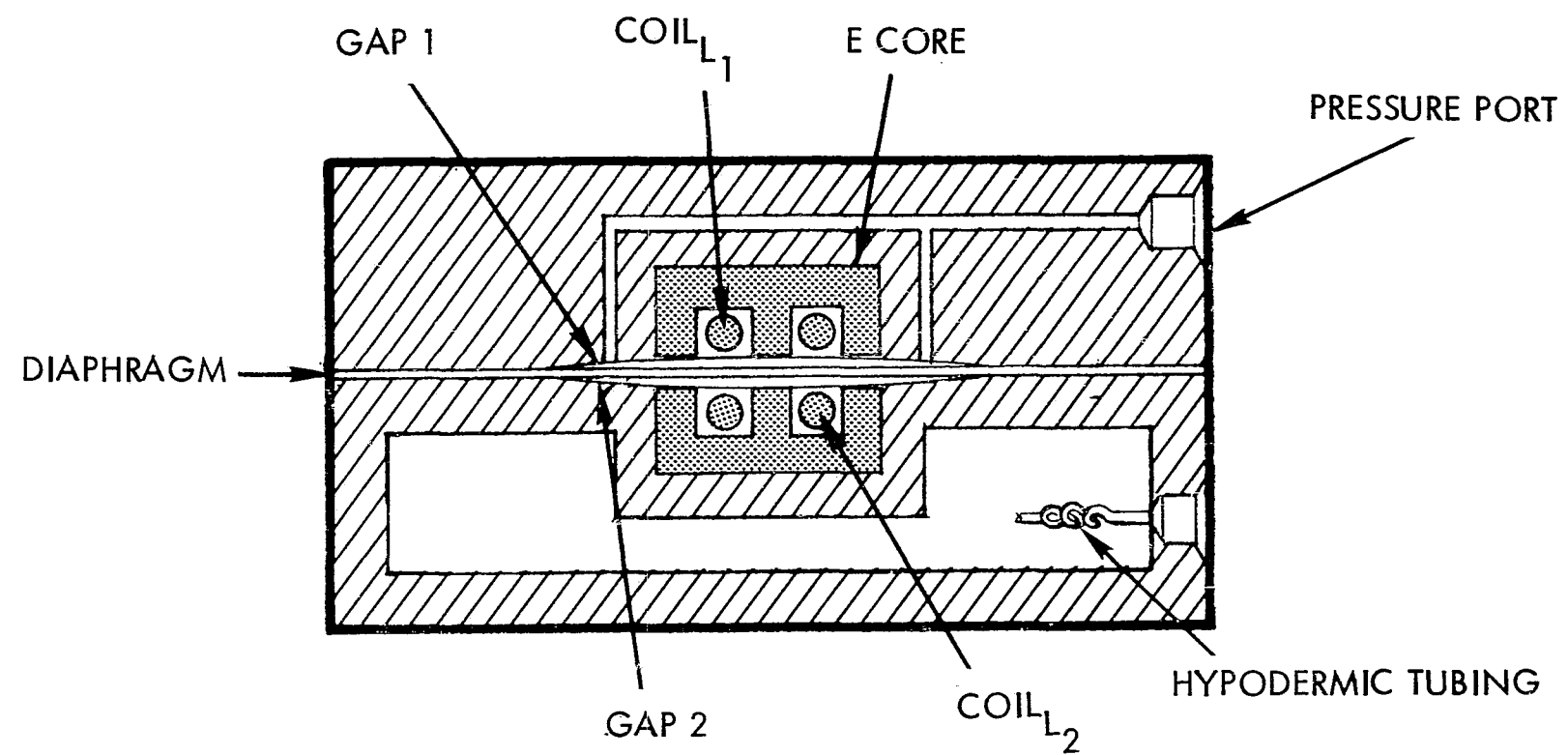


Figure 3-5. Variable Reluctance Pressure Transducer

diaphragm deflection is a function of the applied pressure force, the stiffness of the diaphragm and the stiffness (spring rate) of the enclosed back volume.

The applied force is equal to:

$$F = p' A \quad (3.8)$$

The spring rate of the diaphragm and enclosed back volume is:

$$K_T = K_D + K_g = \frac{4 E t^3}{(1-\nu^2) A} + \frac{A^2 \gamma P_u}{V_B} \quad (3.9)$$

where:

- F = applied force
- p' = variation in pressure
- A = area of diaphragm
- K_T = total spring rate
- K_D = spring rate of diaphragm
- K_g = back volume spring rate
- E = modules of elasticity
- ν = Poisson's ratio
- t = diaphragm thickness
- P_u = static pressure
- V_B = enclosed back volume

The total deflection is thus:

$$\delta = \frac{F}{K_T} = \frac{p' A^2}{\frac{4 E t^3}{(1-\nu^2)} + \frac{A^3 \gamma P_u}{V_B}} \quad (3.10)$$

The diaphragm deflection increases approximately as the fourth power of the diaphragm diameter, which indicates the importance of going to a large diameter diaphragm to detect the small dynamic pressure variations. In actual application, the diaphragm deflection is limited by two plates to prevent damage upon application of a large unbalanced pressure to either side of the diaphragm.

The diaphragm deflection can be detected by a number of different devices. The present design is of the variable reluctance type, similar to the transducer used in the feasibility demonstration tests described in Section 5. This type was selected because all exposed components can be made of stainless steel, thus minimizing possible material compatibility problems. Other possible types include:

- Solid state strain gauges
- Variable capacitance gauge
- Cantilevered piezoelectric pickup

The solid state strain gauge should also be evaluated in the development phase as it possesses certain definite advantages in both simplicity of data processing and high signal output. Material compatibility is the only major problem with this type of device.

3.2 DATA PROCESSOR

3.2.1 Control System

3.2.1.1 System Selection

The control system provides a means of detecting the resonant frequency as well as locking-in the driver element at that frequency. As was shown in Section 2, the cavity pressure in the RIGS system undergoes both a minimum amplitude and a 90-degree phase shift with respect to the driver at the resonant point. Thus either minimum amplitude or phase sensing techniques, or combinations of the two, may be used to determine the resonant frequency. Linear analysis was employed to demonstrate that amplitude-sensing systems are quite sensitive to external noise and are incapable of tracking the desired frequency to the required accuracy. A technique using phase-lock only (employing clipping amplifiers, Schmidt triggers, and a phase comparator circuit) was capable of measuring the desired frequency to the required accuracy, but required a rather large pressure signal resulting in an extremely heavy driver element. The multiplier/filter technique, which utilizes both phase and amplitude information, was found to be superior to other systems in both deadband width and noise toleration, and was selected for further analysis.

3.2.1.2 Principle of Operation

The multiplier/filter sensing technique operates as follows:

If the driver amplitude has the form

$$x = A \sin \omega t \quad (3.11)$$

then the pressure signal will be given by

$$P = B \sin(\omega t + \phi) + c(t) \quad (3.12)$$

where ϕ represents the phase shift between x and P and $c(t)$ represents noise in the output signal. Multiplying x and P together one obtains:

$$x P = A(\sin \omega t) [B \sin(\omega t + \phi) + c(t)] \quad (3.13)$$

which can be simplified to:

$$x P = A c(t) [\sin(\omega t + \phi)] - \frac{AB}{2} [\cos(2\omega t + \phi)] + \frac{AB}{2} \cos \phi \quad (3.14)$$

It is seen that all of these functions except $\frac{AB}{2} \cos \phi$ are time-varying sinusoidal functions. Thus, by passing the signal through a low pass filter, these functions can be removed leaving only the dc signal, $\frac{AB}{2} \cos \phi$. The variations in amplitude and phase angle of this term are shown as a function of frequency in Figure 2-4. Selecting a value of 5 for Q_o , and assuming the driver amplitude is independent of frequency, one obtains the curve shown in Figure 3-6. As may be seen, the value of the dc output ($\frac{AB}{2} \cos \phi$) becomes zero at the resonant frequency. In addition, the rate of change of the dc signal as one approaches the resonant point is quite rapid. The system is thus quite sensitive to small changes in the region of the resonant frequency, and is capable of very good resolution.

A control system which regulates the driver frequency by maintaining the filtered output signal from the multiplier at zero would be continually locked on the resonant frequency. This is the principle of operation of the proposed RIGS control system.

3.2.1.3 Control System Design

Figure 3-7 is a block diagram of the RIGS electronic control system. The individual components are described below.

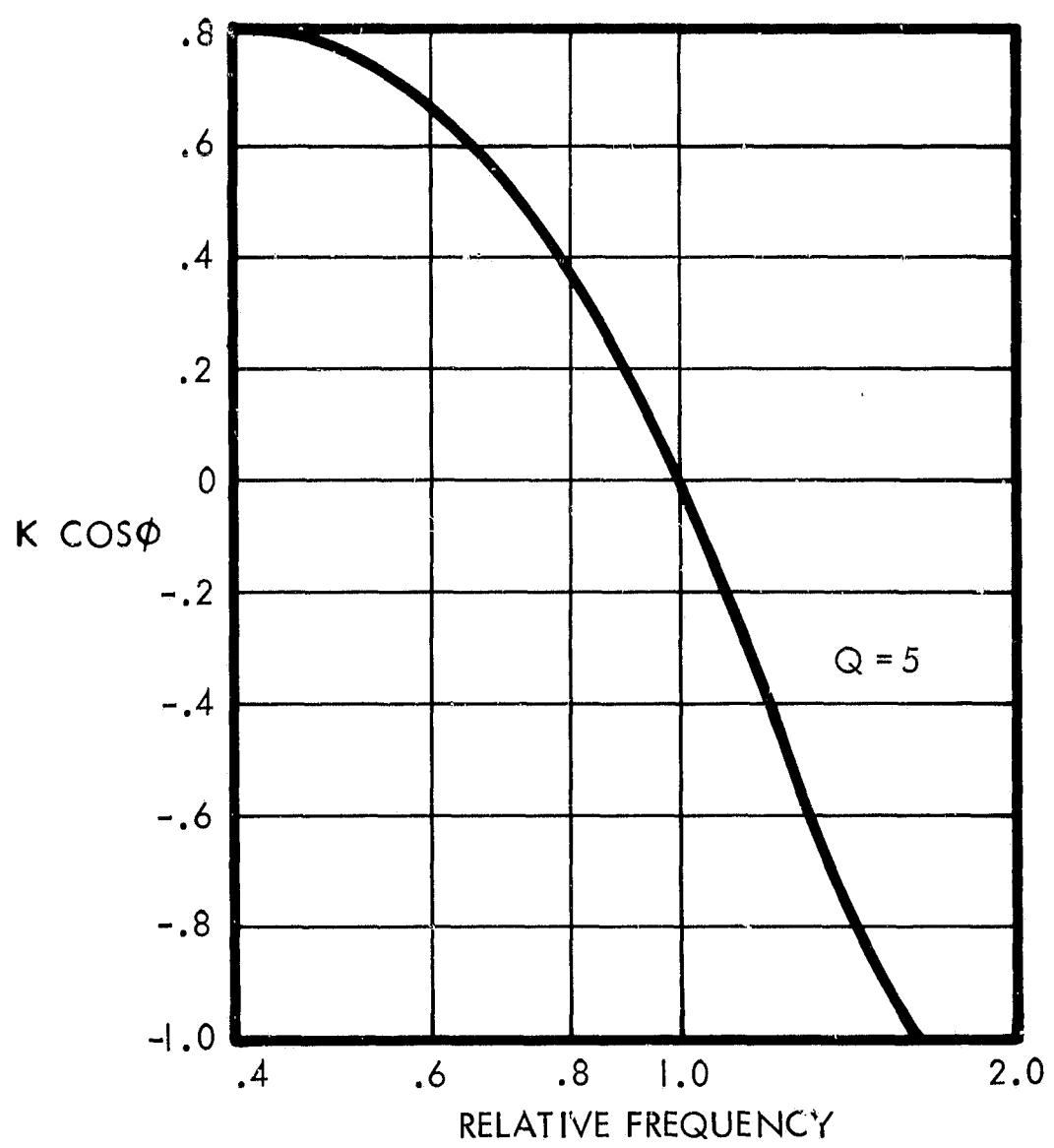


Figure 3-6. Variation of $K \cos \phi$ with Frequency

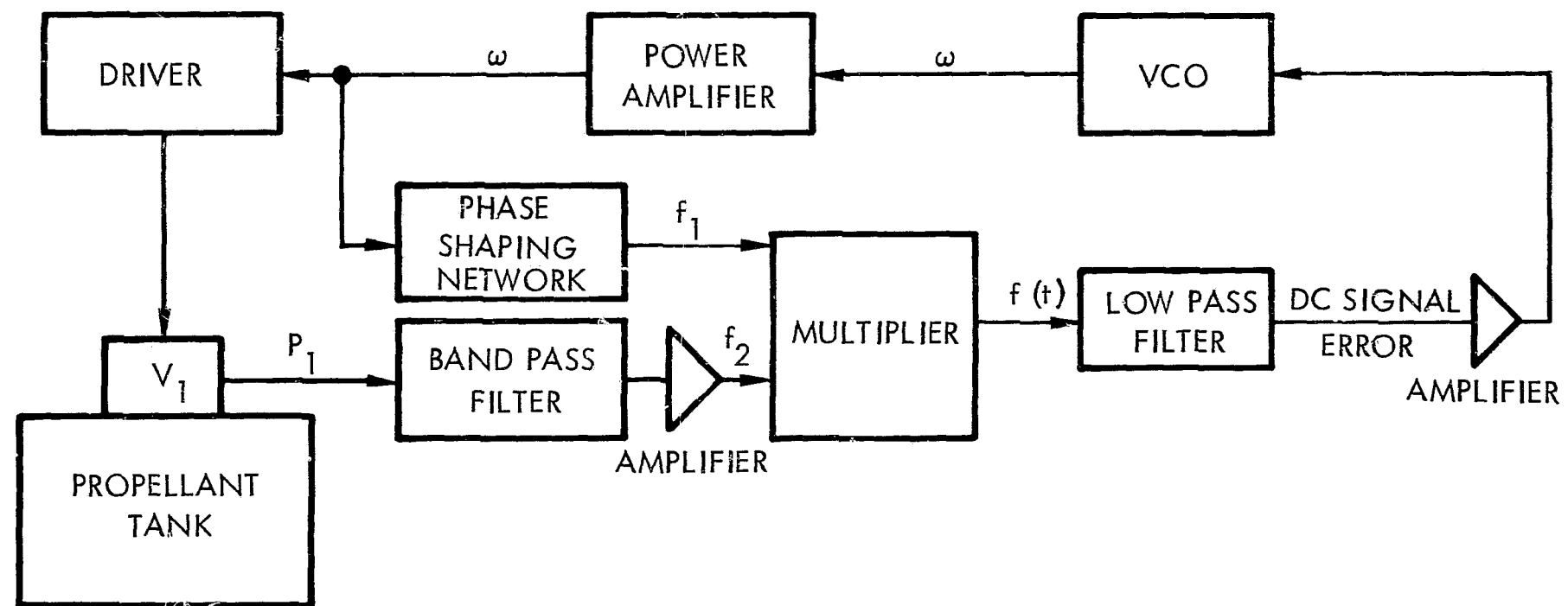


Figure 3-7. Control System Schematic

- Power Amplifier. Amplifies the variable frequency oscillator (VFO) output to the correct level to drive electrodynamic driver at the desired frequency. The output also provides the reference signal for the multiplier.
- Driver/Sensor Assembly. The output of the power amplifier drives the electrodynamic driver. The DSA responds by providing an output pressure signal functionally related to the tank ullage volume.
- Band Pass Filter and Amplifier. The output pressure signal is filtered to remove both dc and very high frequency signals. It is then amplified to provide the proper input level for the multiplier. Results of the preliminary simulation indicate that this component may not be required if sufficient output signal is available directly from the pressure transducer. In this case, the band-pass acoustical filtering is effectively performed by the transducer.
- Multiplier. This component multiplies the filtered signal from the pressure transducer by the reference signal from the power amplifier. The output signal is a complex wave form containing a dc signal proportional to the cosine of the phase shift between the two signals.
- Low Pass Filter and Amplifier. The low pass filter is a long-time-constant filter/integrator which removes all sinusoidal components from the multiplier output except the desired dc signal. This signal is then amplified to serve as the VFO input.

At the resonant frequency, the phase shift, as measured by the phase detector, corresponds to 90° . This corresponds to a dc signal out of the multiplier of zero. When the dc signal is equal to zero, the VFO frequency will stay constant. This point is the desired system resonant point. As can be seen, the loop tends to force the VFO input signal to zero and hence stay locked on the system resonant frequency.

3.2.2 Display Electronics

The display electronics, convert the measured resonant frequency into the propellant mass. The propellant mass is related to the resonant frequency by the following equation:

$$\frac{M}{M_F} = \frac{\rho}{\rho_r} \left(1 - \left(\frac{f_r}{f} \right)^2 \frac{\gamma P}{\gamma_r P_r} \right) \quad (3.15)$$

where:

M	=	propellant mass
ρ	=	propellant density
f	=	resonant frequency
sub F		refers to full tank
sub r		refers to reference condition (tank empty)

The functions ρ/ρ_r and γ/γ_r are generated directly by separate temperature-sensitive thermistor/resistor combinations. The pressure ratio is obtained from a strain gauge pressure transducer. The frequency ratio is obtained from the output of a digital counter gated with the present value of the reference signal. The output of the counter is fed into a squaring module and then multiplied by the product of the pressure and gamma ratios. This signal is then fed into a high gain amplifier acting as a subtractor where a preset reference voltage is subtracted. The signal is now multiplied by the density function to give the propellant mass. A block diagram representation is given in Figure 3-8.

Adjustments are provided on the reference frequency, the reference voltage and the density function to match, respectively, the empty tank frequency, empty tank volume, and measured propellant density.

Additional study is required in order to determine the best configuration of the display system. Although an analog system is shown above, it is possible, particularly with the slow-response requirement, that a small digital system might be preferable.

3.3 RIGS INTEGRATION IN APOLLO SPS TANKS

The preceding discussion assumed that the propellant to be gauged was located in a single, simply-shaped tank and that the gauge could be flange-mounted, externally. In actual practice, such an ideal tank seldom exists and integration of the gauging system into the tank requires a detailed investigation of many interfaces. For this reason, NASA selected the Apollo Service Propulsion System (SPS) for system integration studies. The ground rules for the integration study specified that minimum changes in the tankage were desired and no additional flanges or openings in the basic tank were to be allowed. This caused considerable difficulty in integrating the RIGS into the SPS.

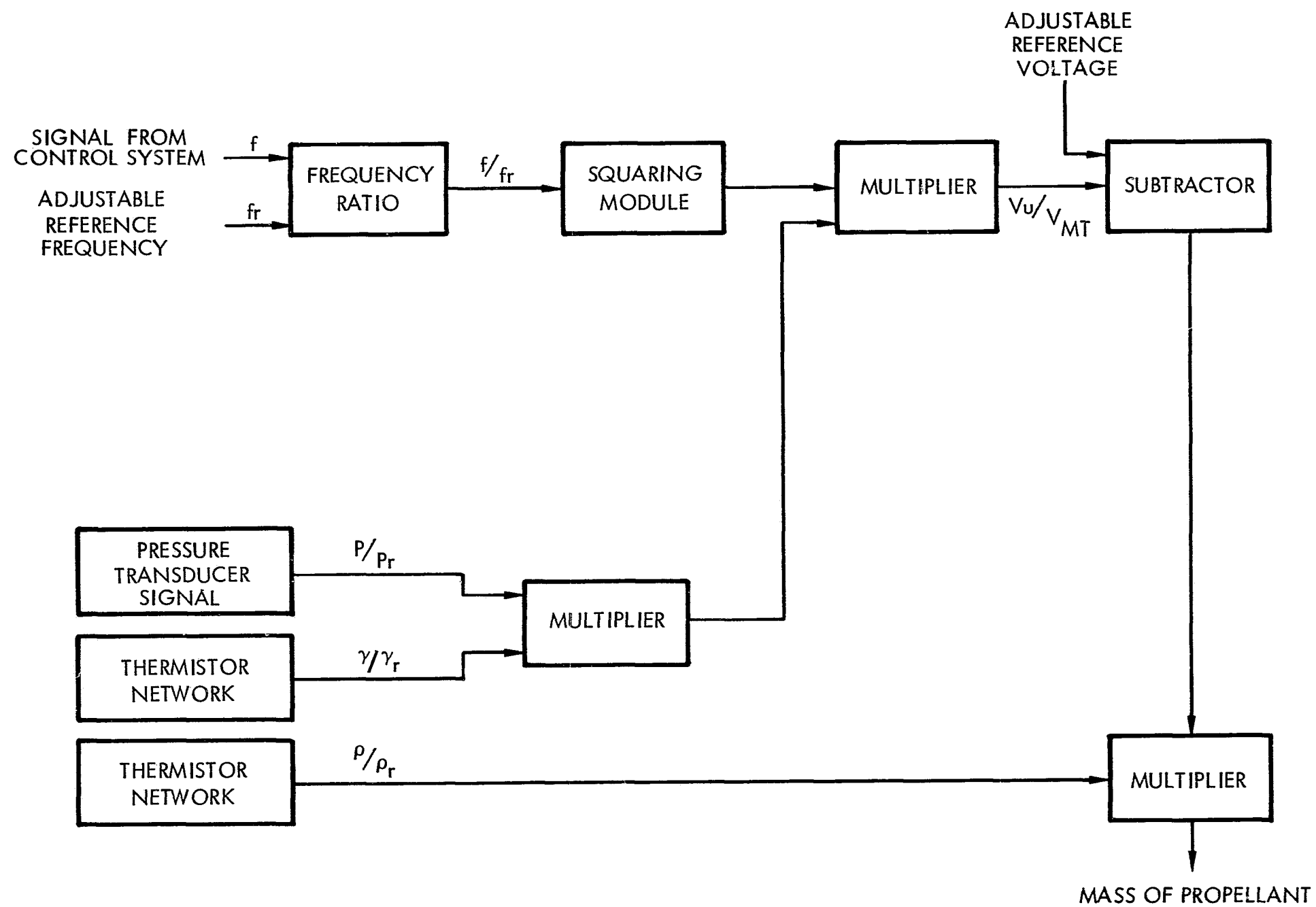


Figure 3-8. Display Electronics

3.3.1 Description of the Apollo SPS Tankage

The SPS tankage is shown schematically in Figure 3-9. There are two series-connected tanks for each propellant. The propellant in the storage tank feeds into the sump tank through a transfer line connecting the two tanks. When the storage tank has been emptied, the sump tank continues to be pressurized through the storage tank and transfer line. Each tank contains a propellant utilization and gauging system (PUGS) located within a 5-inch standpipe in the center of the tank. In addition, the sump tank contains a propellant retention system consisting of the zero-gravity can and a number of retention screens.

3.3.2 Gauge Installation

The best installation area for the gauge would be a 3-inch flange connection to the top of the tank. However, the limitation placed on the RIGS installation - that no new ports or openings be added to the tanks - limited the system installation to areas around the zero-gravity can and the PUGS (see Figure 3-9). A number of possible installation approaches were examined prior to final selection. Some of the more promising ones are shown schematically in Figure 3-10, and are described below:

- Mount gauge assembly on top of PUGS standpipe with reinforced flange at top to take vibration load. This method was rejected because of difficulties in supporting a 4 to 7 pound mass on the end of the long column.
- Mount gauge assembly on top of zero-gravity can surrounding the PUGS standpipe. Unfortunately, insufficient information on the structural characteristics of the zero-gravity can was available, and it appeared doubtful that the zero-gravity can could support the gauge during launch accelerations and vibration. A second difficulty was that the gauge would have to be installed at the same time as the zero-gravity can and could not be removed without removing both the can and the PUGS system, thus complicating maintenance of the gauge. Also, the storage tank does not have a zero-gravity can and a different installation would be required there.
- Mount the gauge on the large, flanged closure at the bottom of the tanks used for installation of the zero-gravity can and PUGS. The pressure signal would be piped through the zero-gravity can to a diaphragm

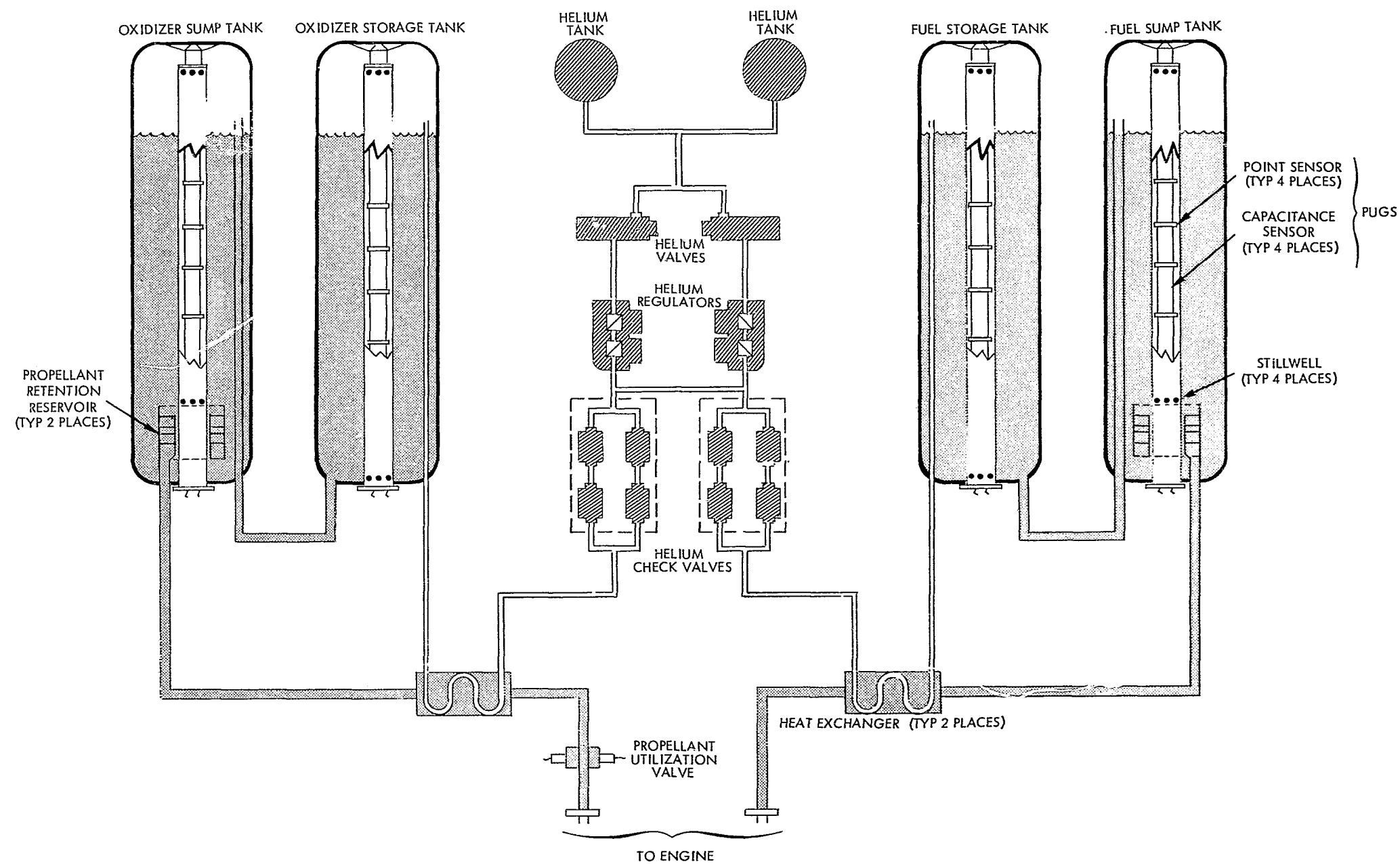


Figure 3-9. Service Propulsion Propellant Feed System

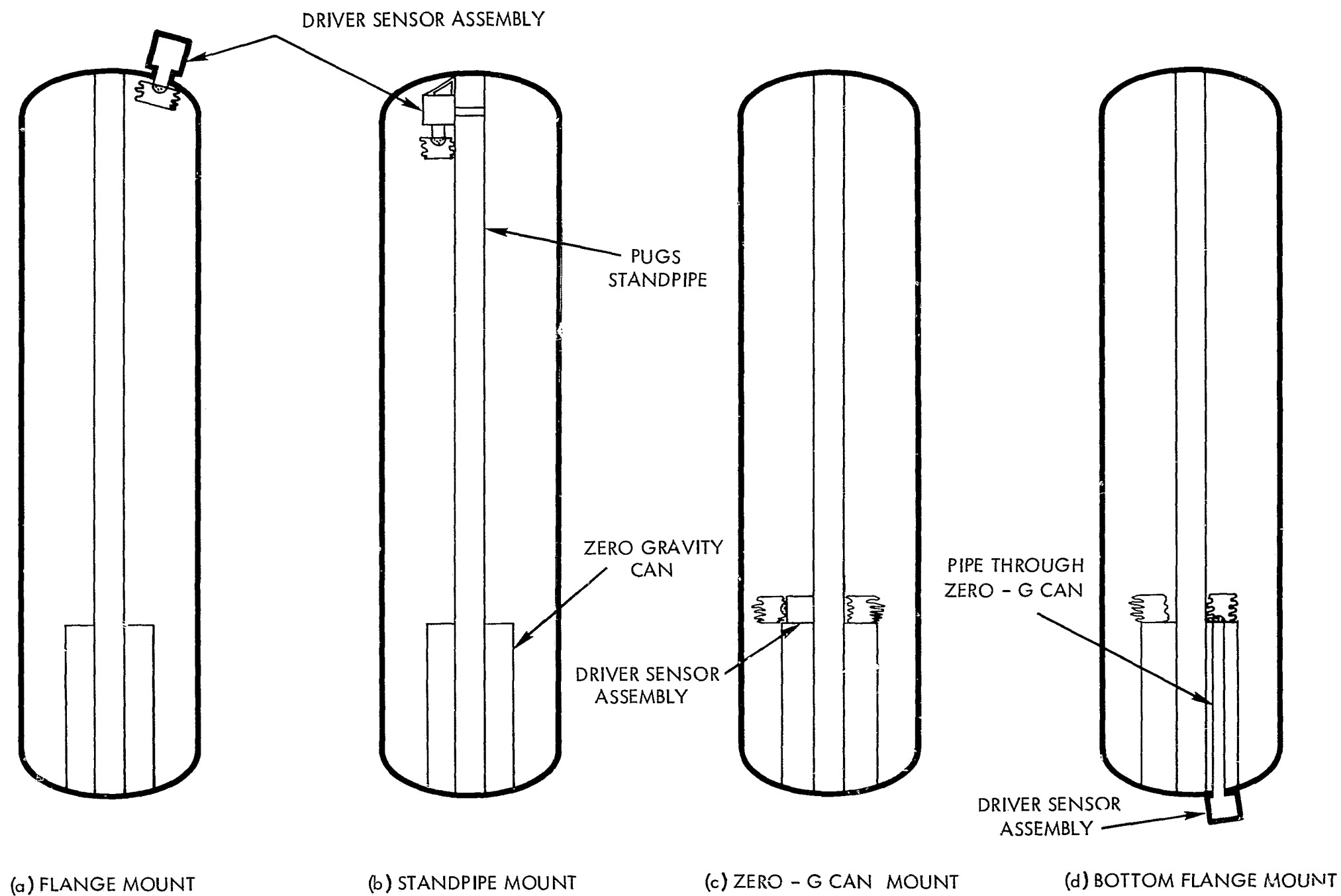


Figure 3-10. Possible RIGS Installations in SPS Tankage

located above the can with both the pipe and diaphragm permanently installed in the zero-gravity can. Some modification of the zero-gravity can would be required. Modification of the flanged closure to include a 4-inch flange would also be required. In the storage tank which does not have a zero-gravity can, the pipe would be supported by the PUGS standpipe.

The third approach was selected and is shown in Figure 3-10d. This installation technique complicates system pressurization since the gauge is submerged beneath liquid during pressurization and it also imposes an additional weight penalty of 1.4 lb over the direct-flanged installation (configuration a).

An additional problem is attenuation of the pressure signal in the piping leading to the larger diaphragm on top of the zero-gravity can. As will be shown in Section 4, the error from this component can be made small by reduction of the maximum system frequency to 3 cps. However, it does not require any new opening or supports in the tank proper and appears to be the only feasible installation method meeting all the ground rules.

3.3.3 Effect of Storage-to-Sump-Tank Transfer Line on RIGS.

The sump tank and storage tank are interconnected by a transfer line as shown in Figure 3-9. When even a small amount of liquid is in this line, the two tanks are essentially acoustically isolated. For this reason, separate RIGS installations are required in storage and sump tanks to provide full-range gauging capability under zero gravity. However, if the storage tank is empty and the line is completely free of liquid, the ullage volumes in the two tanks can interact acoustically and the individual tank measurements become dependent upon the conditions in both tanks.

As the conditions in the transfer line are unpredictable under zero gravity, it is apparent that some positive device is required to prevent this interaction. Two devices seem promising. The simpler, though less positive, device is to install a screen over the outlet of the transfer line in the sump tank. If this screen is wetted, it will serve to acoustically isolate the two tanks. The screen mesh size must be selected to provide negligible pressure drop in the line when liquid is flowing through

the line and thus unfortunately, cannot provide isolation when the screen is completely dry. However, as liquid under zero gravity will preferentially wet the screen, the probability that the screen will be wetted is quite high.

A more positive technique is to provide an inertial damping device such as shown in Figure 3-11. In this device the transfer line is partially blocked during quiescent conditions by a butterfly valve. The butterfly valve is designed to open upon application of a small pressure (less than 0.1 psi) in either direction and, thus, does not serve as a check valve. Acoustical isolation is provided by selecting the moment of inertia of the device such that it has a natural frequency below 0.01 cps when in series with the gas spring rate in either tank.

3.4 MATERIAL COMPATIBILITY

All materials used in the RIGS design were selected for their compatibility with the propellants. On the basis of TRW's extensive experience with these propellants, metallic components are fabricated out of 6061 T6 aluminum, 7075 aluminum, or 347 series stainless steel. The driver magnet assembly which must contain soft iron is coated with a thin layer of crystallized Parylene C. All electrical wires are insulated with teflon and are coated with Parylene C after installation.

The follower diaphragm for the oxidizer tank is made of carboxylnitroso rubber, a product of the Thiokol Chemical Company, which has demonstrated outstanding resistance to N_2O_4 and is presently being used in TRW's LMDE engine. The fuel tank diaphragm is made of ethylene-propylene rubber. The compliance bladders are made of teflon.

3.5 SYSTEM CHARACTERISTICS

3.5.1 System Weight

The estimated weight of the prototype sump tank gauge is presented below. The storage tank gauge weight will be 0.8 lb lighter. The weight of the isolation device between the sump and storage tanks is 0.6 lb.

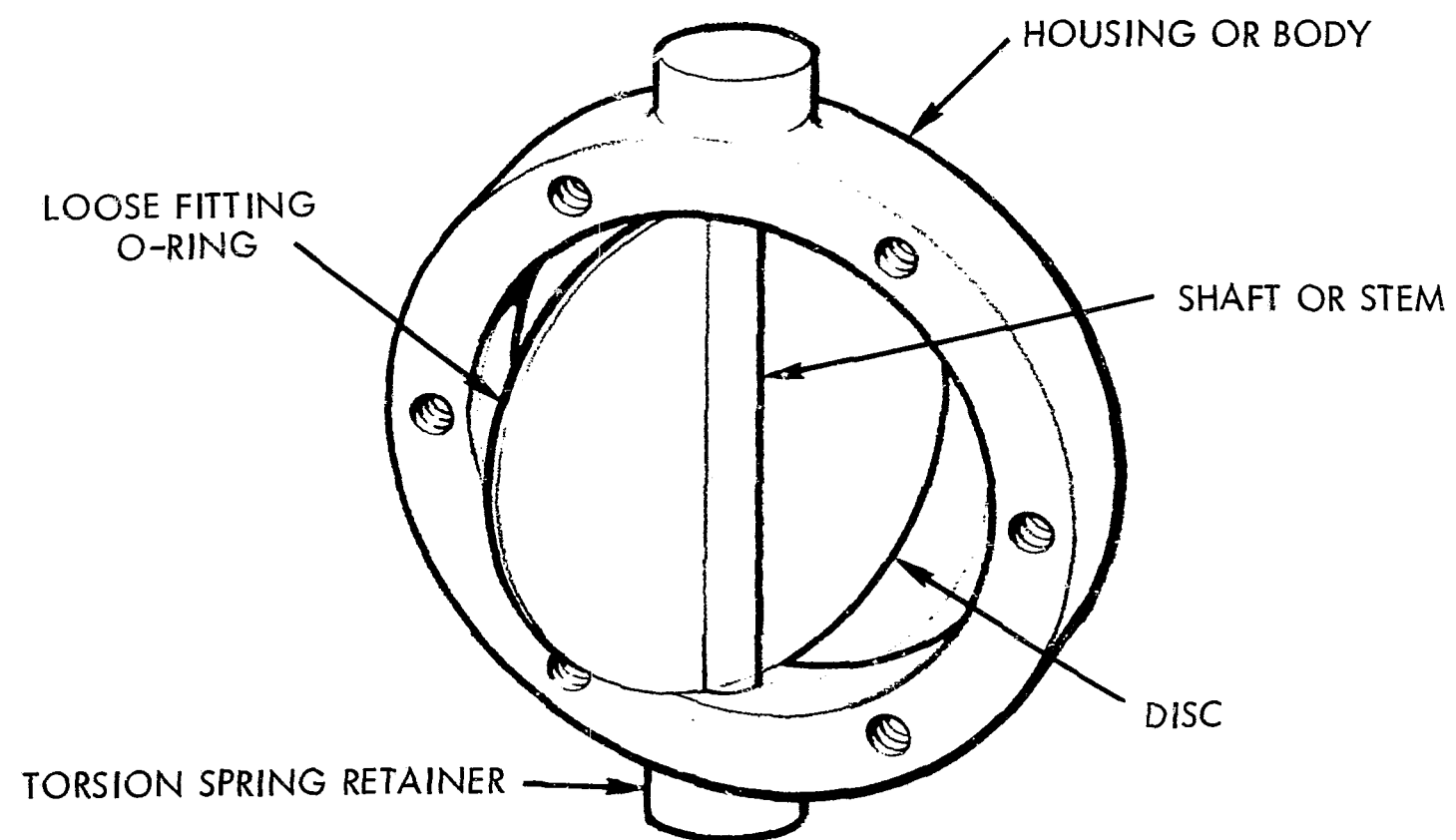


Figure 3-11. Inertial Damping Device

<u>Sensor/Driver Assembly</u>	<u>Weight, lb</u>
Electrodynamic driver	3.50
Can assembly and flange	1.94
Driver bellows, end plates, and coil	0.28
Follower piston and diaphragm	0.31
Fill valve and flange	0.21
Pressure transducer (dynamic)	0.11
Pressure transducer (static)	0.10
Miscellaneous	<u>0.30</u>
	6.75
<u>Installation in Zero-Gravity Can</u>	
Tube and supports	1.0
Bladder	<u>0.3</u>
	1.3
<u>Data Processor</u>	
Control system	0.7
Display electronics	<u>0.6</u>
	1.3
Total Weight/ Tank	<u>9.35 lb</u>

3.5.2 System Power Requirements

The primary power requirements for the RIGS system are for the electrodynamic driver and the power amplifier. The driver requires 3.4 watts of power. Based on typical efficiencies for power amplifiers, the total system power requirement including the data processor and control system is 7 watts/tank.

3.5.3 System Performance

Detailed analyses of the system performance characteristics are given in Section 4. The following is a summary of the results:

System accuracy: Empty tank: ± 0.85 percent of full tank mass.
25 percent full tank: ± 1.25 percent of full tank mass.
97 percent full tank: ± 0.85 percent of full tank mass.

System response: Continuous tracking.
System time constant 5 to 10 seconds.

Operational periods: Inactive during boost and SPS engine firing.
Immediately after firing, error can be as high as 8 percent, depending on the duty cycle.
Recovers to specified accuracy within 5-30 minutes.

4. SYSTEM ANALYSIS

4.1 ANALYSIS OF ERROR SOURCES

The system discussed in the preceding sections was somewhat idealized. It was assumed, for example, that the measured gas spring rate was simply $\left(\frac{\gamma P A^2}{V}\right)$, which neglects the wave characteristics of the infrasonic system and assumes that lumped parameters may be used to approximate it. It was also assumed that the ullage volume was one continuous gas space, that the ratio of specific heats, γ , of the mixture of gases could be defined, and that the process was essentially adiabatic. In the following sections, the accuracy of these and other assumptions will be examined in detail.

4.1.1 Wave Transmission Effects

4.1.1.1 Wave Transmission Through the Gas

The pressure wave generated by the follower piston moves at sonic velocity and takes a finite time to traverse the ullage gas space. The lumped parameter representation of the system (Section 2) assumes that the entire ullage space responds at one time. An appreciable error can therefore be generated if the transit time of the wave is not negligible compared to the period of the pressure wave.

The maximum effective error from this source may be calculated by use of transmission line theory. For a wave traveling through a gas, the acoustical impedance to flow is:

$$Z = -j Z_o \cot \left(\frac{2 \pi \ell}{\lambda} \right) \quad (4.1)$$

where:

Z = acoustical impedance

Z_o = characteristic impedance of line = $\frac{\rho c_a}{A}$

ρ = gas density

c_a = acoustic velocity

ℓ = line length

A = area through which wave travels

$$\lambda = \text{wave length} = \frac{2\pi c_a}{\omega}$$

$$\omega = \text{angular velocity}$$

The pressure seen at the driver will be the product of the impedance and the volume flow ($j\omega\Delta V$):

$$\Delta P = j\omega\Delta V Z = \frac{\omega \rho c_a \Delta V}{A} \cot \left(\frac{\omega l}{c_a} \right) \quad (4.2)$$

When ω is small (i.e., low frequency),

$$\cot \frac{\omega l}{c_a} \cong \frac{c_a}{\omega l} \quad \text{and} \quad \Delta P' = \frac{\rho c_a^2 \Delta V}{A l}$$

Substituting for the acoustic velocity:

$$c_a = \sqrt{\frac{P_o \gamma}{\rho}}$$

where P_o is the system static pressure and γ is the ratio of the specific heats, then

$$\frac{\Delta P'}{P} = \gamma \frac{\Delta V}{V}$$

where V is the volume $A l$.

This is the adiabatic gas law assumed in Section 2. For other than low frequencies, the error is the difference between the $\Delta P'$'s calculated by Equations (2.1) and (4.2):

$$\epsilon \equiv \frac{\Delta P - \Delta P'}{\Delta P'} = \frac{\Delta P}{\Delta P'} - 1 \quad (4.3)$$

Expanding the expression for the cotangent in Equation (4.2) and taking only the first two terms:

$$\Delta P = \frac{\omega \rho c_a \Delta V}{A} \cot \left(\frac{\omega l}{c_a} \right) = \frac{\omega \rho c_a \Delta V}{A} \left[\frac{c_a}{\omega l} - \frac{\omega l}{3 c_a} \dots \dots \right]$$

$$\frac{\Delta P}{\Delta P'} = 1 - \frac{\omega^2 l^2}{3 c_a^2} = 1 - \frac{\omega^2 l^2 \rho}{3 P_o \gamma} \quad (4.4)$$

$$\epsilon = - \frac{\omega^2 l^2 \rho}{3 P_o \gamma}$$

For the frequency range of 0.5 to 3 cps and a 12-foot-long tank filled with gas, this error is appreciably less than 0.1 percent. This condition may be corrected for if the gas configuration is known, but since the ullage gas location will not be known during periods of zero gravity, the error can be made as small as desired by selection of a sufficiently low driver frequency.

4.1.1.2 Wave Transmission Through the Liquid

The RIGS system is designed to operate primarily during extended periods of zero gravity. Under these conditions, the ullage volume may consist of discontinuous gas pockets separated by liquid. In order for the system to operate accurately, the pressure signal from the piston must be transmitted through the liquid to submerged pockets as shown in Figure 4-1. In addition, the prior discussion presumed that the follower piston was located in the ullage gas and transmitted the pressure wave directly to the submerged gas. However, in zero gravity, some of the liquid could be directly on the piston. Under these conditions, the liquid in contact with the piston would have to be accelerated and would act as if it were part of the piston mass. In order to prevent this, it is necessary to provide a gas cavity between the follower piston and the actual tank enclosure as shown in Figure 4-2.

The enclosure consists of a pliable diaphragm containing gas and possessing surface area roughly equivalent to the cross-sectional area of the tank. It serves to transform the long stroke/small area motion of the driven piston to a small stroke/large area motion, which is more effective in transmitting the pressure wave through the liquid. It acts in a manner similar to an output transformer on an amplifier, matching the impedance of both the driver and the liquid/ullage combination. However, in order to effectively communicate with the submerged gas pocket, it is still necessary to accelerate any propellant mass located between the pliable diaphragm and the ullage gas. This results in a reduction in the

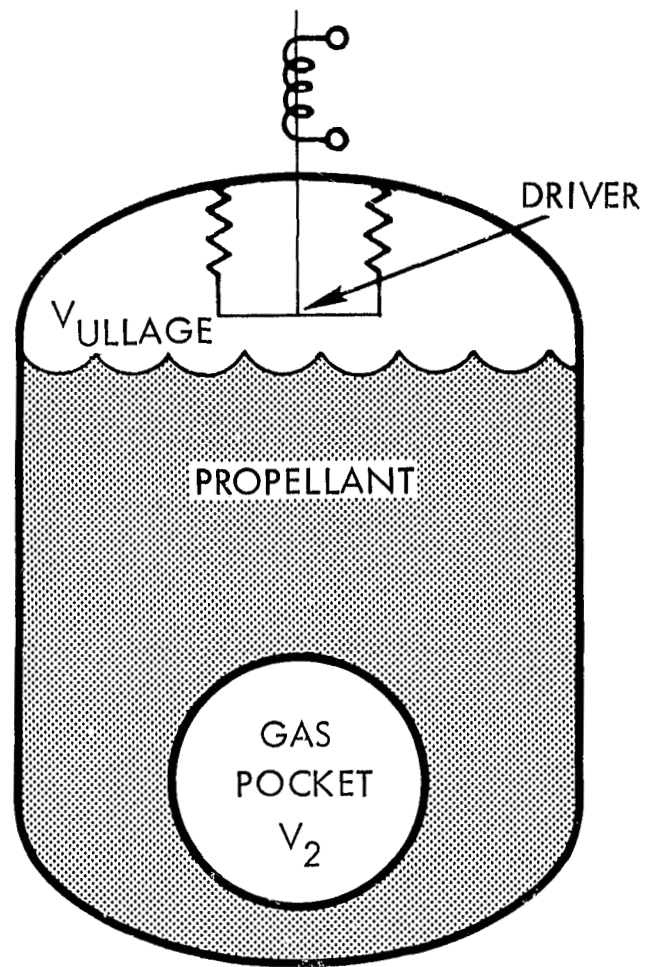


Figure 4-1. Submerged Gas Pocket

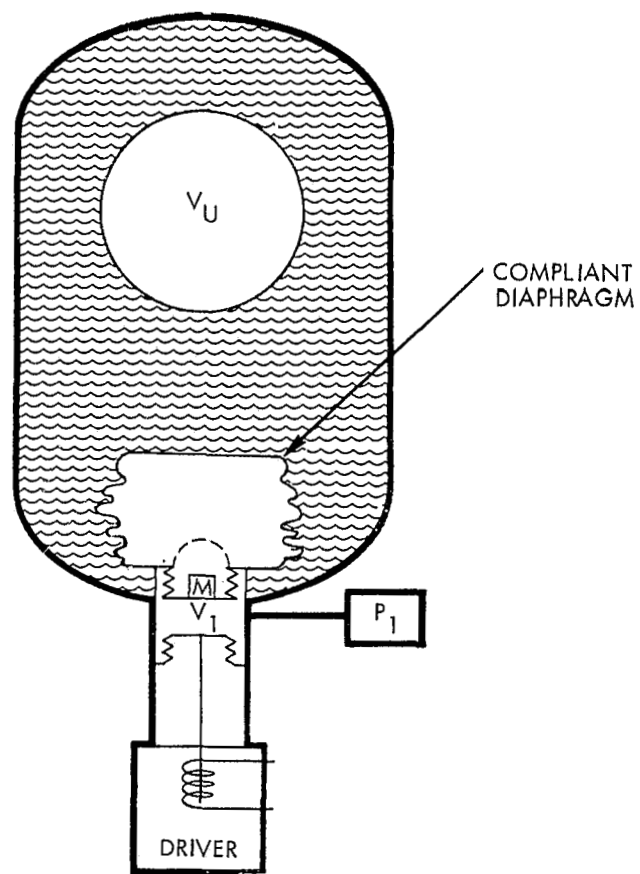


Figure 4-2. Transmission Through Liquid by a Compliant Diaphragm

measured gas spring rate. The effective spring rate of the submerged gas pocket is given by (see Section 3.1 of Volume 1 for the derivation):

$$K_g' = K_g \left(1 - \frac{\omega_r^2 \rho_\ell \ell_\ell V_u}{\gamma A P} \right) \quad (4.4)$$

and

$$\epsilon' = 1 - \frac{K_g'}{K_g} = \frac{\omega_r^2 \rho_\ell \ell_\ell V_u}{\gamma A P} \quad (4.5)$$

where:

K_g' = apparent spring rate

K_g = true gas spring rate

ω_r = angular velocity at resonance = $2\pi f_r$

ρ_ℓ = liquid density

ℓ_ℓ = liquid length

V_u = gas ullage volume

V_{MT} = empty tank volume

f_{MT} = resonant frequency at V_{MT}

A = area of diaphragm

ϵ' = fractional error in ullage volume

The resonant frequency f_r is related to the resonant frequency of the empty tank f_{MT} by the relation:

$$\left(\frac{f_r}{f_{MT}} \right)^2 = \frac{V_{MT}}{V_u} \quad (4.6)$$

Substituting this relationship into Equation (4.5) leads to

$$\epsilon' = \frac{4 \pi^2 f_{MT}^2 \rho_\ell \ell_\ell V_{MT}}{\gamma A P} \quad (4.7)$$

The length of the liquid path between the diaphragm and the submerged volume is a function of the liquid volume. In this analysis it was

assumed that a sphere of liquid completely surrounds the diaphragm and that the liquid length is the radius of the sphere. Thus,

$$\ell_{\ell} \cong \left[\frac{3}{4\pi} (V_{MT} - V_u) \right]^{1/3}$$

Substituting this approximation into Equation (4.7) leads to:

$$\epsilon'_{\max} = \frac{4\pi^2 \left[\frac{3}{4\pi} (V_{MT} - V_u) \right]^{1/3} \rho_{\ell} V_{MT} f_{MT}^2}{\gamma AP} \quad (4.8)$$

The error ϵ' is the fractional error based on the ullage volume.

Expressing the error in terms of the fraction-of-full tank volume and letting

$$y = \frac{V_u}{V_{MT}},$$

$$\epsilon_{\max} = y \epsilon'_{\max} = \frac{4\pi^2 \rho_{\ell} V_{MT}^{4/3} \left[\frac{3}{4\pi} (1 - y) \right]^{1/3} y f_{MT}^2}{\gamma AP}. \quad (4.9)$$

In Figure 4-3, the maximum error from this source is plotted for the Apollo SPS oxidizer tank for a number of tank-empty resonant frequencies. As may be seen, to keep the error from this source to less than ± 1 percent at all times, the tank-empty resonant frequency must be less than 0.5 cps. This conclusion leads to the selection of a tank-empty frequency of 0.5 cps.

4.1.1.3 Wave Transmission in Piping

As mentioned in Section 3.3, the pipe which transmits the signal from the follower piston to the pliable diaphragm can cause some error. The primary error source is that associated with the acceleration of the mass of the gas column within the pipe. The error from this source is, as shown above for the liquid:

$$\epsilon' = 1 - \frac{K_g'}{K_g} = \frac{\omega_r^2 \rho_g \ell_g V_u}{\gamma AP} \quad (4.10)$$

where, as above, ϵ' is the fractional error in the measured gas volume, and the subscript g refers to ullage gas. Thus,

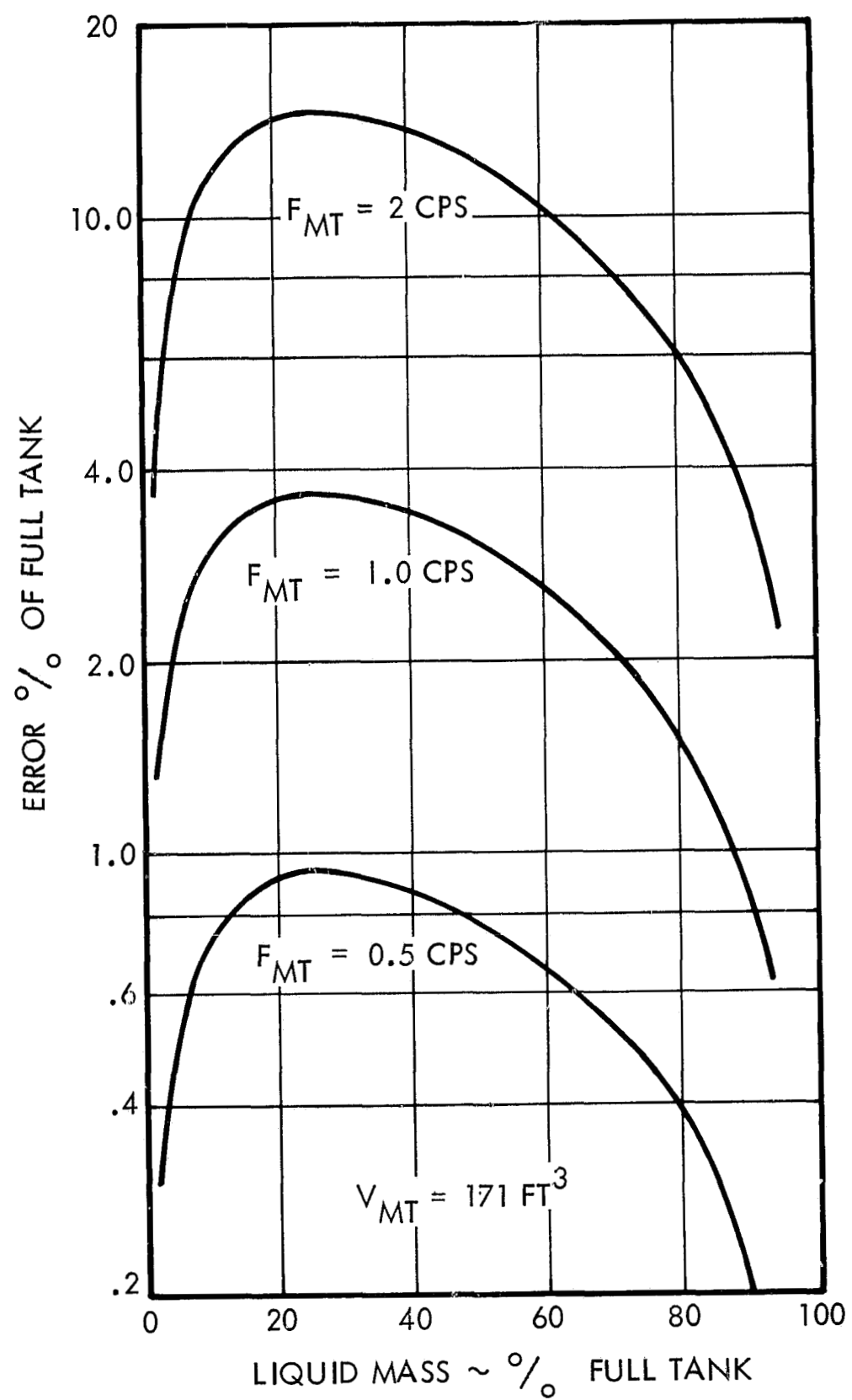


Figure 4-3. Error Due to Signal Transmission Through Liquid as a Function of Empty Tank Frequency

$$\epsilon = y \epsilon' = \frac{\omega_r^2 \rho_g \ell_g V_u^2}{\gamma A P V_{MT}} \quad (4.11)$$

where ϵ is the error in fraction-of-full tank volume. Since

$$\omega_r^2 = \omega_{MT}^2 \frac{V_{MT}}{V_u}$$

and

$$\frac{P}{\rho_g} = RT$$

then

$$\epsilon = \frac{\omega_{MT}^2 \ell_g V_{MT}}{\gamma A R T} y \quad (4.12)$$

Substituting in the values for the SPS tankage

$$f_{MT} = 0.5 \text{ cps}$$

$$V_{MT} = 150 \text{ ft}^3$$

$$\ell_g = 51 \text{ inches}$$

$$D = 4 \text{ inches}$$

one obtains

$$\epsilon = 0.0061 \frac{V_u}{V_{MT}}$$

The error is obviously greatest (0.6 percent) near the tank-empty condition and varies linearly with the ullage volume. As the quantity of this error is predictable, it can be corrected for in the data processor within ± 0.1 percent of full tank volume.

4.1.2 Variable Ullage Gas Properties

The assumption was made that the ratio of specific heats, γ , was accurately known. As the ullage gas is composed of a mixture of propellant vapor and helium in varying proportions, this is not always the case. In Figure 4-4 the variation of γ in the ullage gas is shown as a function of the partial pressure and temperature of N_2O_4 . Figure 4-5 shows a

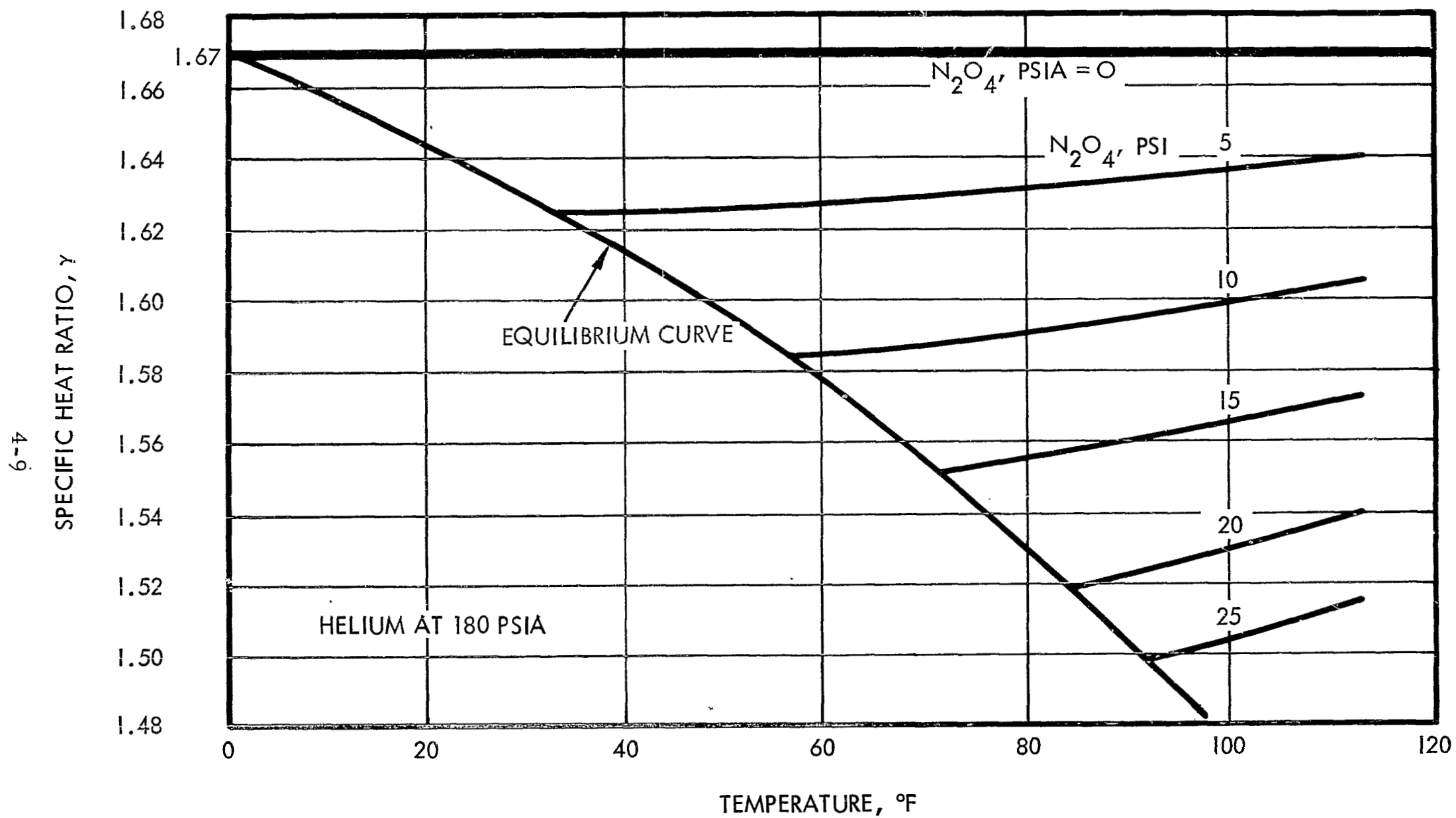


Figure 4-4. Variation of Gamma with N_2O_4 Concentration and Temperature

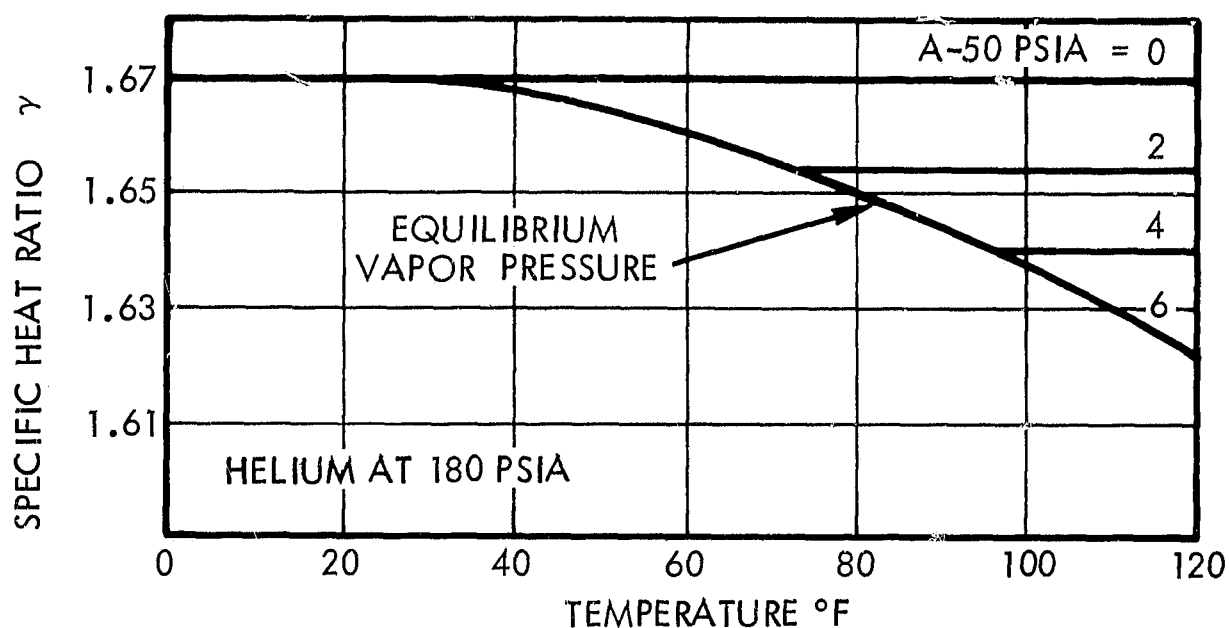


Figure 4-5. Variation of Gamma with Aerozene-50 Vapor Composition and Temperature

similar set of curves for Aerozene-50. The maximum propellant vapor concentration at any temperature will be the equilibrium vapor pressure as higher concentrations will result in condensation. However, during and immediately after engine firings, the propellant vapor will be diluted by the influx of pure helium pressurant gas. After the transient, the vapor concentration will slowly build back up until equilibrium is approached.

As the ullage volume measurement is directly proportional to the ratio of specific heats, γ , any error in the γ will cause a proportional error in the ullage volume. Thus, the measured volume may be appreciably in error during and immediately after a lengthy firing. As shown in Sections 2.1 and 4.1 of Volume 1, the departure from equilibrium becomes quite small within 20 minutes after a disturbance, using very conservative assumptions. Actual equilibrium restoration times should be considerably shorter. In addition, the maximum error experienced during the transient is dependent on the amount of helium introduced and thus upon the actual duty cycle.

4.1.3 Heat Transfer to the Ullage Gas

It was also assumed that the expansion and compression of the ullage gas occurred adiabatically. The assumption is not completely valid as heat is transferred at the gas/liquid and gas/wall interfaces. This transfer of heat reduces the effective (or detected) value of γ in the ullage gas and can result in errors. A simplified analysis of this problem indicates that the heat transfer affected zone extends a maximum of 1 inch from an interface for the selected frequencies, and that the quantity of heat transferred would lead to an error of about 5 percent in γ within this 1-inch zone. In Figure 4-6, the maximum error from this source is plotted as a function of liquid volume, assuming the ullage gas is spherically shaped. While the maximum error from this source is only 0.35 percent at the tank-empty condition, it should be noted that a large increase in the surface area of the gas/liquid interface could result in appreciable errors. Fortunately, such conditions are improbable under zero gravity.

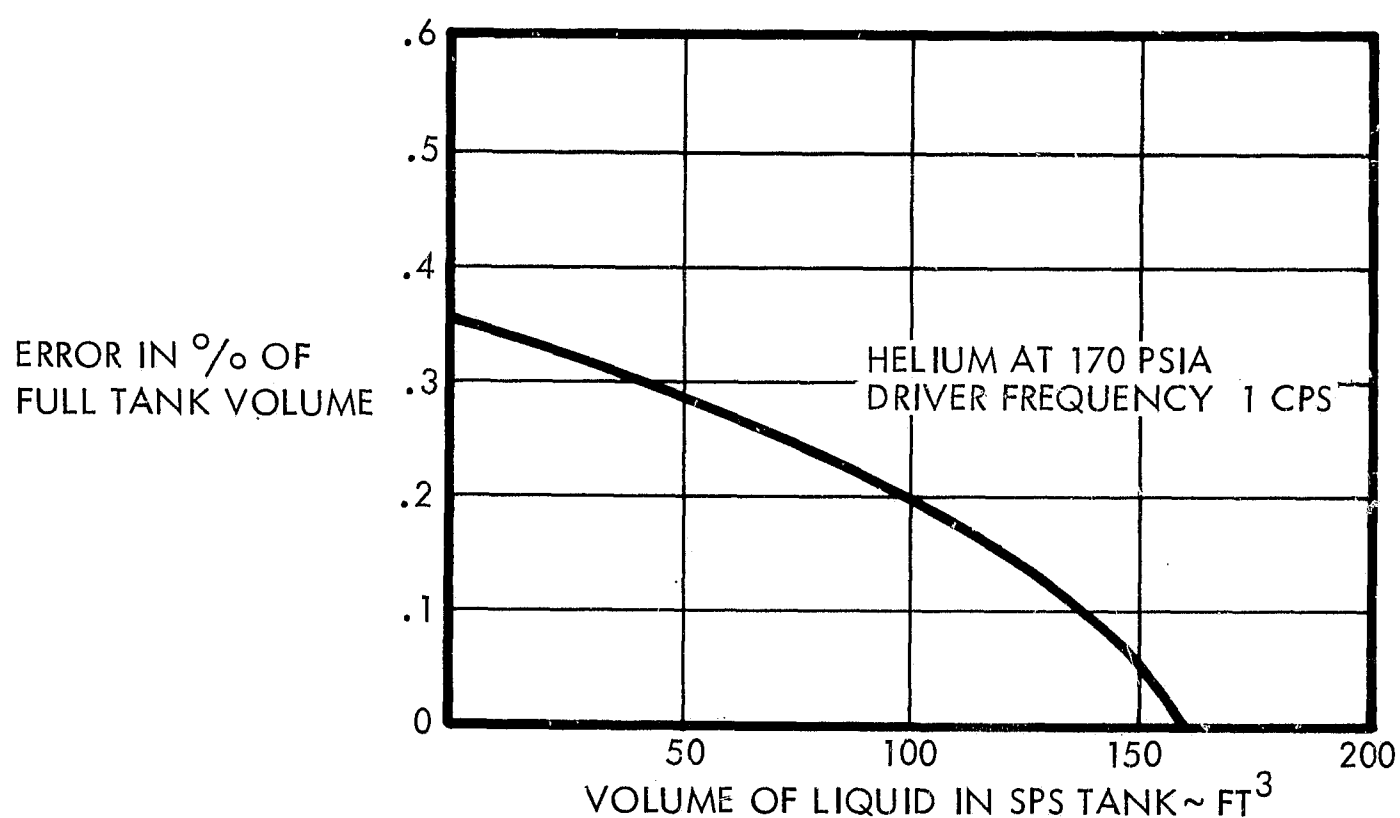


Figure 4-6. Error Caused by Heat Transfer to the Ullage Gas

4.1.4 Acoustically Isolated Regions

Certain regions of a propellant tank may be acoustically isolated from the RIGS system, and the system is not capable of detecting propellants in these locations. Within the SPS tanks, as shown in Figure 3-2, the volume in the zero-gravity can and in the PUGS standpipe are such acoustically isolated regions. As the zero-gravity can is designed to remain full, this propellant quantity is simply added to the gauged quantity without introducing any error. This is similar to the present practice on the PUGS system.

The PUGS standpipe, on the other hand, does not remain full. During and immediately after each firing the propellant in the standpipe is proportional to the height of liquid in the tank. If the same quantity of propellant remained thereafter in the standpipe, this could be corrected for by increasing the gauged quantity by the fixed percentage of 1.21, which is the ratio of the cross-sectional area of the standpipe to that of the tank.

However, the liquid quantity in the standpipe may change during extended periods of zero gravity. The same effects that cause the standpipe volume to be acoustically isolated, namely surface tension and relatively small openings, will tend to keep the liquid trapped in the standpipe and prevent additional liquid from entering. The liquid will pass through the holes only under the influence of an appreciable pressure differential. The maximum change in the liquid quantity will be proportional to the maximum possible change in the pressure level. If this variation is conservatively assumed to be ± 10 percent, the error from this source is limited to ± 0.12 percent of the full tank volume.

4.2 ERROR ANALYSIS OF THE RIGS SYSTEM

A linear analysis of the RIGS system was carried out by assuming that each error source was completely independent. Two major types of error source were considered; system errors which relate to basic uncertainties in the physical quantities being measured, and measurement errors which are a function of the precision with which a particular measurement can be made. The magnitude of the system errors was assessed by analysis of the system behavior under extreme conditions, which were assumed to represent the 3σ variation in each parameter. The magnitude of the measurement errors was established by determining the accuracy limitations of comparable equipment.

4.2.1 System Error Sources

Most of the system error sources have been discussed in Section 4.1. The errors were evaluated assuming that the measurements were made at least 30 minutes after the SPS engine has fired. Additional system error sources are: the uncertainty in the empty tank volume (± 0.35 percent), and the uncertainty in the true propellant specific gravity (± 0.2 percent).

The contributions of the individual system error sources are shown in Figure 4-7 as a function of tank volume. The total system error was obtained by root sum squaring of the component errors. As can be seen in Figure 4-7, the maximum error of 1.1 percent occurs at 25 percent tank-full condition and the major system error source is caused by the uncertainty in transmission time of the pressure signal through the liquid.

4.2.2 Measurement and Data Processing Errors

Errors contributed by the measuring devices, the control system, and the mechanics of the data processor were evaluated (see Table 4-1). The basic equation for the data processor is given by

$$\Phi \equiv \frac{M}{M_{\text{full}}} = \frac{\rho}{\rho_r} \left[1 - \left(\frac{f_r}{f} \right)^2 \frac{\gamma}{\gamma_r} \frac{P}{P_r} \right] [1 + K(\Phi)] \quad (4.13)$$

where M is the propellant mass and the subscript r applies to a reference condition of the empty tank filled with helium gas at nominal pressure and temperature. The full mass (M_{full}) represents the equivalent mass if the tank were completely filled with liquid rather than with the loaded quantity. The function $K(\Phi)$ represents those functions (standpipe volume, piping error) for which corrections must be made as a linear function of the liquid volume.

The errors have been split into three categories:

- Offset errors, which cause a random but constant error at all times
- Rate errors, which cause a random error proportional to the signal

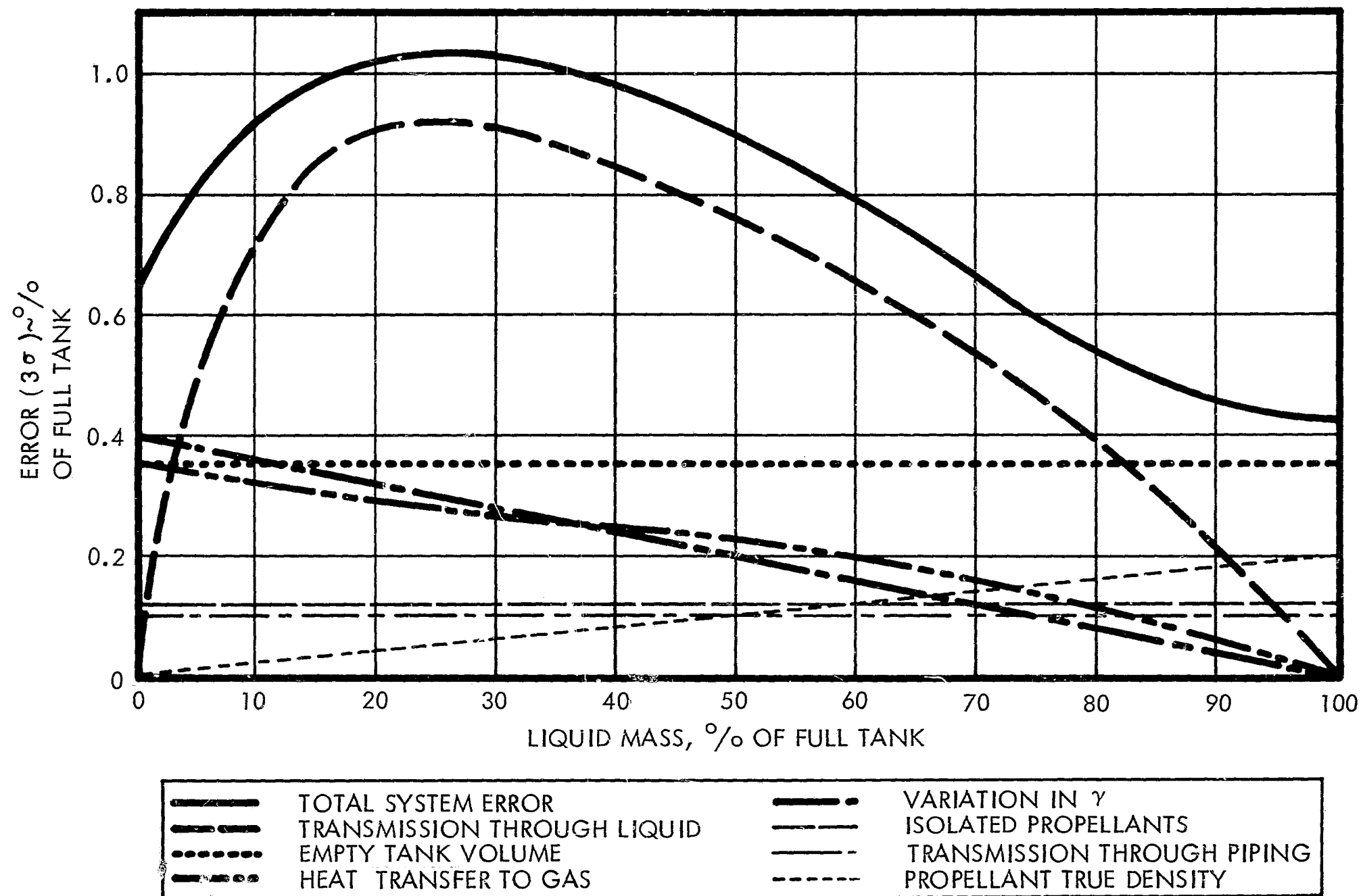


Figure 4-7. System Error Sources as a Function of Liquid Mass

- Noise errors, which cause a random error independent of the signal

Table 4-1. Measurement and Data Processing Errors (3σ)

	Offset % of full scale	Rate % of indicated	Noise % of full scale
Reference Voltage Drift	± 0.1	± 0.1	
Servo Dead Band	± 0.2		± 0.4
Temperature Compensation (density)		± 0.15	± 0.2
Temperature Compensation (gamma)		± 0.10	± 0.15
Uncertainty in K (Φ)	± 0.1	± 0.1	
Setting of Tank-Empty Frequency		± 0.2	
Pressure Correction	± 0.2	± 0.2	± 0.2
Total Error	± 0.31	± 0.36	± 0.51

These errors result in an overall measurement error for each tank of ± 0.61 percent of the full scale reading, plus ± 0.36 percent of the propellant remaining. These errors must be added to the system errors.

4.2.3 Total Error for RIGS System

The total (3σ) error for the RIGS system is shown in Figure 4-8. This error was obtained by root sum squaring of the component errors. The most significant source of error is again the uncertainty in signal transmission through the liquid.

4.3 CONTROL SYSTEM ANALYSIS

4.3.1 System Simulation

This section presents the results of a computer simulation and associated analyses performed to determine a suitable control system configuration for the RIGS application. The control system selected utilizes a multiplier/filter combination to lock in on the frequency at which the pressure signal is 90 degrees out of phase with the reference signal to the driver. The control system was described in Section 3.2 and, as described in Section 5, the principle of operation has been

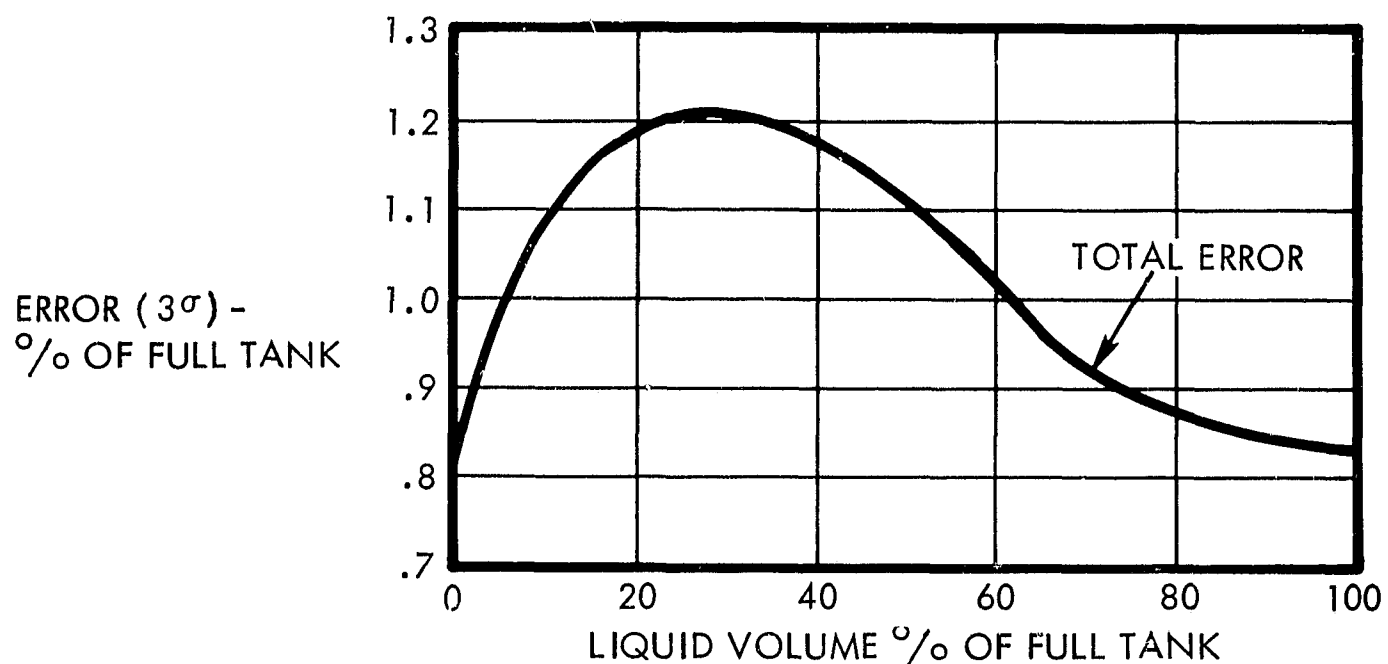


Figure 4-8. RIGS Error as a Function of Liquid Volume

successfully demonstrated by the complete closed loop operation of the feasibility demonstration hardware.

The selected control loop did not lend itself to linear analysis because of the nonlinearities introduced by the resonant nature of the input signal and by the multiplier circuit. It was therefore necessary to simulate the system to obtain the control system characteristics. The system simulation was performed on an analog computer.

The basic RIGS zero-gravity gauging system as implemented on the analog computer is shown in block diagram form in Figure 4-9. The corresponding implementation of the tank transfer function is shown in Figure 4-10. The results of a typical run, demonstrating the lock-on capability of the system, are shown in Figure 4-11. It can be seen that starting with an initial 25 percent offset in frequency, it takes approximately 7 seconds for the system to lock on to the correct frequency for either the full or empty tank condition. The time to lock on is primarily set by the 10-second integrating filter at the multiplier output.

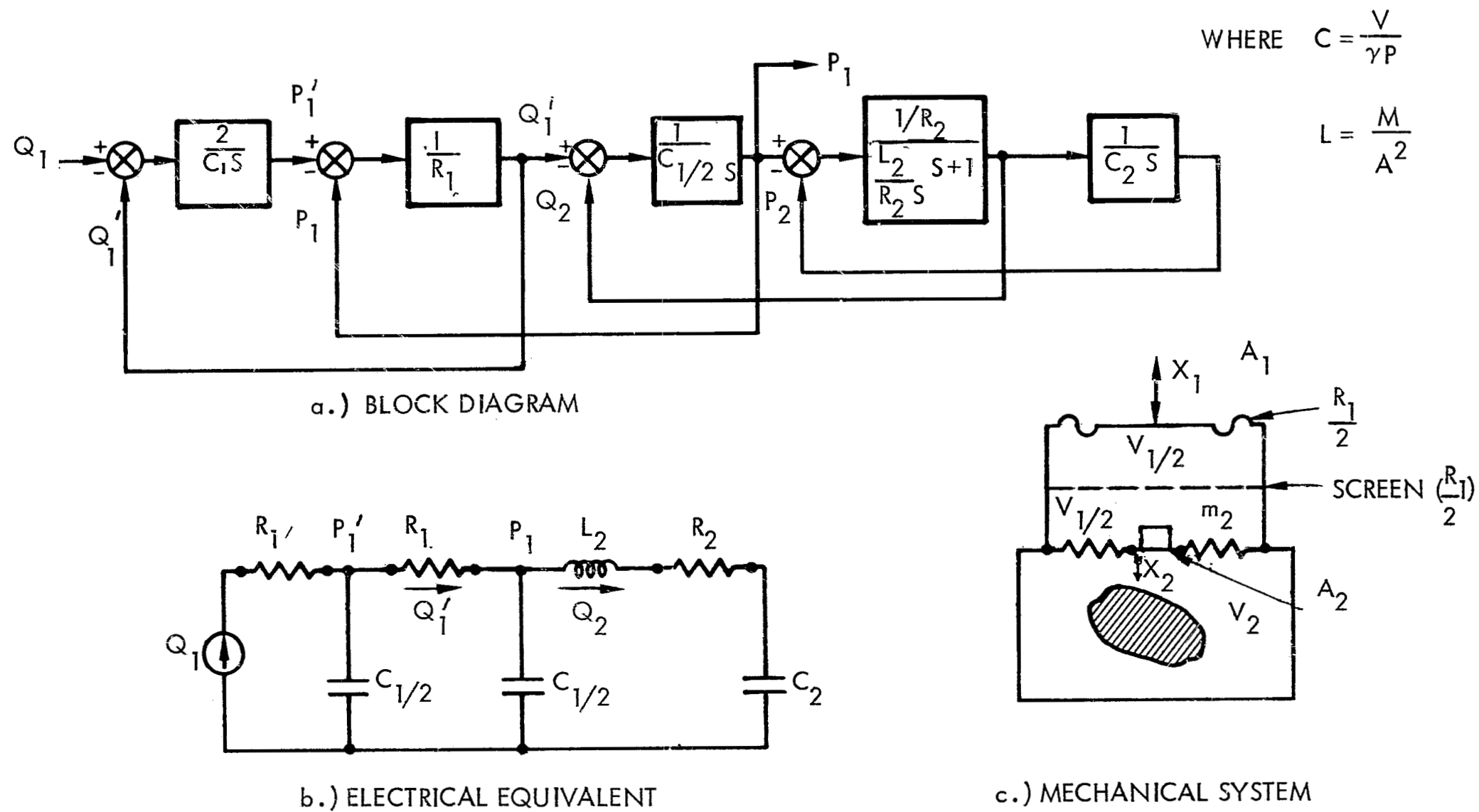


Figure 4-10. Block Diagram of Driver Cavity and Propellant Tank Transfer Function

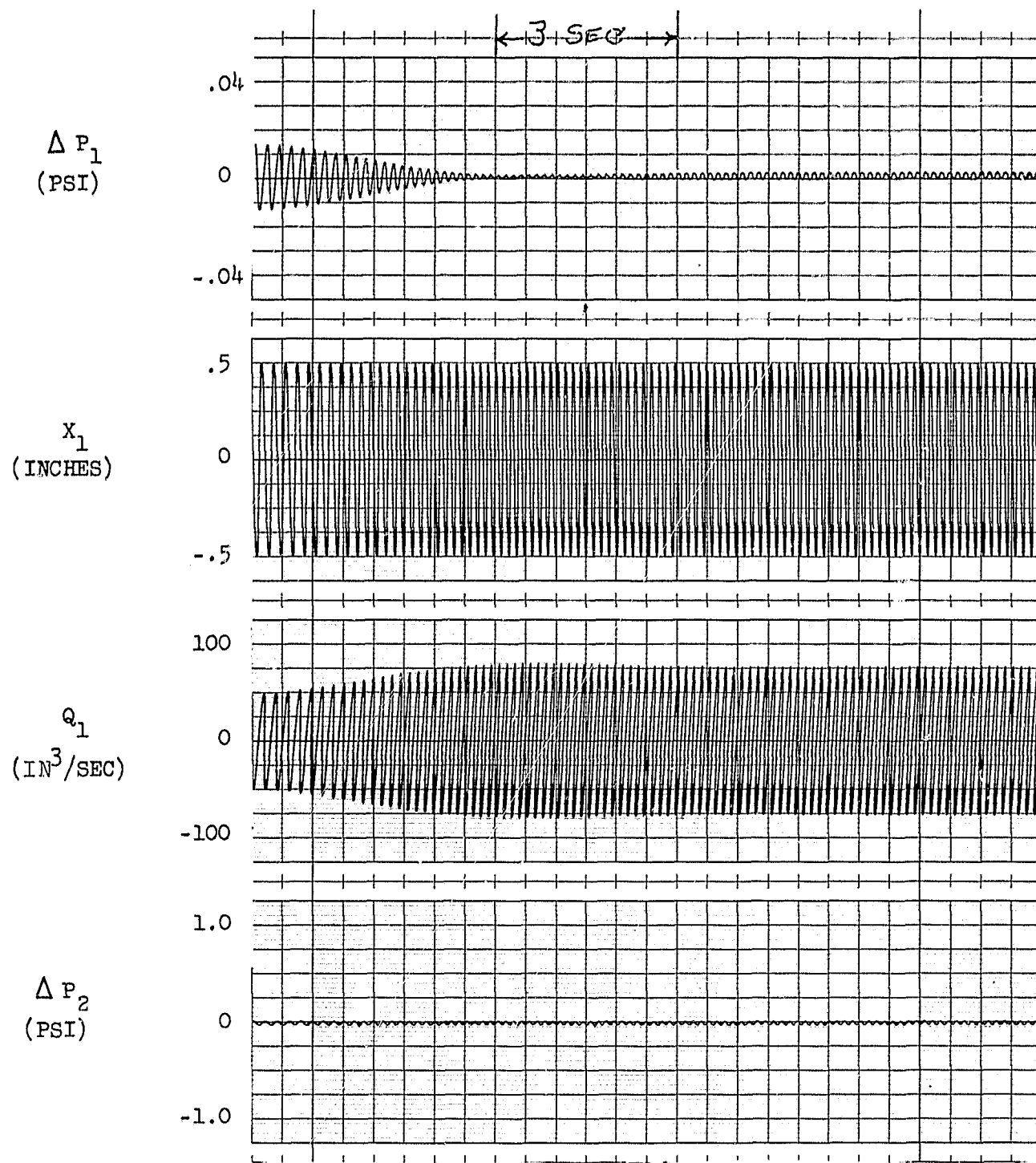


Figure 4-11a. Computer Traces of Zero-G Gauging System Response
(Ullage Volume = 13 ft³)

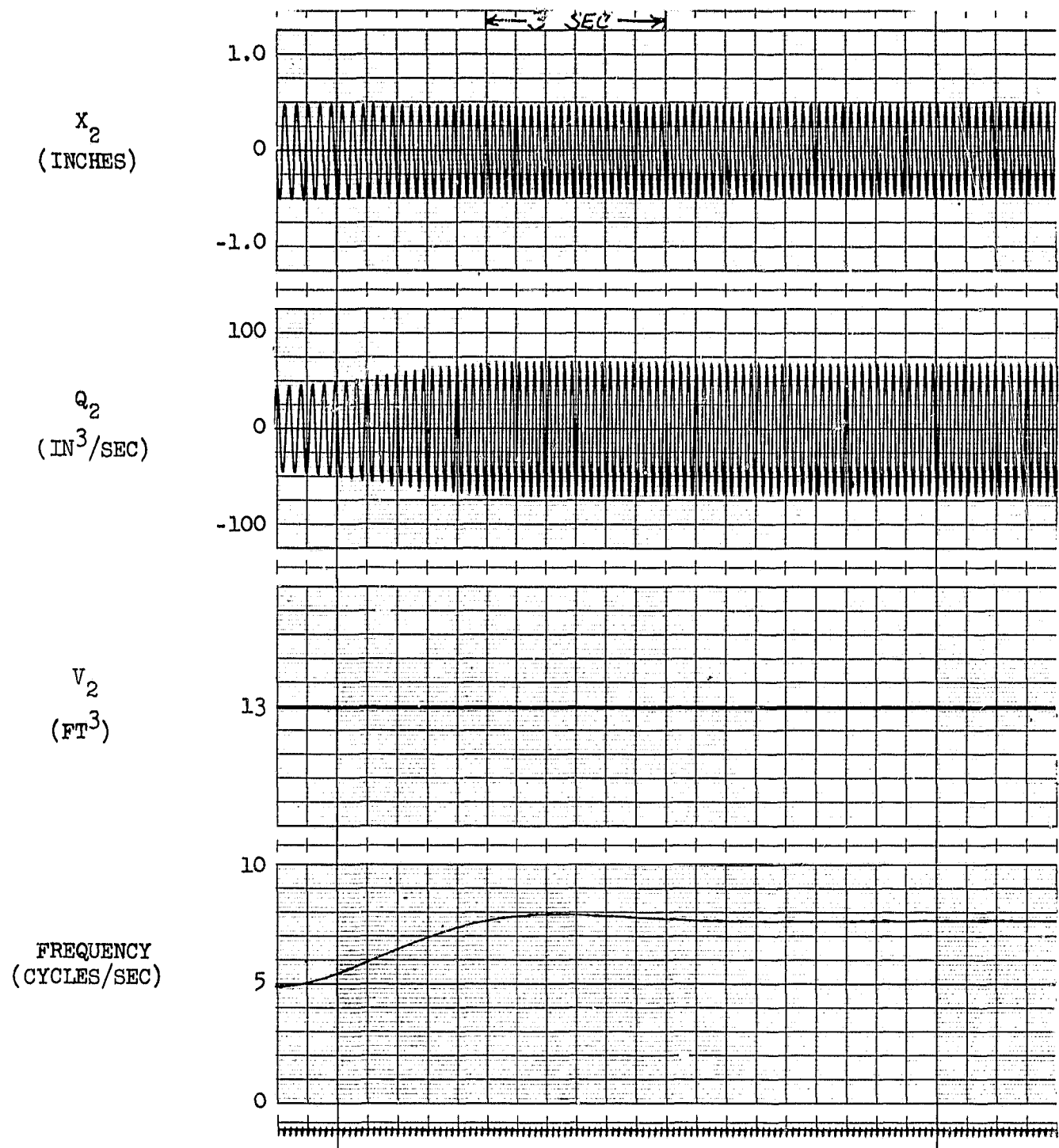


Figure 4-11b. Computer Traces of Zero-G Gauging System Response (Ullage Volume = 13 ft³)

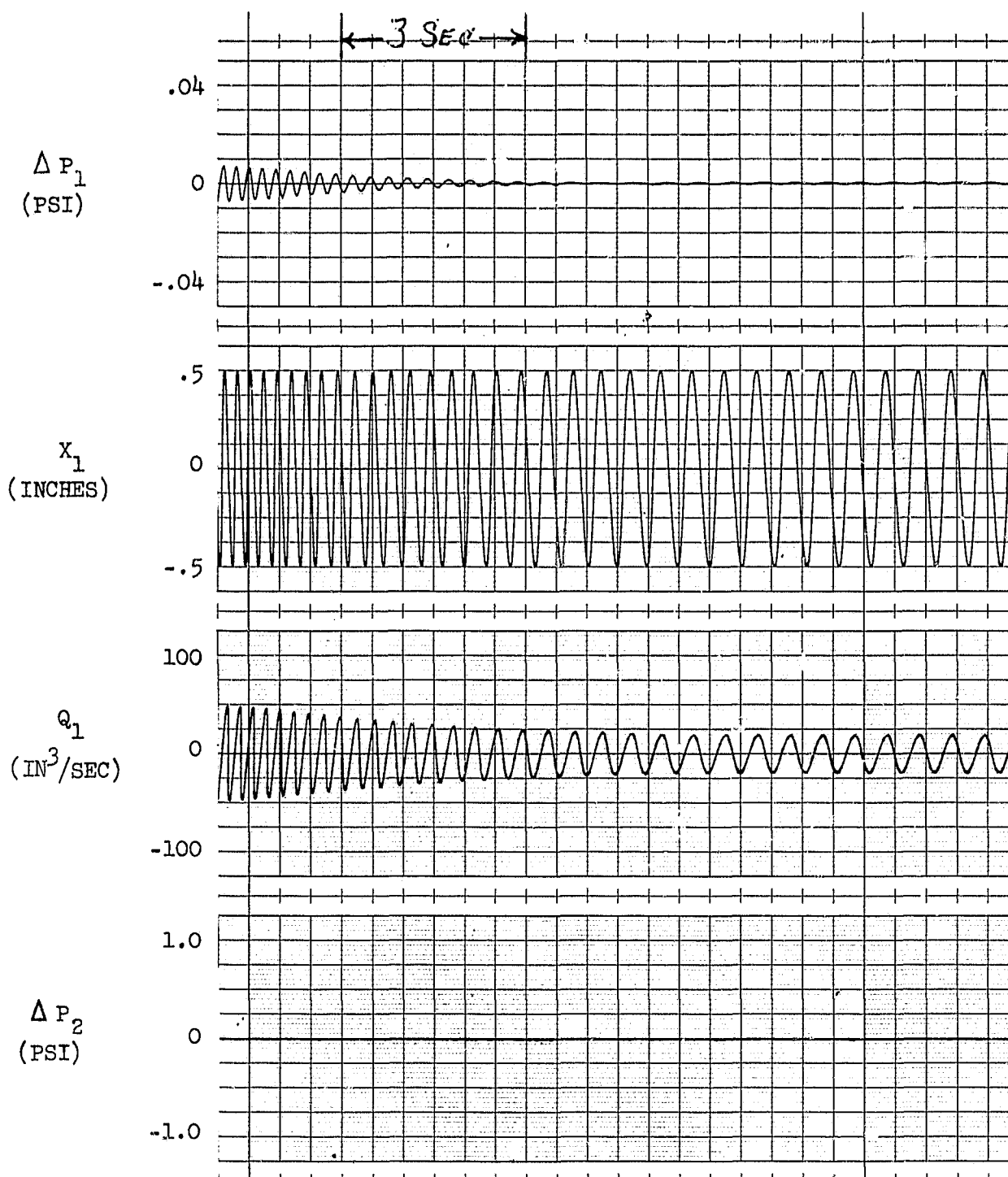


Figure 4-11c. Computer Traces of Zero-G Gauging System Response
(Ullage Volume = 179.4 ft³)

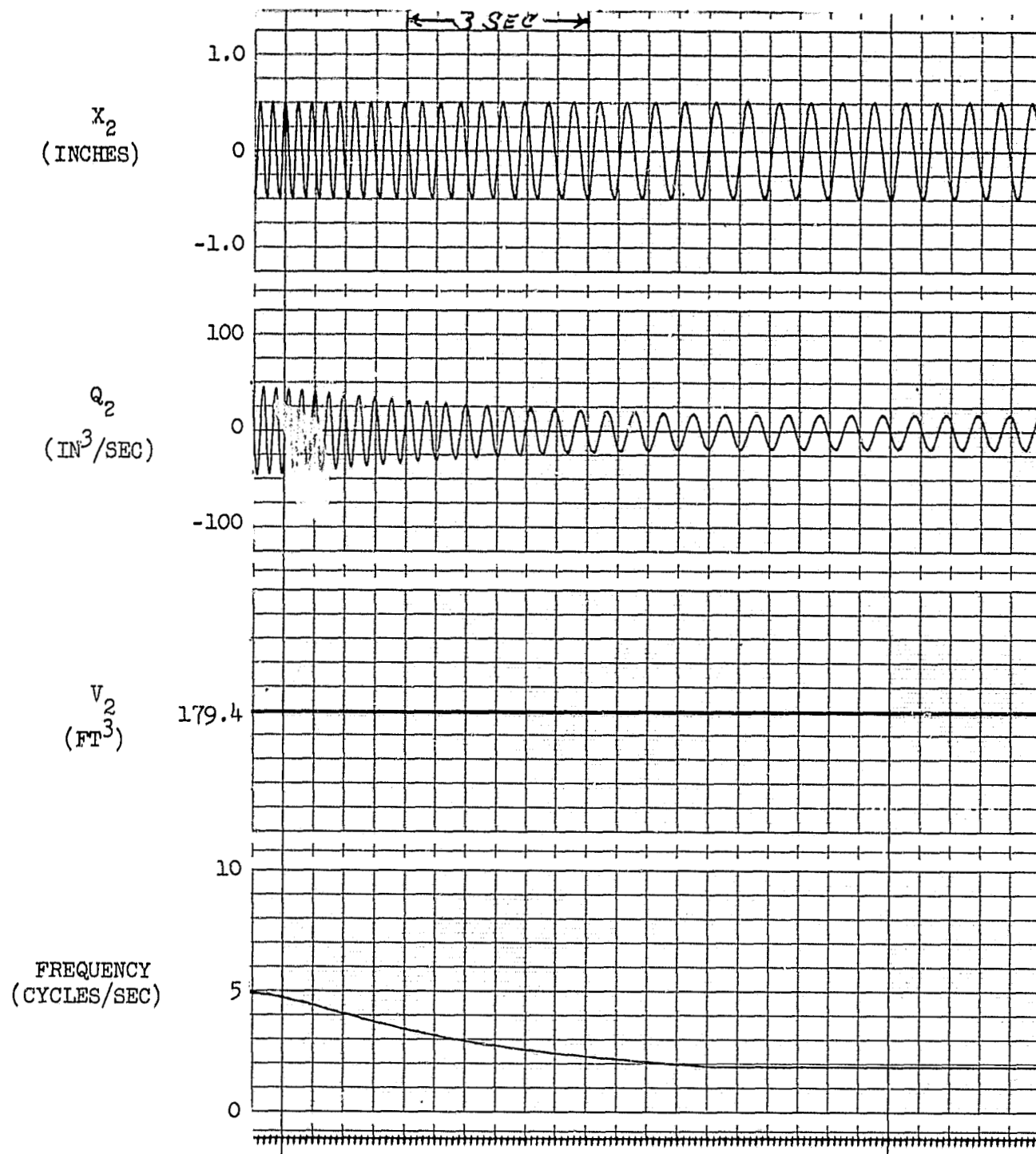


Figure 4-11d. Computer Traces of Zero-G Gauging System Response (Ullage Volume = 179.4 ft³)

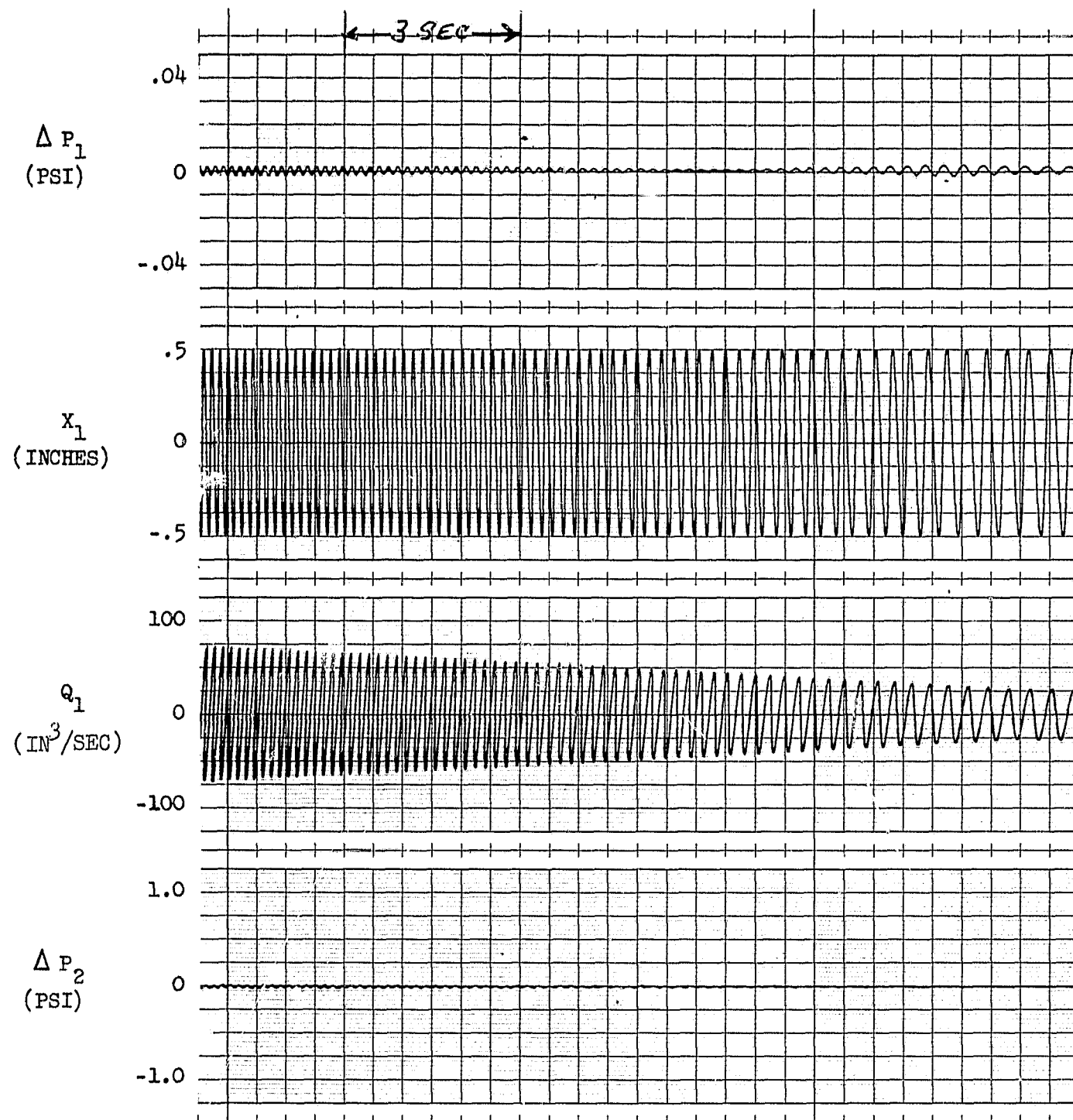


Figure 4-12a. Computer Traces of Zero-G Gauging System Response as Ullage Volume Varies

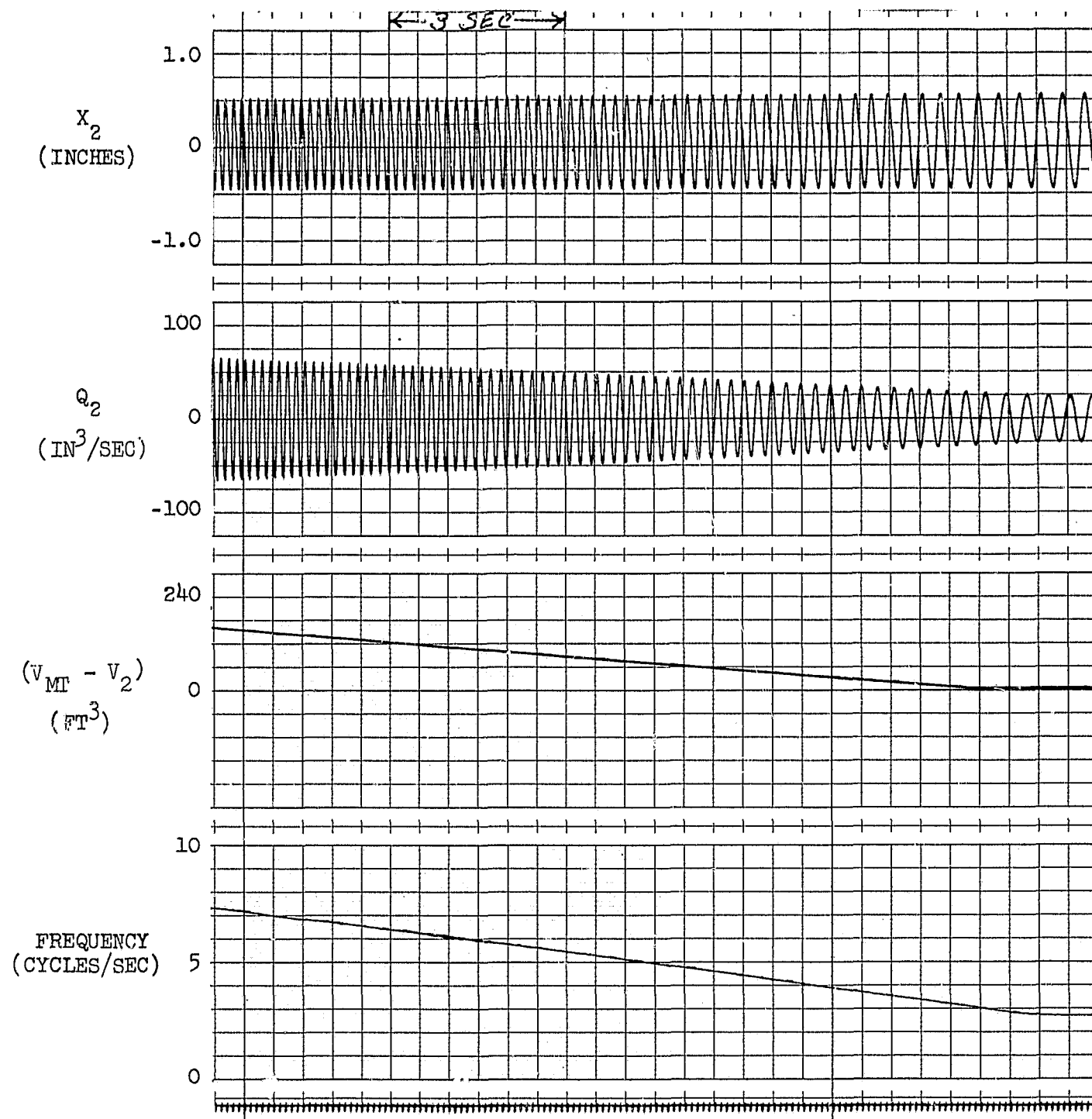


Figure 4-12b. Computer Traces of Zero-G Gauging System Response as Ullage Volume Varies

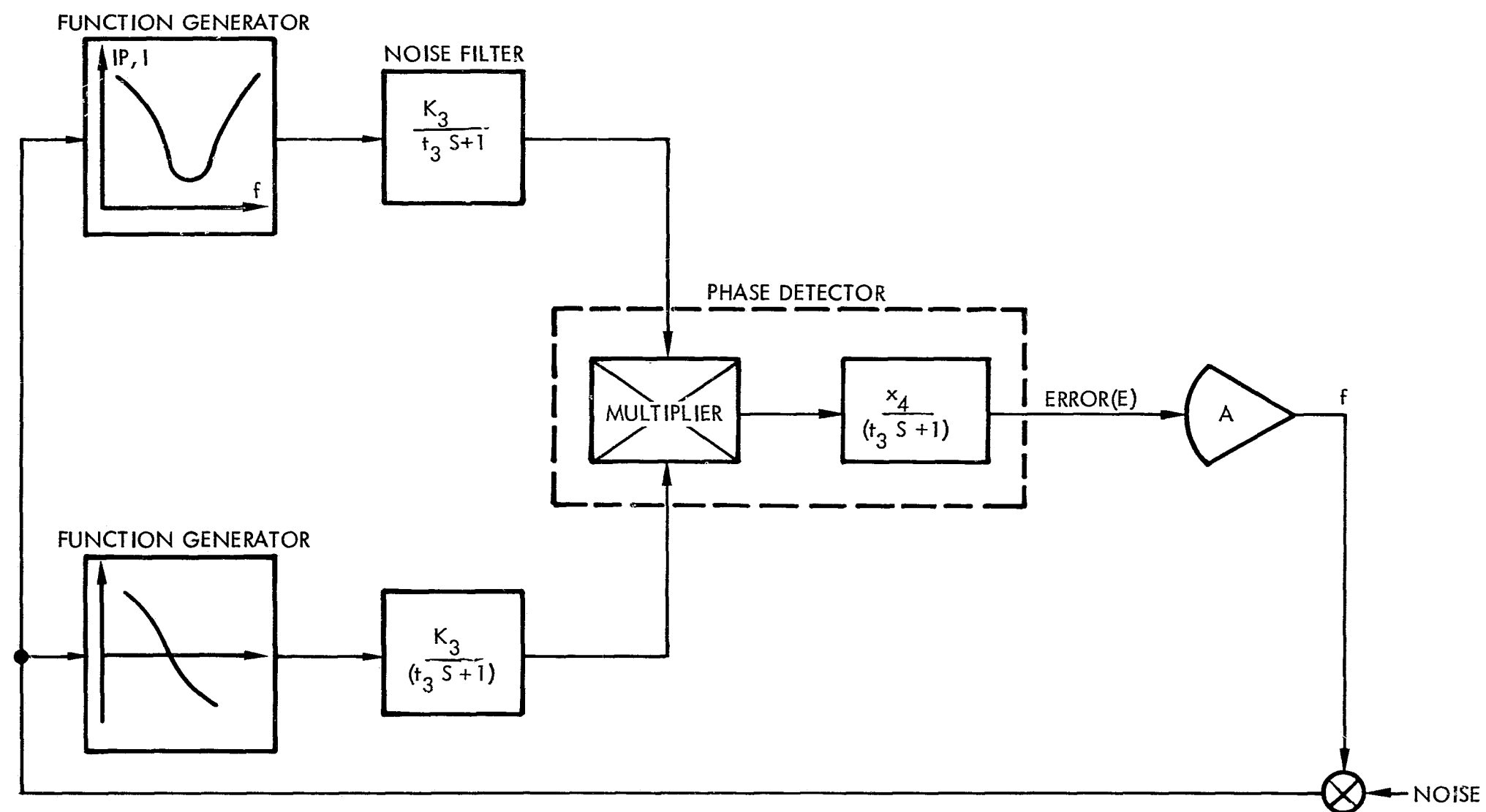


Figure 4-13. Block Diagram Based on DC Signal Implementation

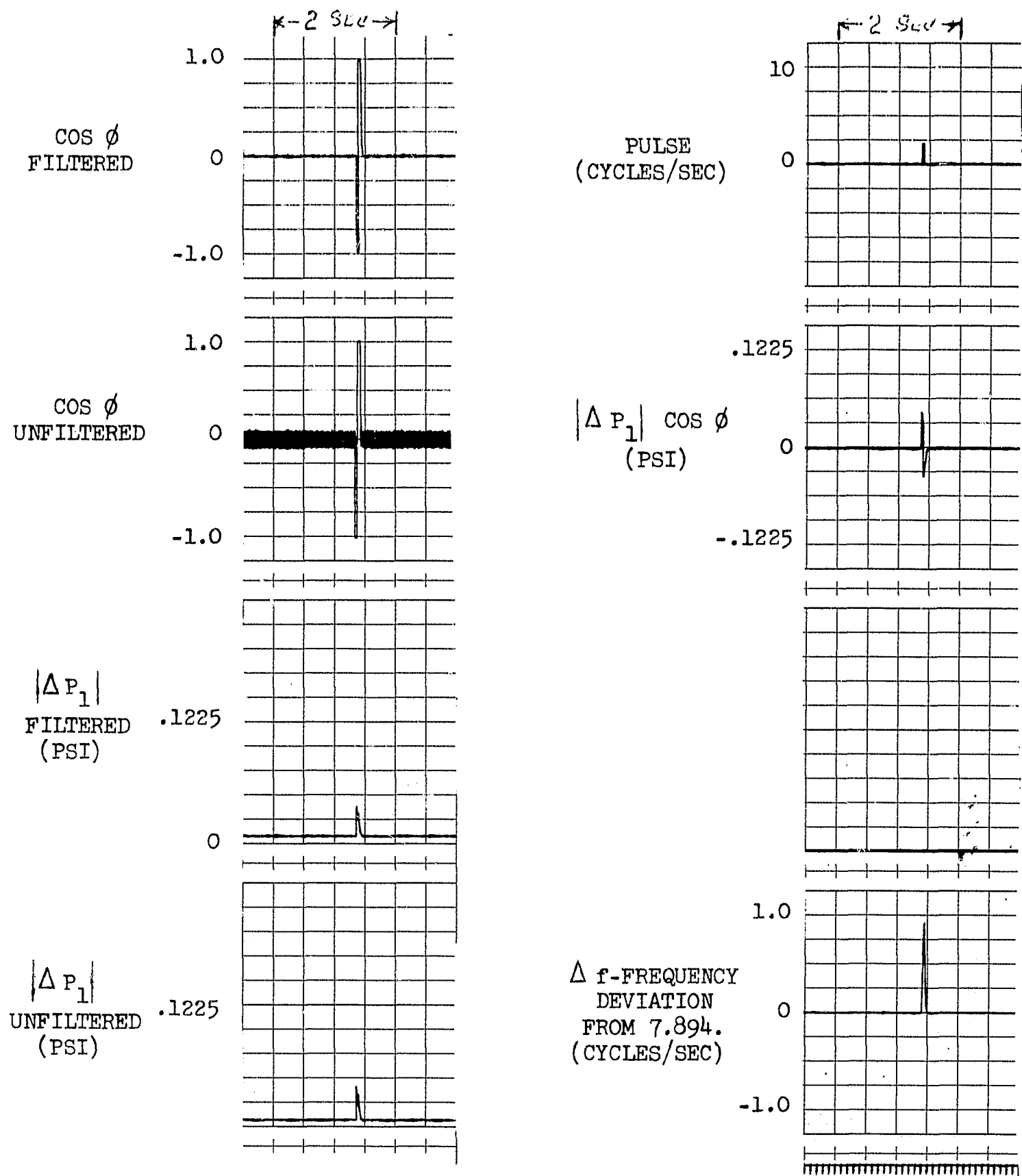


Figure 4-14a. Computer Traces for Zero-G Gauging System Response to a 30 msec Pulse (Ullage Volume = 13 ft³)

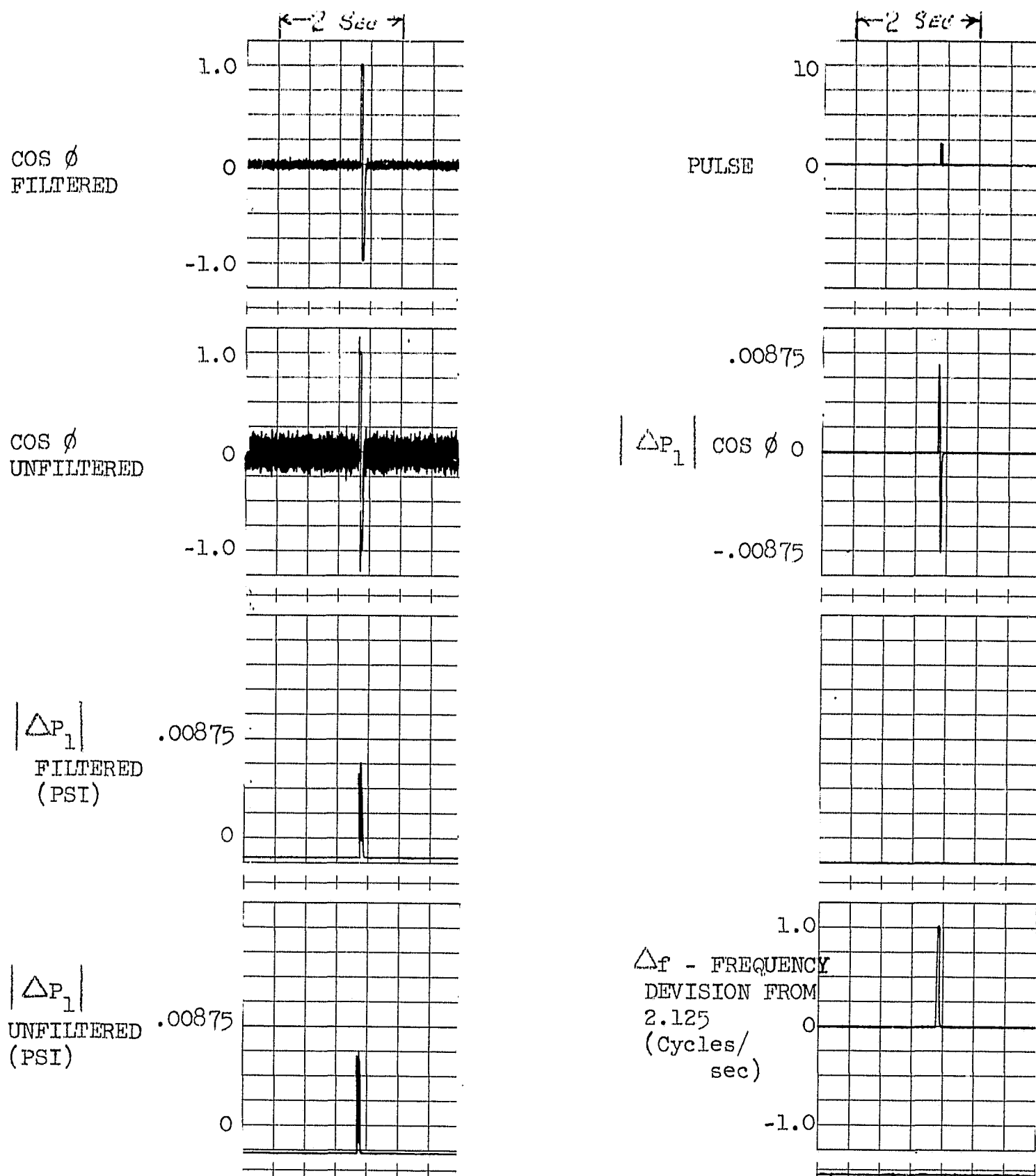


Figure 4-14b. Computer Traces of Zero-G Gauging System Response to a 30 msec Pulse (Ullage Volume = 179.4 ft³)

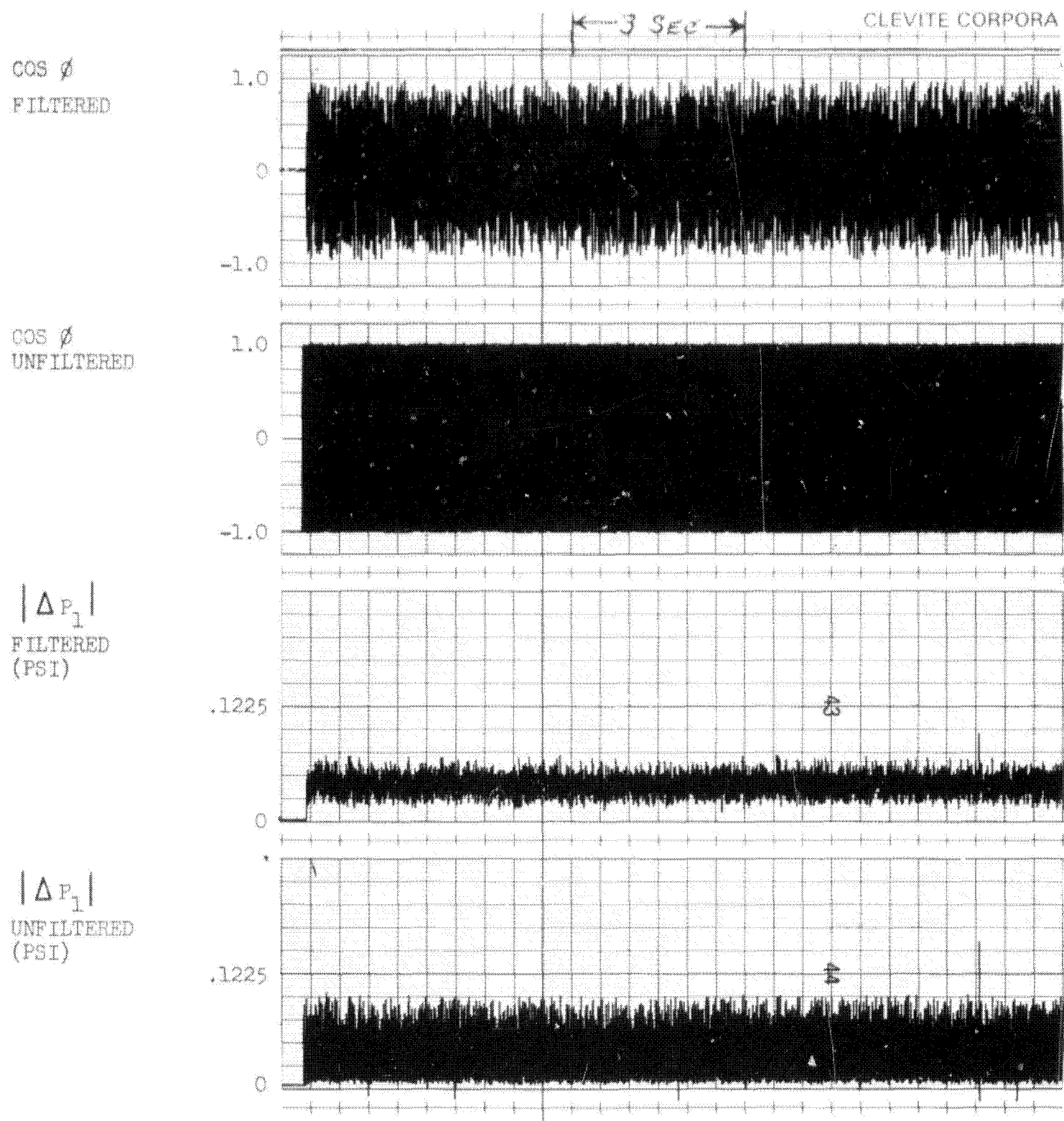


Figure 4-15a. Computer Traces of Zero-G Gauging System Response to a Gaussian White Noise Input (Wideband); Ullage Volume = 179.4 ft³

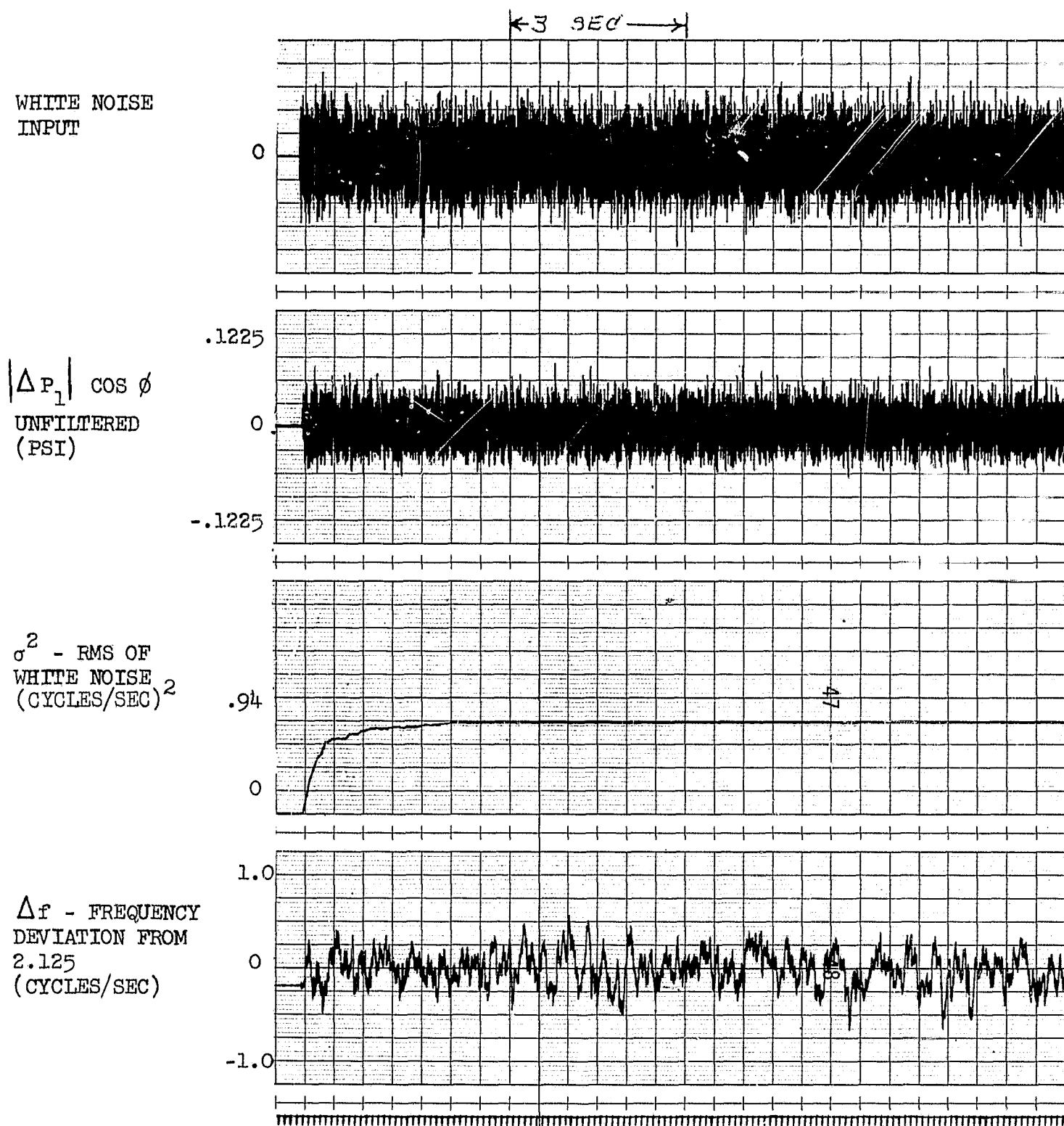


Figure 4-15b. Computer Traces of Zero-G Gauging System Response to a Gaussian White Noise Input (Wideband); Ullage Volume = 179.4 ft³

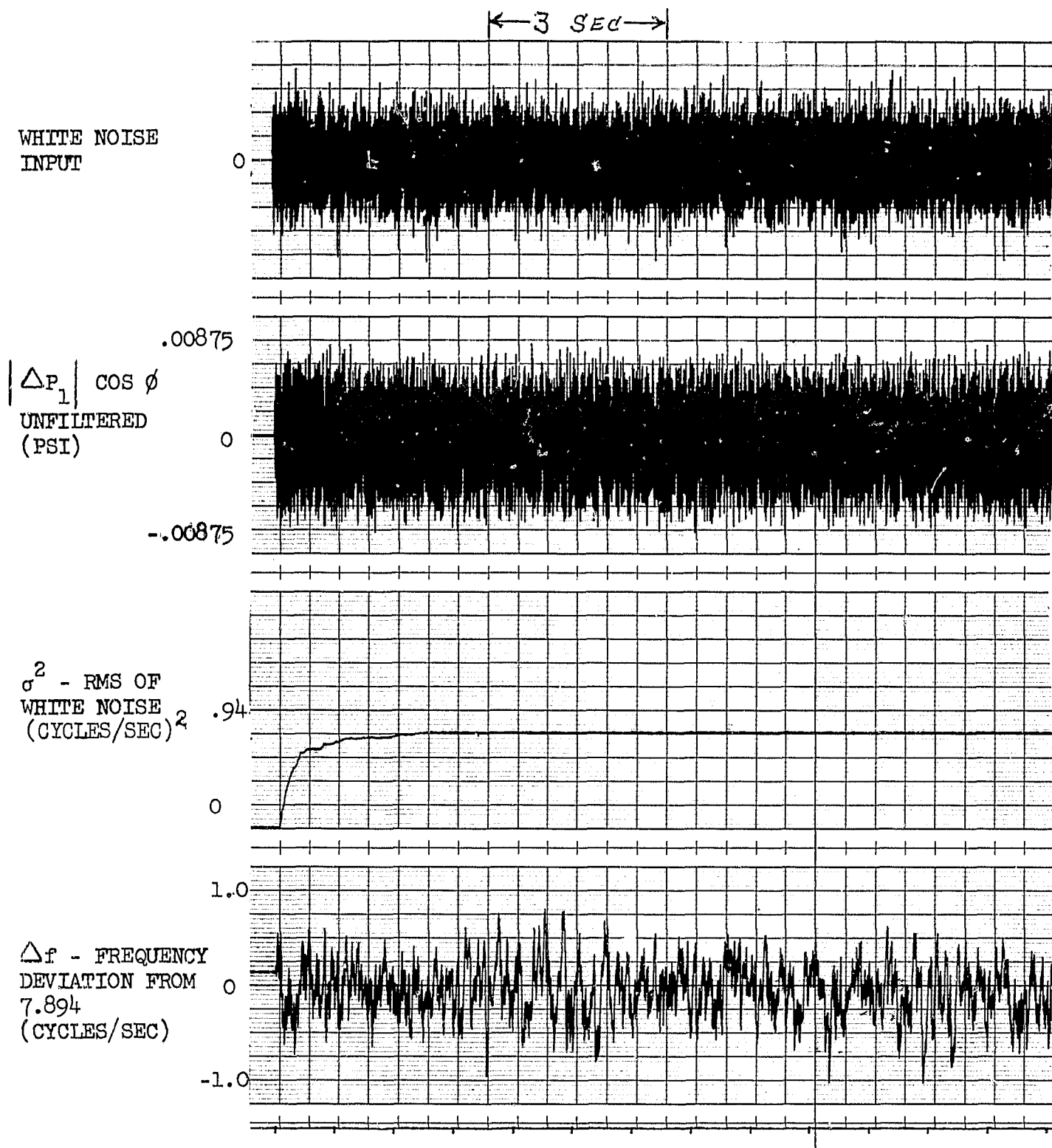


Figure 4-15c. Computer Traces of Zero-G Gauging System Response to a Gaussian White Noise Input (Wideband); Ullage Volume = 13 ft³

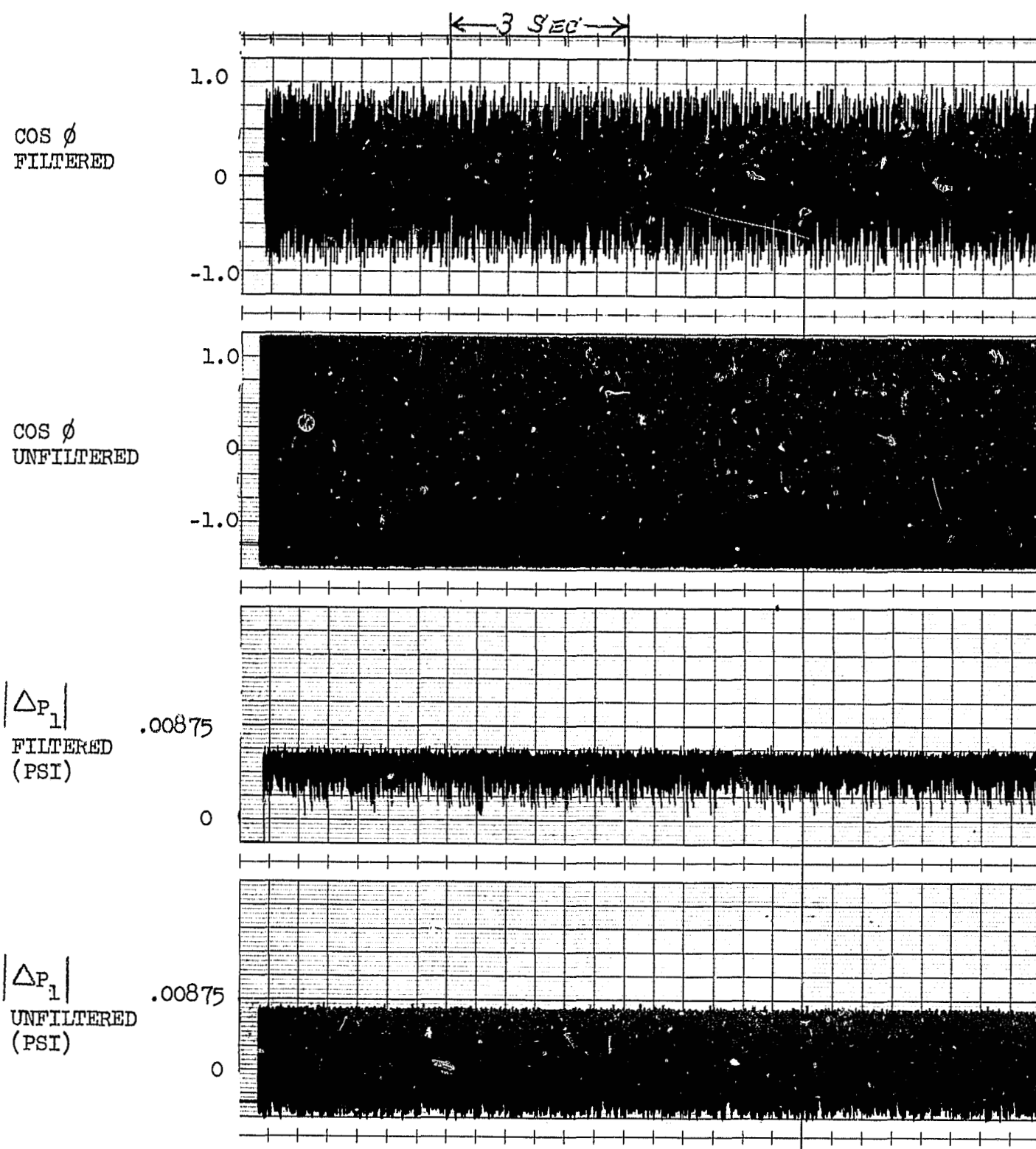


Figure 4-15d. Computer Traces of Zero-G Gauging System Response to a Gaussian White Noise Input (Wideband); Ullage Volume = 13 ft³

to ± 15 percent) would be experienced by measuring the instantaneous value of the frequency. However, by averaging the frequency over a 10-second period, the net error in frequency is maintained below ± 0.25 percent. Since the actual display system will employ a 10-second filter, the noise in the instantaneous frequency signal will not produce any appreciable error. As can be seen from Figure 4-15, the white noise introduced was at least an order of magnitude greater in amplitude than the measured pressure signal.

4.3.2 Conclusions

It was concluded from the above analyses that the system is extremely stable under all conditions, and steady state recovery of the system is always assured. System operation in the presence of either white noise or random pulses resulting in signal-to-noise ratios of 0.1 or less is feasible provided the output signal is filtered through a 10-second time-constant filter. As high response data are not required during zero-gravity, this is not a limitation. With the 10-second filter on the output, the error in the frequency can be held to less than ± 0.25 percent.

For optimum performance in the presence of external noise, the amplifier gain after the multiplier should be 100 and the loop filter time-constant should be at least 10 seconds. Under these conditions the system requires about 5 to 10 seconds to recover from an offset.

4.4 RIGS FAILURE MODE AND RELIABILITY ANALYSIS

A preliminary failure mode and reliability analysis estimate was performed for the RIGS. The results of this analysis are shown in Table 4-2. A limitation on the accuracy of the analysis was the lack of detailed information on most of the electronics in the data processor. Data from electronic equipment of greater complexity than would actually be used with RIGS was employed in the analysis for conservatism. Data from generic components similar to those comprising the RIGS system was examined, a failure rate determined, and all apparent failure modes consolidated into a limited number of general failure mode classifications. The probability of occurrence of these classifications were estimated based on available data. Each failure mode classification was then examined for its applicability and effect on the RIGS. The failure rates

associated with all modes determined to be applicable and sufficient to produce a RIGS failure were totaled and then applied to a reliability model. The total RIGS failure rate was calculated to be 1.4×10^{-5} failures/hour. This value applied to a 30-day mission yields an estimated reliability of 0.990.

TABLE 4-2
 RESONANT INFRASONIC GAUGING S
 FAILURE MODE AND EFFECTS ANALYSIS - I

<u>SYSTEM COMPONENT</u>	<u>GENERIC COMPONENT FAILURE MODES (CONSOLIDATED)</u>	<u>ESTIMATED GENERIC FAILURE MODE %</u>	<u>GENERIC COMPONENT ESTIMATED FAILURE MODE</u>
<u>SENSOR/DRIVER ASSEMBLY</u>			
DRIVER ASSEMBLY			
Electrodynamic Driver (Coil-magnet-shaft-guide ring assembly)	1. Inoperative (electrical failure)	60	0.2x10 ⁻⁶
	2. Inoperative (mechanical failure - sticking or jammed)	40	
Driver Bellows (metallic)	1. Leak (small)	90	2.8x10 ⁻⁶
	2. Leak (large leak or rupture)	10	
	3. Change in spring rate (small)	≈0	
	4. Change in spring rate (large)	≈0	
Electronic Amplifier	1. Out of tolerance or inoperative	100	0.5x10 ⁻⁶
RESONANT ELEMENT ASSEMBLY			
Follower Piston			0.6x10 ⁻⁶ (Dis
(Elastomer diaphragm with convolutions, and guide bushing)	1. Leak (small)	90	0.08x10 ⁻⁶ (SI
	2. Leak (large leak or rupture)	10	

FOLDOUT FRAME /

E 4-2
GAUGING SYSTEM (RIGS)
ANALYSIS - RELIABILITY ESTIMATE

Application: 30 days
2 cycles/sec - 5,184,000 cycles
Bellows shaft travel≈ 25 inch

GENERIC COMPONENT ESTIMATED FAILURE MODE	FAILURE MODE APPLICABILITY TO RIGS	APPLICABLE FAILURE MODE FAILURE RATE	EFFECT OF APPLICABLE FAILURE MODE ON THE RIGS
2x10 ⁻⁶	Yes	0.12x10 ⁻⁶	RIGS failure - no volume displacement can be achieved.
	Yes	0.08x10 ⁻⁶	RIGS failure - the design consists of low tolerance fits resulting in sufficient "slop" in the system to make sticking or jamming failures less probable.
.8x10 ⁻⁶	N/A	N/A	N/A - the design will function satisfactorily with a small leak.
	Yes	0.28x10 ⁻⁶	RIGS failure - back volume gas could fill the piston cavity or mix with the gas between the pistons.
	N/A	N/A	N/A - the design will function satisfactorily with a small spring rate change.
	Yes	≈0	RIGS inaccurate measurement - the bellows spring rate is a factor in the volume displacement for a given applied force.
5x10 ⁻⁶		0.5x10 ⁻⁶	RIGS failure
6x10 ⁻⁶ (Diaphragm)			
08x10 ⁻⁶ (Shaft or bushing)	N/A	N/A	N/A - the design will function satisfactorily with a small leak.
	Yes	0.06x10 ⁻⁶	RIGS failure - the driven gas volume would flow into the volume displaced by the large area bladder.

TABLE 4-2 CONTINUED

<u>SYSTEM COMPONENT</u>	<u>GENERIC COMPONENT FAILURE MODES (CONSOLIDATED)</u>	<u>ESTIMATED GENERIC FAILURE MODE %</u>	<u>GENERIC COMPONENT ESTIMATED FAILURE MODE</u>
Follower Piston (continued)	3. Change in spring rate (small)	≈0	
	4. Change in spring rate (large)	≈0	
	5. Inoperative (mechanical failure - sticking or jammed shaft-bushing, contamination)	100	
PRESSURE TRANSDUCER (Differential)	1. Fitting leak	1	1.4×10^{-6}
	2. Out of tolerance.	79	
	3. Inoperative	20	
LARGE SURFACE AREA BLADDER	1. Leak	100	0.6×10^{-6}
FILL VALVE	1. Leak	100	≈0 (Reduced)
BACK VOLUME CAN AND TUBE JOINT	1. Leak or rupture	100	0.04×10^{-6}

4-2 CONTINUED

<u>GENERIC COMPONENT ESTIMATED FAILURE MODE</u>	<u>FAILURE MODE APPLICABILITY TO RIGS</u>	<u>APPLICABLE FAILURE MODE FAILURE RATE</u>	<u>EFFECT OF APPLICABLE FAILURE MODE ON THE RIGS</u>
	N/A	N/A	N/A - the design will function satisfactorily with a small change in spring rate.
	Yes	≈ 0	RIGS inaccurate measurement - the follower piston spring rate is required to be small relative to the gas spring rate.
	Yes	0.08×10^{-6}	RIGS failure - the design consists of low tolerance fits resulting in sufficient "slop" in the system to make sticking or jamming failures less probable.
1.4×10^{-6}	Yes	0.01×10^{-6}	RIGS failure - the back volume gas would be lost.
	N/A	N/A	N/A - system operation requires only a pressure reading (not accuracy).
	Yes	0.28×10^{-6}	RIGS failure - no measurement would be achieved.
0.6×10^{-6}	Yes	0.6×10^{-6}	RIGS failure - propellant would wet the follower piston.
≈ 0 (Redundant seal)	Yes	≈ 0	RIGS failure - back volume gas would be lost (a redundant seal will be utilized on the valve lessening the probability of this failure).
0.04×10^{-6}	Yes	0.04×10^{-6}	RIGS failure - back volume gas would be lost (redundant o-rings are utilized at the joint).

TABLE 4-2 CONTINUED

<u>SYSTEM COMPONENT</u>	<u>GENERIC COMPONENT FAILURE MODES (CONSOLIDATED)</u>	<u>ESTIMATED GENERIC FAILURE MODE %</u>	<u>GENERIC COMPONENT ESTIMATED FAILURE MODE</u>
<u>DATA PROCESSOR</u>			
CONTROL SYSTEM			
Power Amplifier	1. Out of tolerance or inoperative	100	1×10^{-6}
Band Pass Filter and Low Power Amplifier	1. Out of tolerance or inoperative	100	0.5×10^{-6}
Multiplier	1. Out of tolerance or inoperative	100	3×10^{-6}
Low Pass Filter and Amplifier	1. Out of tolerance or inoperative	100	0.5×10^{-6}
DISPLAY ELECTRONICS			
Temperature Transducer (Thermistor)	1. Equivalent to an open circuit 2. Equivalent to a short circuit	75 25	1.4×10^{-6}
Pressure Transducer	1. Fitting leak 2. Out of tolerance 3. Inoperative	1 79 20	1.4×10^{-6}
Remainder of system (approximately as complex as a multiplier and 2 or 3 low power amplifiers)	1. Out of tolerance or inoperative	100	4.5×10^{-6}

For 30 da

2 CONTINUED

<u>GENERIC COMPONENT ESTIMATED FAILURE MODE</u>	<u>FAILURE MODE APPLICABILITY TO RIGS</u>	<u>APPLICABLE FAILURE MODE FAILURE RATE</u>	<u>EFFECT OF APPLICABLE FAILURE MODE ON THE RIGS</u>
1×10^{-6}	Yes	1×10^{-6}	RIGS failure
0.5×10^{-6}	Yes	0.5×10^{-6}	RIGS failure
3×10^{-6}	Yes	3×10^{-6}	RIGS failure
0.5×10^{-6}	Yes	0.5×10^{-6}	RIGS failure
1.4×10^{-6} F/hr	Yes	1.0×10^{-6}	RIGS failure
	Yes	0.4×10^{-6}	RIGS failure
1.4×10^{-6} F/hr	Yes	0.01×10^{-6}	RIGS failure - loss of gas.
	Yes	1.1×10^{-6}	RIGS inaccurate measurement.
	Yes	0.28×10^{-6}	RIGS failure - no measurement would be achieved.
4.5×10^{-6}			
	Yes	4.5×10^{-6}	RIGS failure
	TOTAL	14.35×10^{-6}	

For 30 day mission, the estimated RIGS reliability is $e^{-720(14.35 \times 10^{-6})} = \underline{0.990}$

5. FEASIBILITY DEMONSTRATION TEST PROGRAM

5.1 INTRODUCTION

A series of tests was performed to demonstrate the ability of a RIGS-type system to detect propellant tank resonant frequencies and to show that the resonant frequency varied as predicted with ullage volume. Since the objective of these tests was a feasibility demonstration of the RIGS operating principles, available off-the-shelf equipment was used and all test equipment design emphasized flexibility and simplicity.

The feasibility demonstration was extremely successful. In addition, to demonstrating both of the above goals, it was possible to demonstrate the satisfactory operation of a complete closed-loop system capable of locking-on to the system resonant frequency within $\pm 1/2$ percent. This accuracy was demonstrated with the system in both the upright and inverted positions.

5.2 DESCRIPTION OF TEST HARDWARE

The test hardware is shown schematically in Figure 5-1, and the actual test setup is shown in Figures 5-2, 5-3, and 5-4. The hardware consisted of the driver/sensor assembly and a large tank having a measured volume of 69,410 ml. The driver/sensor assembly, shown in Figure 5-1, was mounted on a base plate which was bolted to the top of the tank. It contained a follower piston (the resonant element) and a driver piston which was firmly sealed in its bore by an O-ring. The follower piston was weighted to the desired value and sealed loosely in its bore with an O-ring lubricated with molybdenum disulfide powder. The volume between these two pistons, the driver volume, V_1 , was approximately 2 cubic inches. The driver piston was driven by a variable-speed dc electric motor with a variable-stroke cam drive capable of being adjusted from zero to a maximum stroke of $\pm 1/16$ inch. The shaft connecting the drive piston to the cam follower was held in a pair of linear ball bearings in order to minimize frictional loads, and was sealed by an O-ring seal to partially balance the pressure loads on the piston. The motor employed a Ward Leonard type drive to obtain its variable speed capabilities. Good speed stability was obtained from approximately 2 to 200 cps, which was adequate for the detection of the resonant frequencies in the feasibility demonstration tank. The assembly was designed to accommodate a variety of resonant diaphragms in addition to the piston,

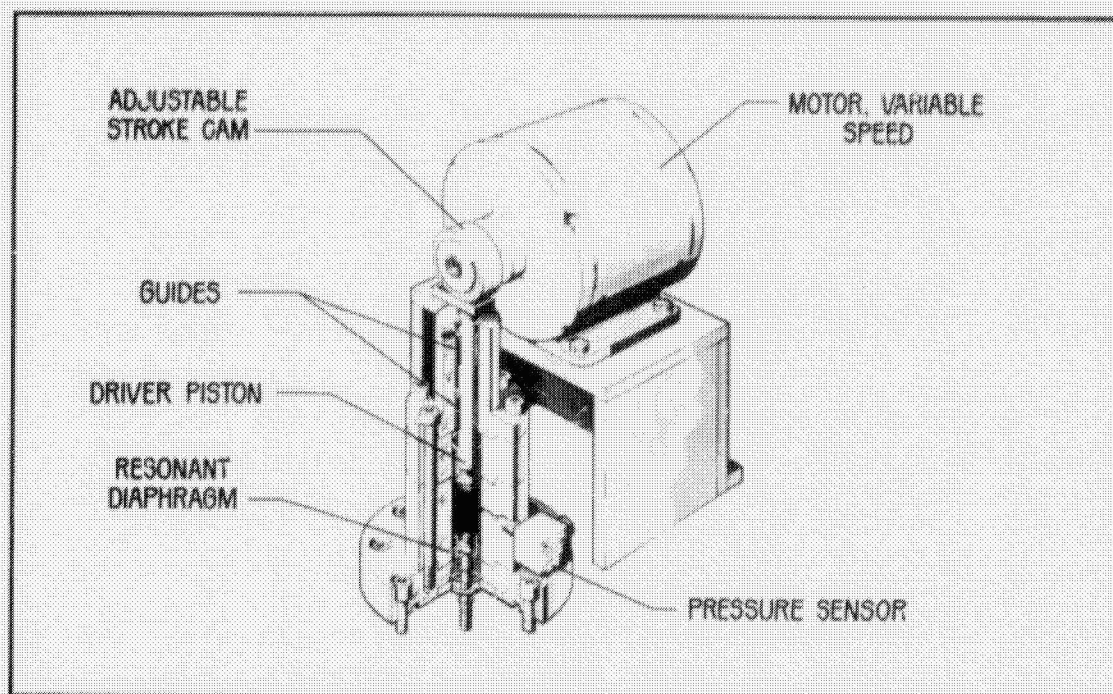


Figure 5-1. Feasibility Test Fixture

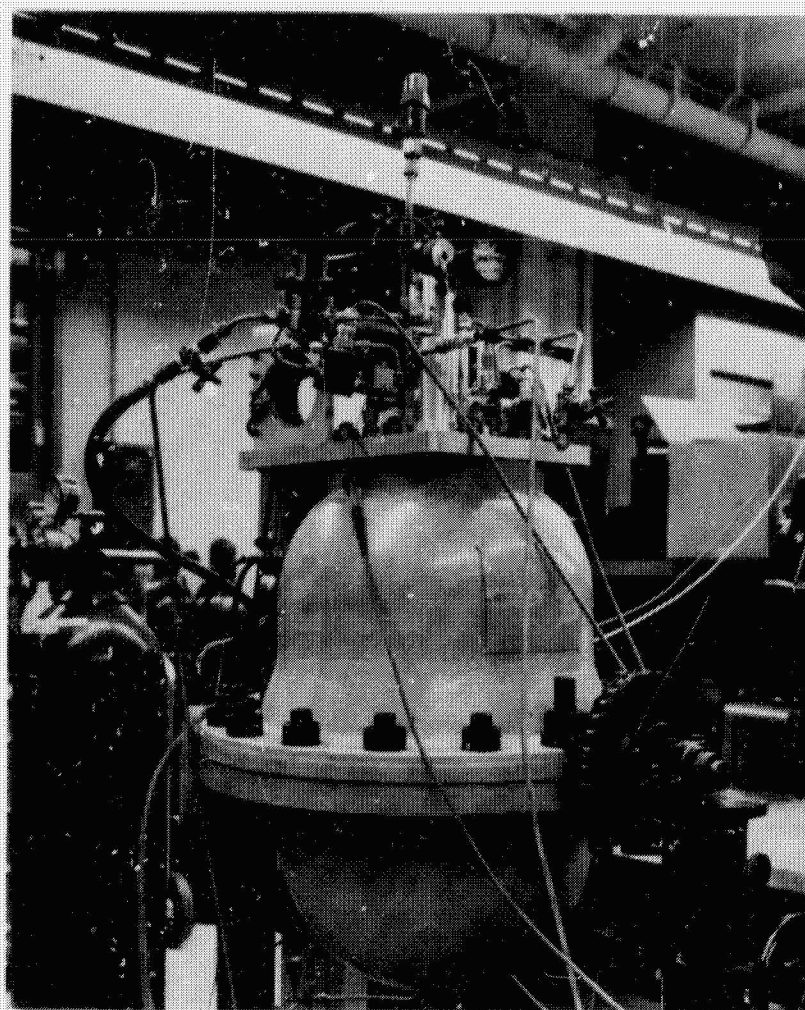


Figure 5-2. Feasibility Test Hardware

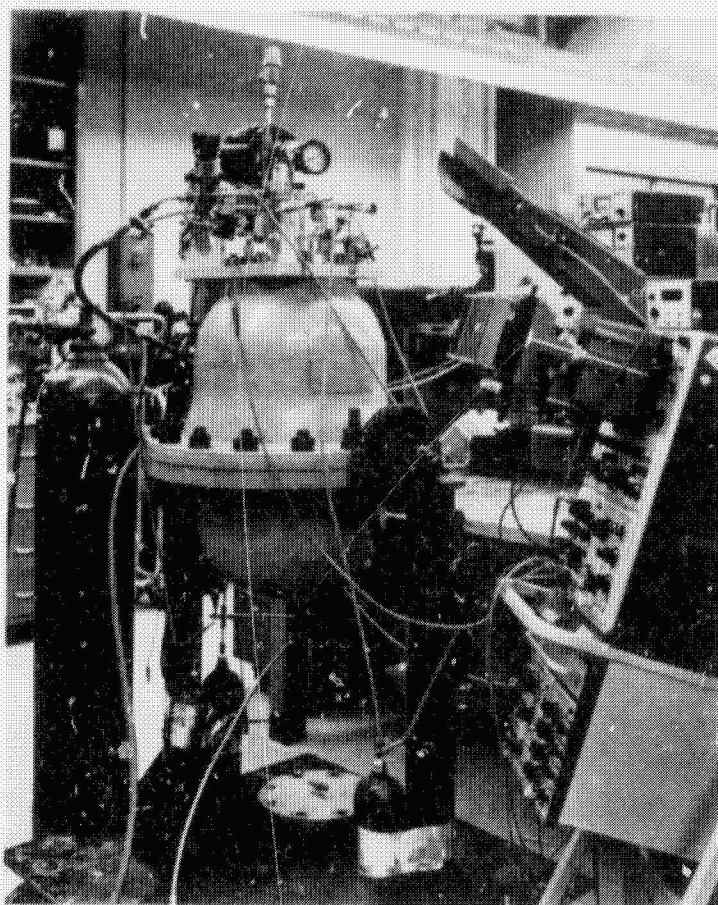


Figure 5-3. Feasibility Test Hardware

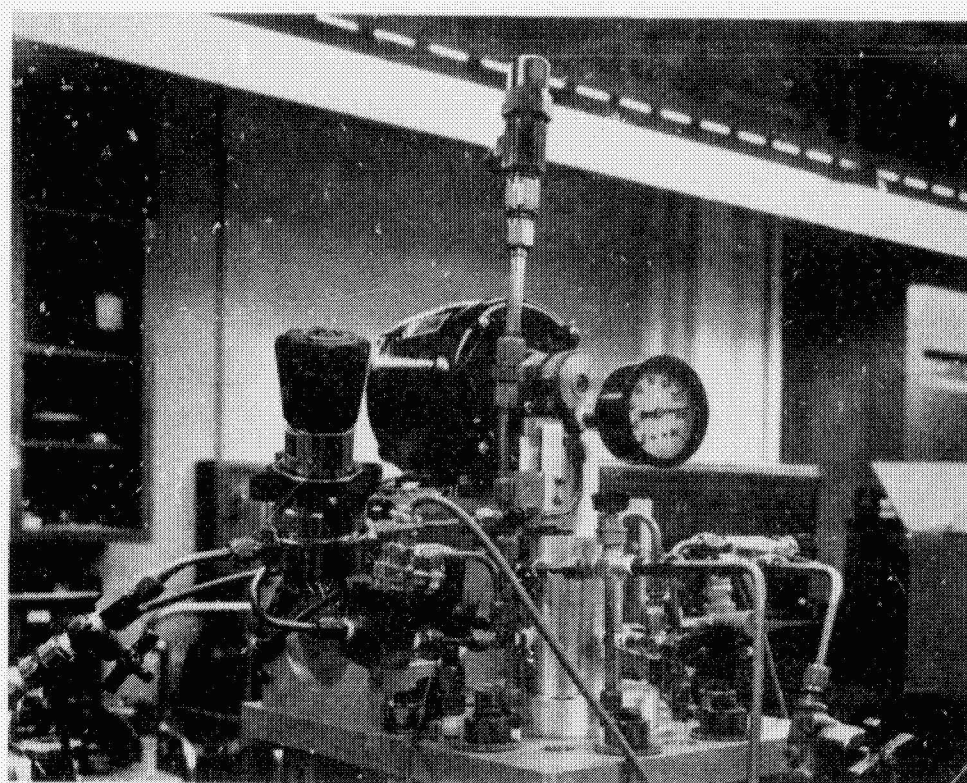


Figure 5-4. Feasibility Test Driver and Sensor Assembly

but as satisfactory results were obtained with the follower piston, no diaphragms were tested.

Linear position transducers were provided on both the driver and the follower pistons. The transducer on the follower piston ensured that the piston was truly in a free-floating position and was stroking smoothly within its bore. The pressure transducers were provided to measure tank pressure, driver cavity pressure, and the differential pressure between the driver cavity and the tank. Piezoelectric differential pressure transducers were used for all three measurements. The driver cavity pressure transducer employed a 0.1 psig diaphragm, while the other two transducers utilized 1.0 psig diaphragms. In order to measure only the dynamic component of the pressure signal, one port of the differential pressure transducer was referenced to the system static pressure. This was accomplished by providing a reference volume on one port of the transducer which was connected to the propellant tank volume through a suitably snubbed line. Actual propellant tank pressure was read from a conventional Bourdon tube pressure gauge and may be considered accurate to 2 percent.

5.3 TEST RESULTS

5.3.1 Initial Testing

The initial tests served to check out the apparatus and to ensure proper operation of all system components. It was noted that the output pressure signal was quite sensitive to the actual follower piston location, and that by a judicious positioning, the friction on the follower piston could be minimized. Maintaining the follower piston in this position and performing a frequency sweep, the resonant point location was quite apparent. Frequency sweeps were accomplished manually at propellant volumes varying from 80 percent of full tank down to tank-empty conditions. Data were recorded by photographing an oscilloscope screen. Typical data are presented in Figure 5-5. When the data from this test were reduced, it was found that the measured response agreed within ± 4 percent of the theory.

It soon became apparent that, using this approach, the resolution, particularly near the tank-empty conditions, could not be appreciably improved. As the piston had appreciable viscous damping, the Q_0 of the system was only about 3 to 5 and both the phase and amplitude of the

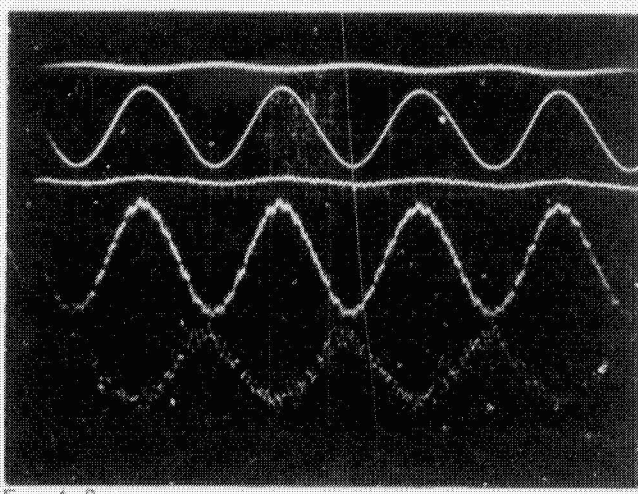
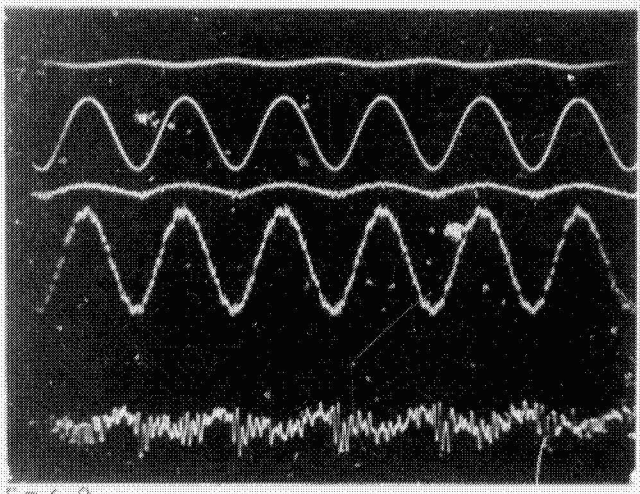
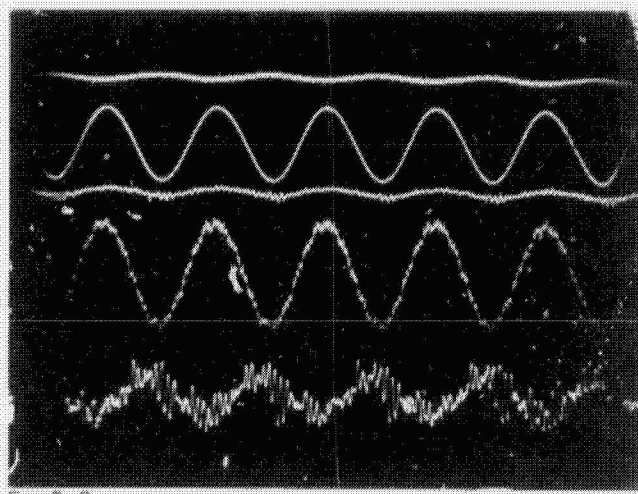
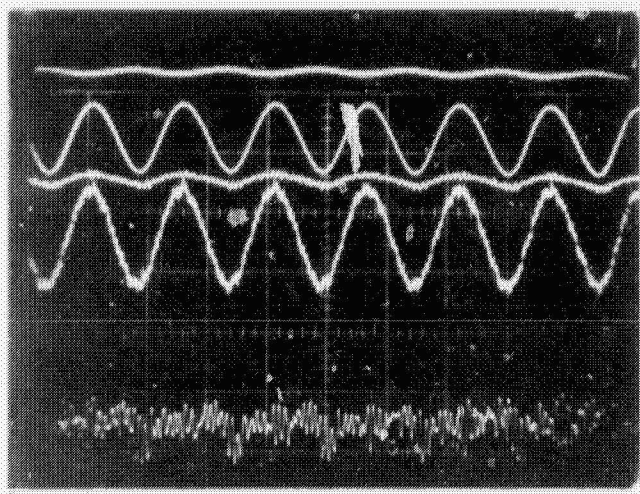
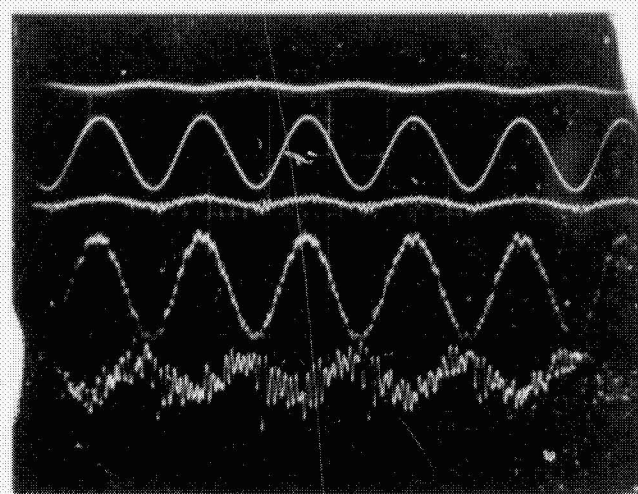
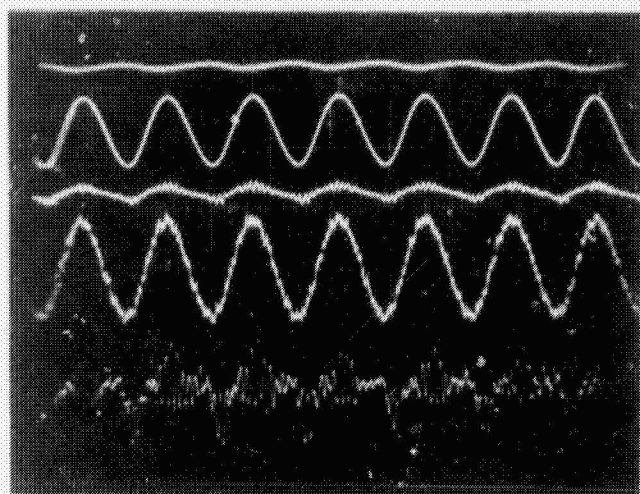
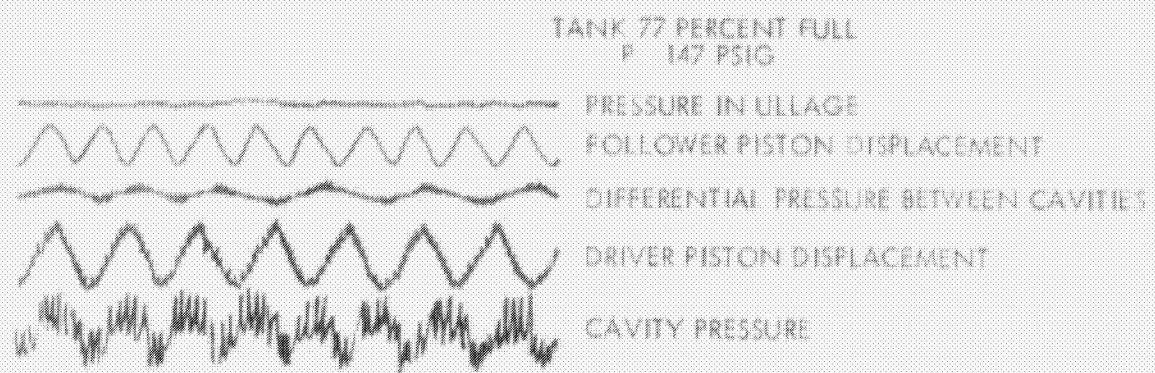
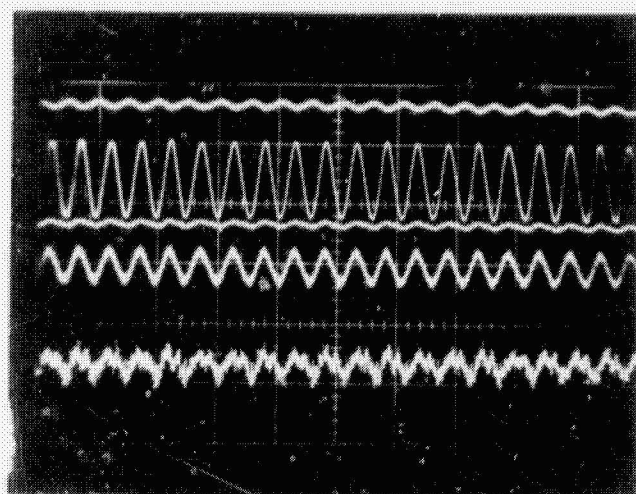
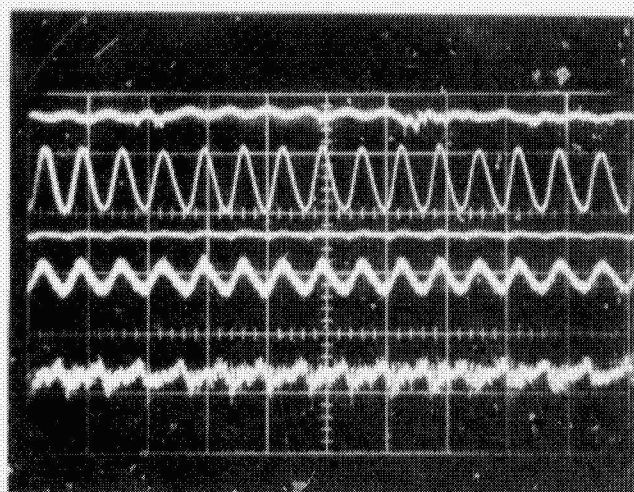


Figure 5-5a. System Response at Constant Volume and Variable Frequency

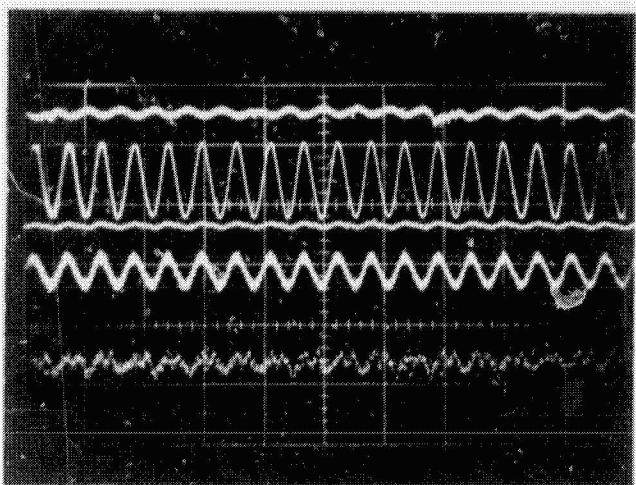
TANK 23 PERCENT FULL



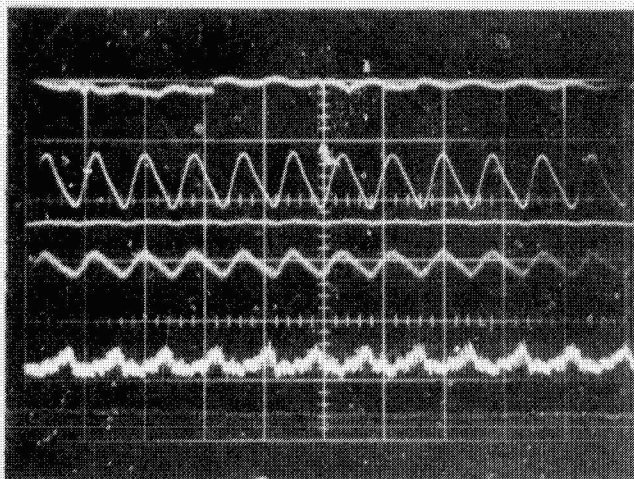
F 3.9 CPS



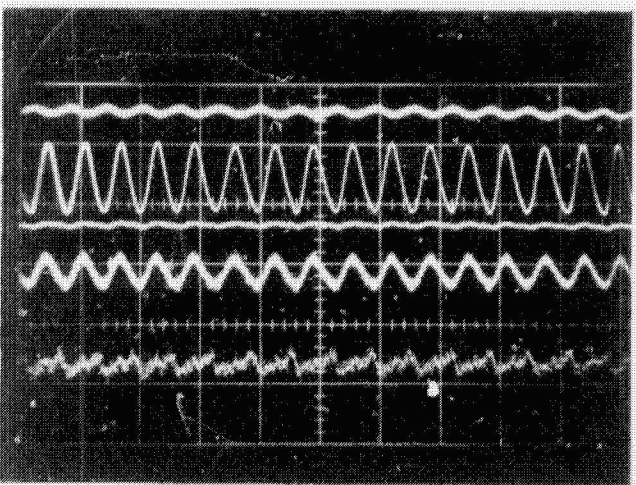
F 2.9



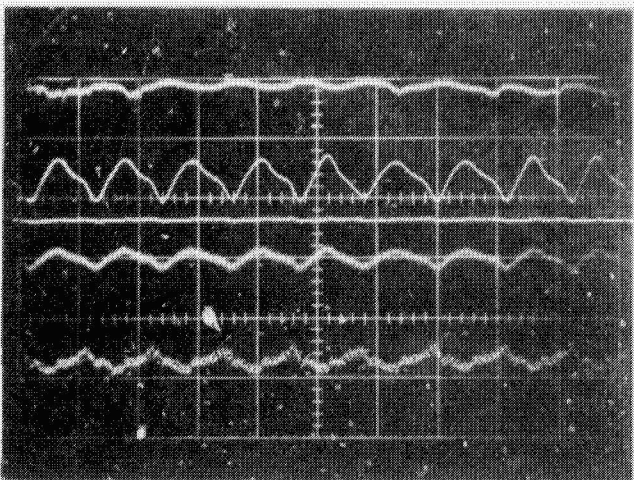
F 3.5



F 2.4



F 3.2



F 1.8

Figure 5-5b. System Response at Constant Volume and Variable Frequency

signal varied too slowly. Because of this, the phase could not be read from the oscilloscope to an accuracy of better than ± 10 percent. Figure 5-6 shows the amplitude data for a typical test. In addition, the speed control on the dc motor was not sufficiently tight to maintain the frequency within ± 2 percent. The tests were quite encouraging as they did demonstrate the validity of the basic concept. However, in order to demonstrate the accuracy potential of the concept, an automated means of measuring the resonant point was required. It was decided to use a multiplier/filter combination similar to that described in Section 3.2.

5.3.2 Closed Loop Testing

A closed loop control system was incorporated into the test assembly and is shown schematically in Figure 5-7. The control system was similar to that proposed for the prototype gauge, but used off-the-shelf Philbrick operational components. The motor speed control was modified to permit the use of a regulated power supply controlled by an operational amplifier. The two input signals to the multiplier were first filtered through two matched bandpass (2-10 cps) filters. One signal was the driver cavity dynamic pressure, while the reference signal was the driver piston position. The output from the multiplier was filtered by an integrating amplifier with a 10-second time constant to remove all time-varying components. The remaining dc component of the multiplier signal was used to control the motor speed.

A series of tests were then performed in which 4 liters of water were removed from the tank at each data point, starting with the tank approximately 80 percent full and continuing to the tank-empty condition. The system successfully returned each time to the new resonant frequency. The system could not successfully track during the transient because of leakage around the free piston. The pressure fluctuation during liquid removal was sufficient to cause the free piston to travel against the stops. The system, however, recovered after the liquid flow ceased, and successfully determined the resonant frequency without adjustment.

The oscilloscope photographs of the system response are shown in Figure 5-8. It will be noted that the reference signal (V_1) into the multiplier is appreciably skewed from a normal sinusoidal wave shape,

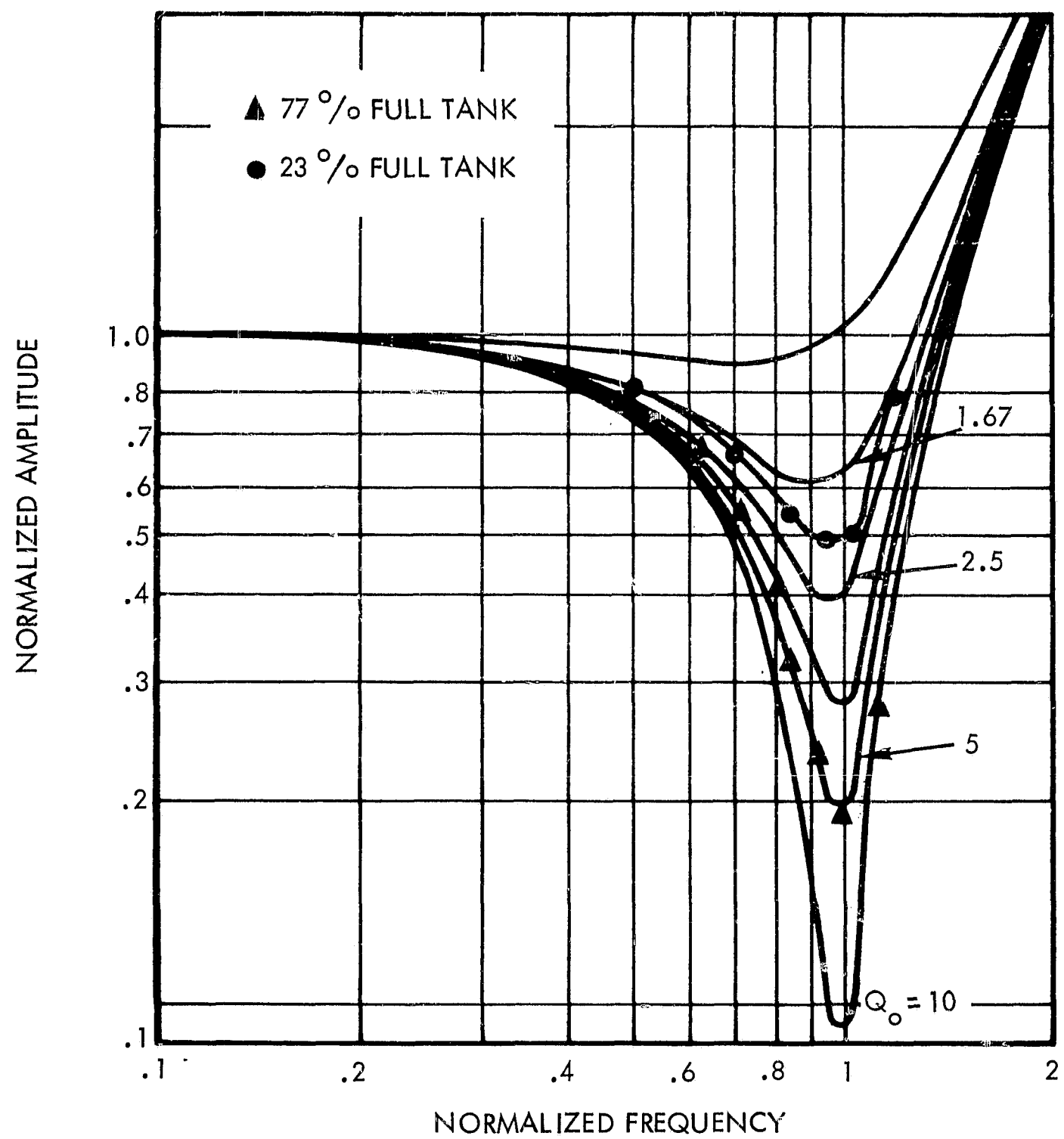
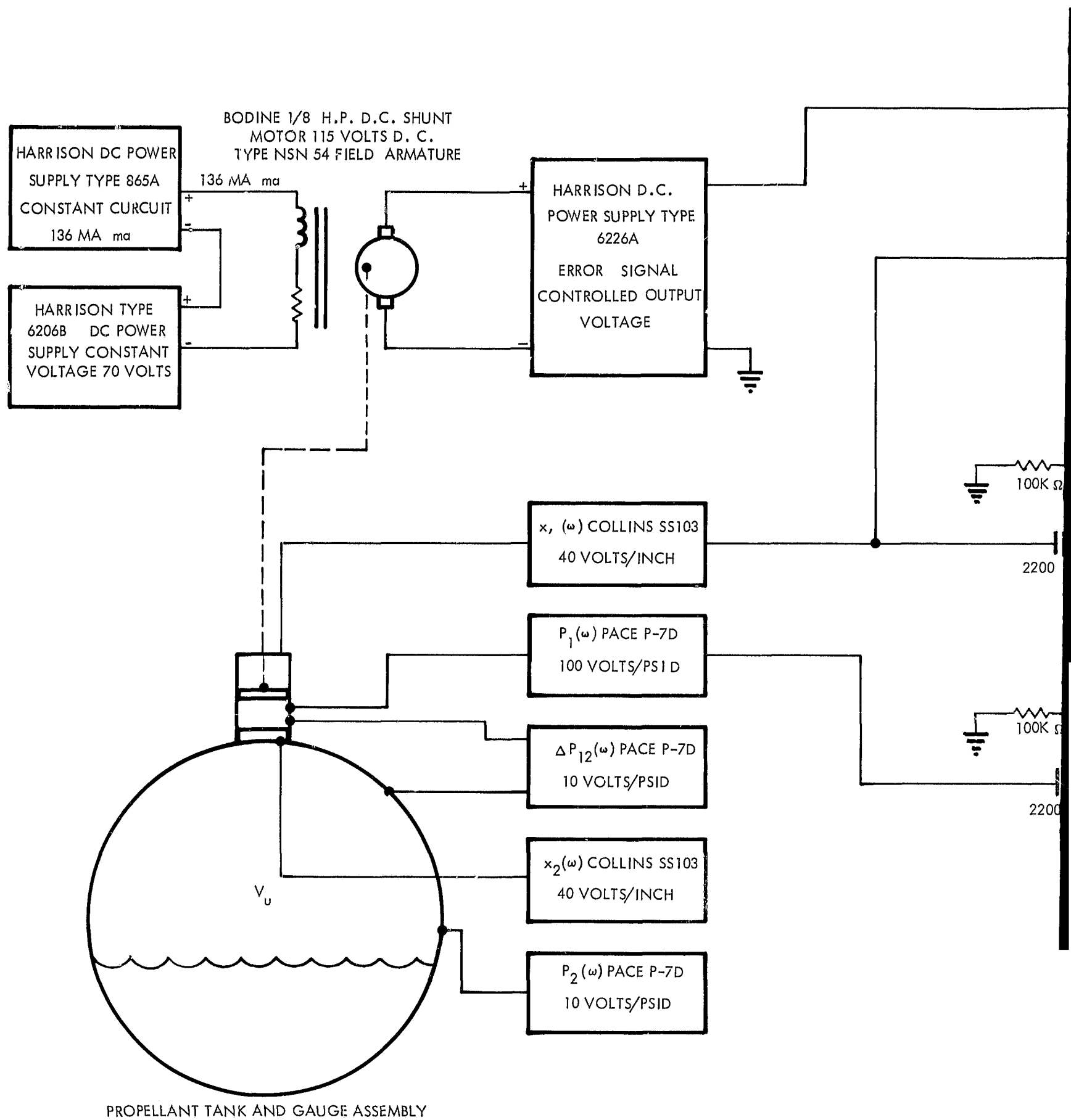


Figure 5-6. Amplitude Response for RIGS Feasibility Test



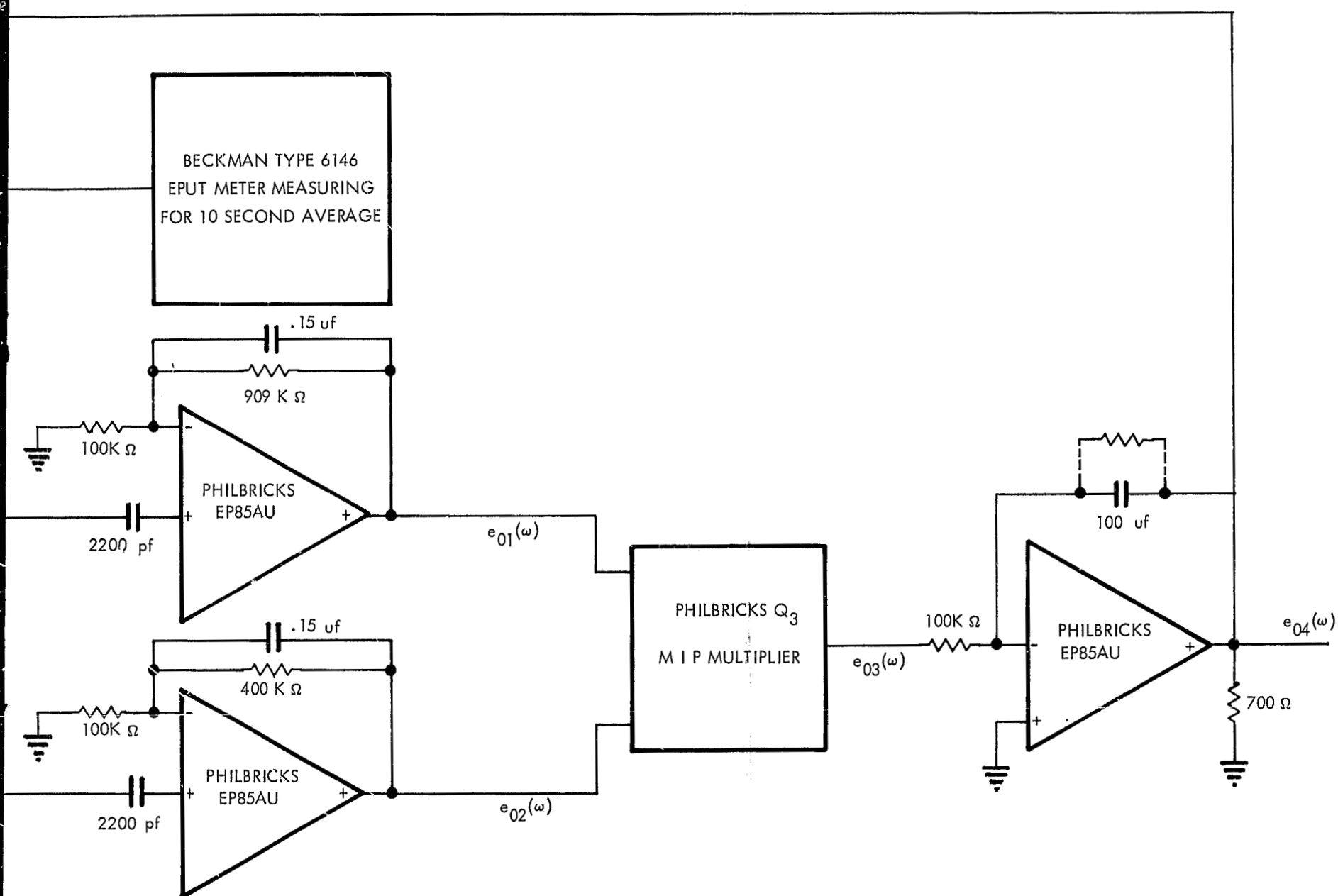
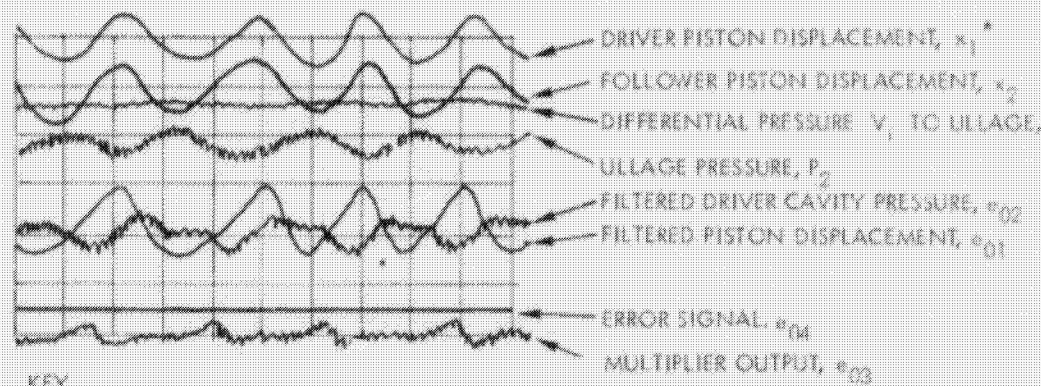
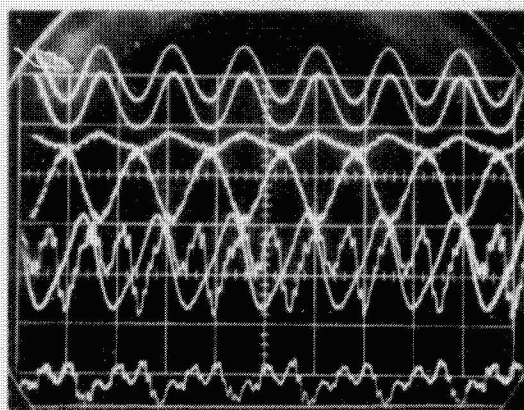


Figure 5-7. Feasibility Test Closed Loop Control System

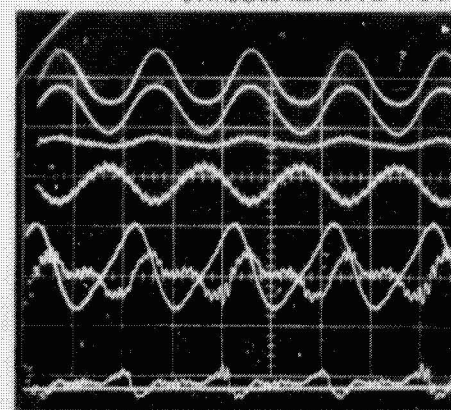


KEY

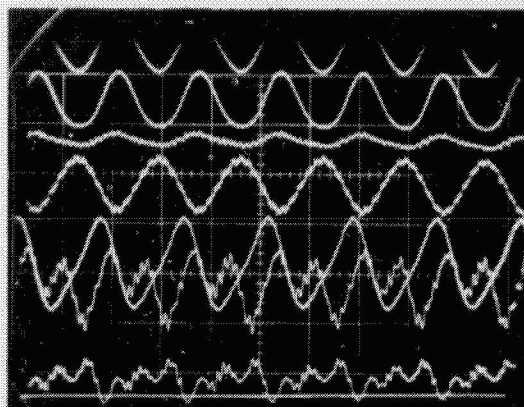
*SYMBOLS REFER TO FIGURE



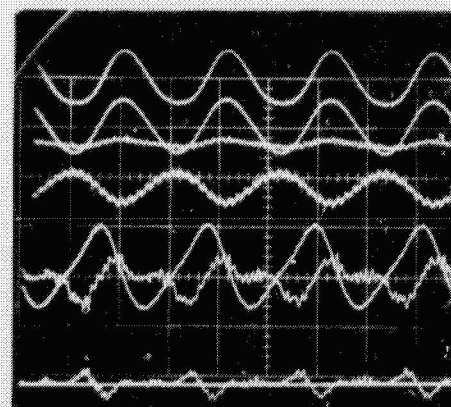
a) ULLAGE VOLUME - 12,000ML



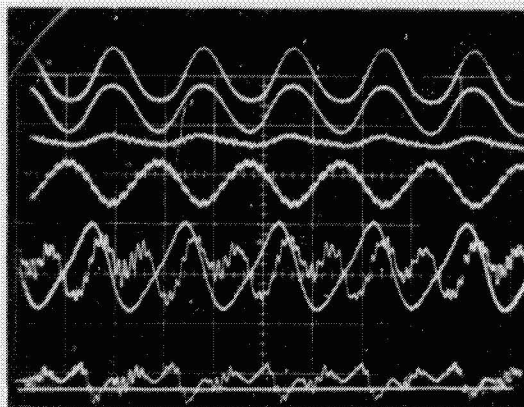
d) 24,000ML



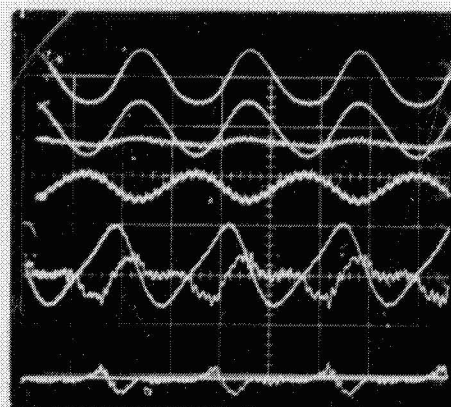
b) 16,000ML



e) 28,000ML



c) 20,000ML



f) 32,000ML

DISPLACEMENT, x_1
 ON DISPLACEMENT, x_2
 PRESSURE V_1 TO INFLAGE, AP_{12}
 RE, P_2
 CAVITY PRESSURE, 002
 DISPLACEMENT, 001

004
 PUT, 003

SYMBOLS REFER TO FIGURE 5-7

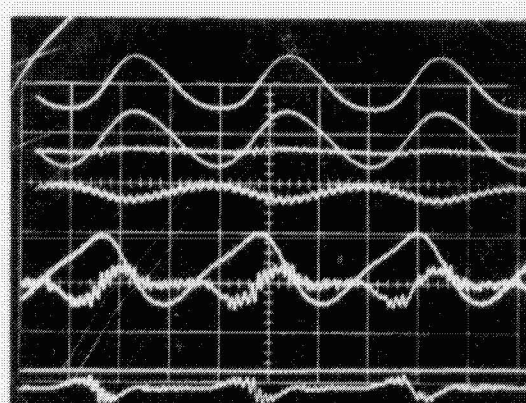
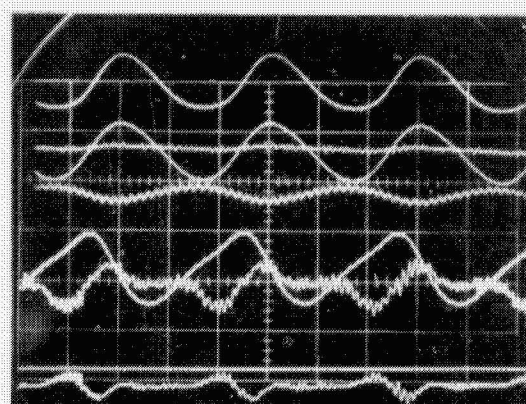
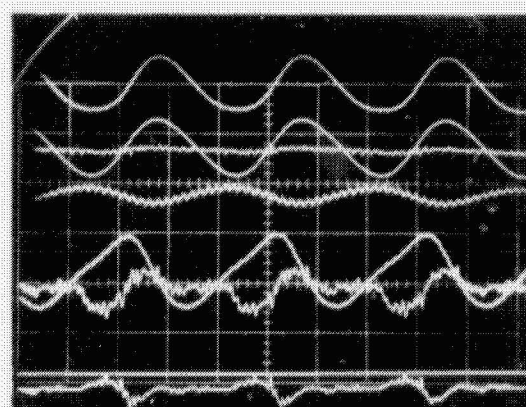
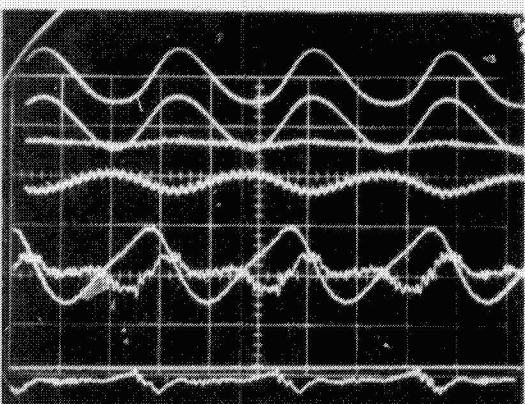
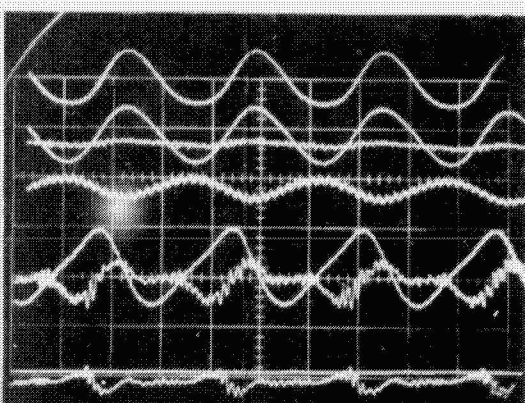
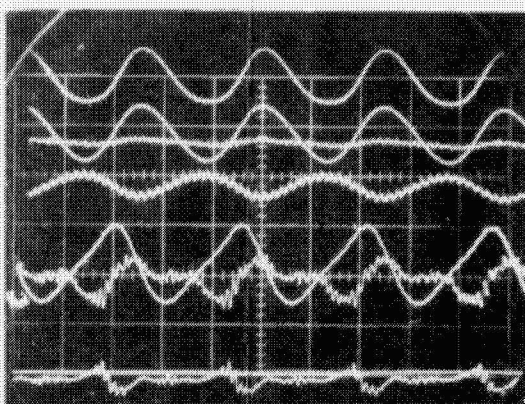
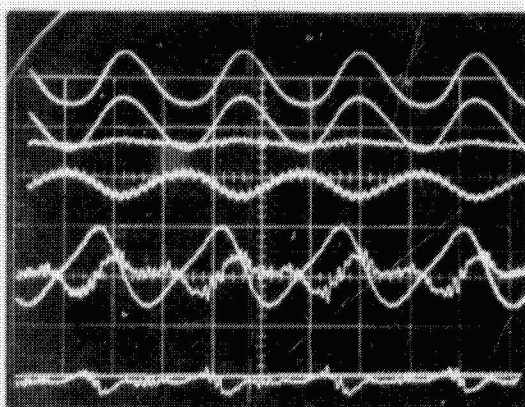
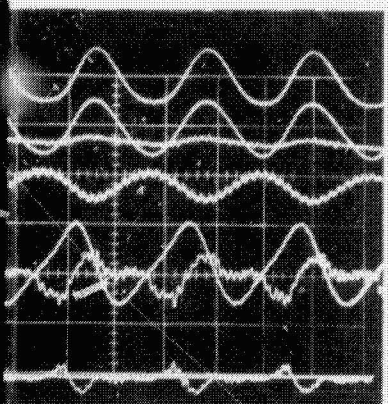
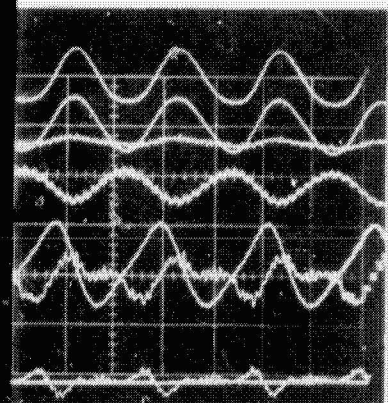
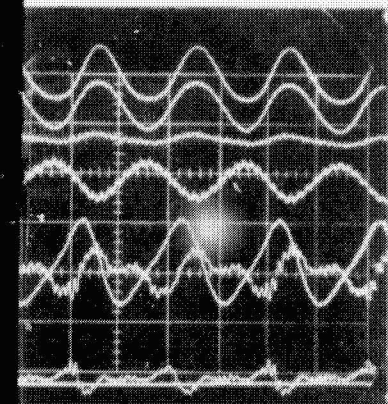


Figure 5-8. Closed-Loop System Response at Resonance

particularly near the tank-empty condition. This is a result of the uni-directional force on the cam which generated large second harmonic components. Despite the presence of the harmonics on the reference signal, the system successfully locked on to the correct frequency. The results of the test are shown in Figure 5-9. Except for two points, all of the data fell within $\pm 1/2$ percent of the predicted frequency, or ± 1 percent of the predicted volume. It was believed that the apparent error for the two points was caused by extraneous pulses being generated by the oscillograph time mark system entering into the digital frequency meter used to measure the frequency. This was later verified as described in Section 5.3.3.

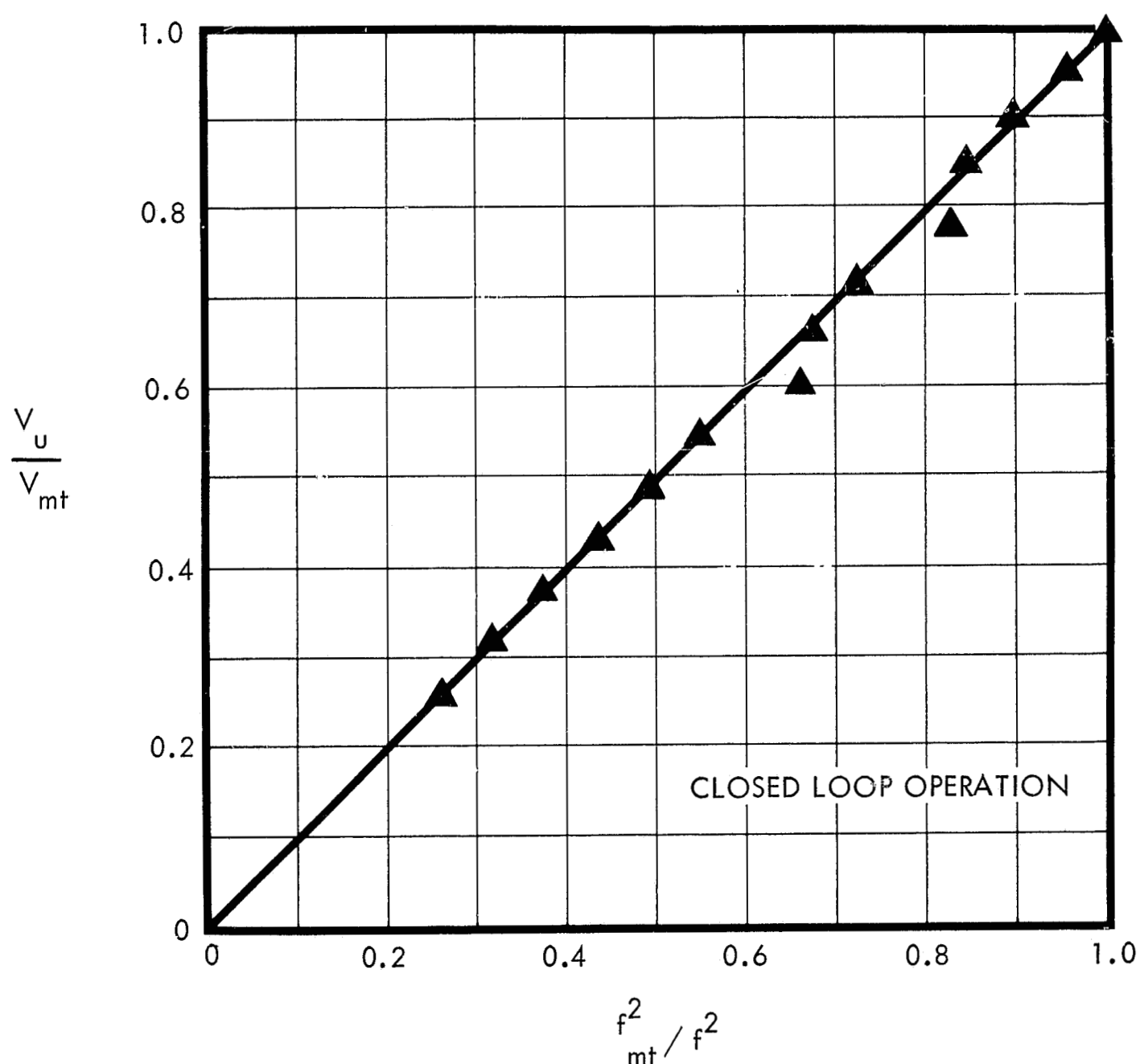


Figure 5-9. Performance of Feasibility Demonstration System

5.3.3 Additional Testing

The testing reported above demonstrated the basic feasibility of the RIGS concept. However, the tests were performed with the propellant tank in an upright position. In this orientation, the gauge was in direct communication with the entire ullage volume without any intervening liquid. In order to demonstrate the zero gravity gauging capability of the RIGS system, it was necessary to show that the use of a large area diaphragm (discussed in Section 4.1) would permit the infrasonic wave to be transmitted through the liquid to an isolated gas pocket without signal loss or phase shift. Since a test of this type was beyond the scope of the original contract, TRW undertook to demonstrate this feature in a series of company-sponsored tests.

The tests were performed by incorporating a hemispherical rubber diaphragm in the center of the tank, as shown in Figure 5-10. In the inverted position (RIGS at bottom), the tank was filled with the desired quantity of water and pressurized with nitrogen to 175 psig. As shown schematically in Figure 5-10, the ullage gas was thus contained in two gas pockets separated by the liquid quantity. The follower piston was replaced by a weighted sphere to permit operation in the inverted position.

A series of closed-loop tests was performed to determine the resonant frequency as a function of the ullage volume. The results are plotted in Figure 5-11. Also, additional data were taken with the tank in the upright position using the piston. As described in Section 5.3.2 and shown in Figure 5-9, initial tests of the system in this configuration had yielded ± 1 percent accuracy except for two data points which were believed to be caused by extraneous signals entering the digital frequency meter. The results of the test rerun, also shown in Figure 5-11, verified this explanation. As may be seen, the data from both the inverted and upright position tests are within ± 1 percent of the expected curve. These test results conclusively demonstrate the gauging ability of the RIGS independent of liquid location.

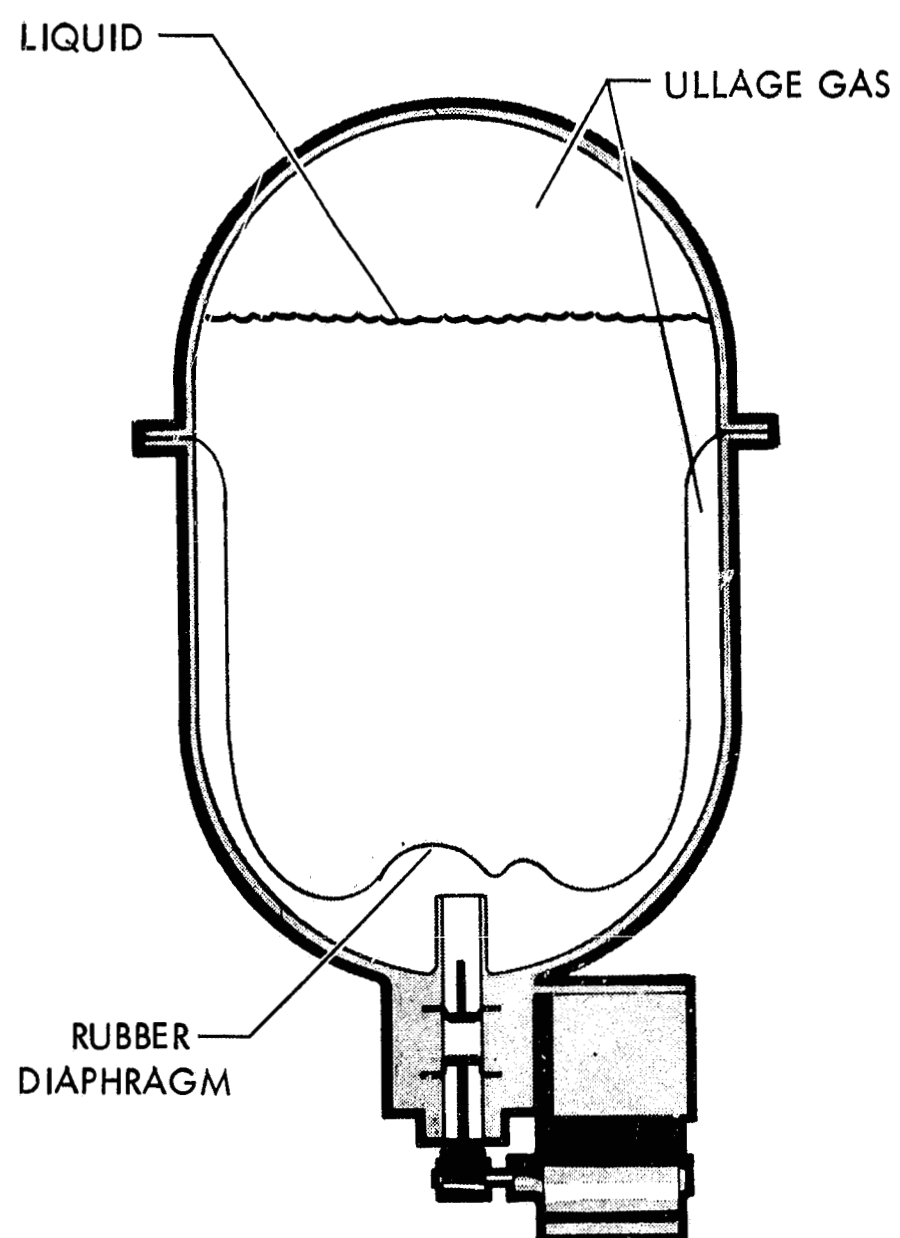


Figure 5-10. Inverted Tank Tests with Rubber Diaphragm

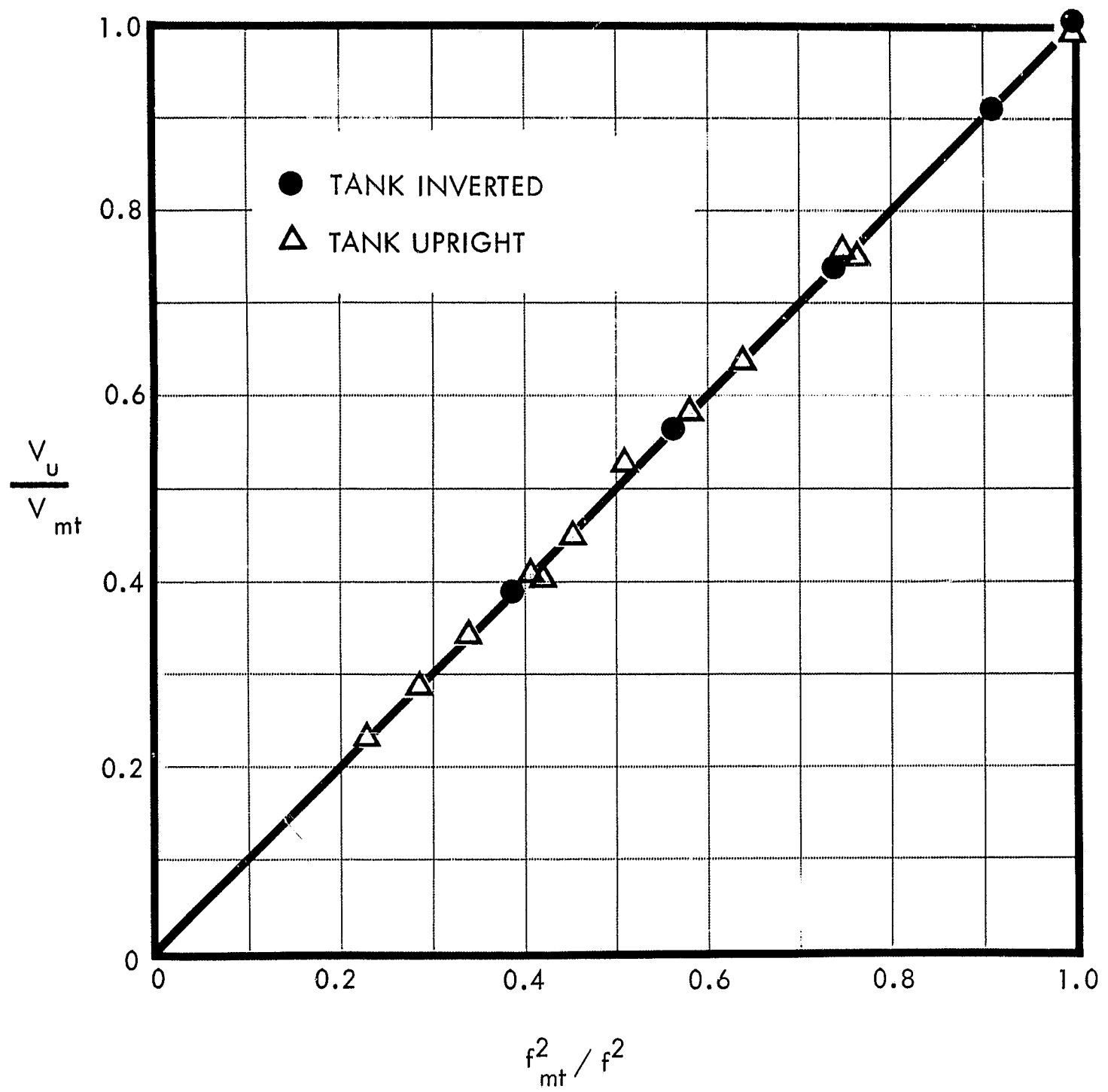


Figure 5-11. Performance of Feasibility Test System - Tank in Upright and Inverted Positions

6. CONCLUSIONS

The objectives of the Phase II portion of the Feasibility Study of Positive Gauging Systems were to:

- o Perform feasibility tests of the RIGS gauging concept
- o Analytically evaluate operational and integration problems for application of RIGS to the Apollo SPS tankage
- o Complete a prototype RIGS gauge design and evaluate system performance

The operating principle of the RIGS system was successfully demonstrated using subscale tankage and boilerplate hardware and components. During closed-loop operation of the system, the propellant volume was measured to an accuracy of ± 1 percent. These tests were performed with the tankage in both the normal and inverted positions, thus demonstrating the ability of the RIGS to gauge propellants independent of the gravity field. All identifiable operational and integration problems for application of the RIGS system to the Apollo SPS tankage were analytically evaluated. Each was satisfactorily resolved within an overall gauging system accuracy of ± 1 percent. Design of prototype hardware was carried out and indicated that a four-tank gauging system for the SPS application would weigh 38 pounds and require about 28 watts of power.

The results of this program have demonstrated the soundness of the RIGS concept and provide a firm basis for initiation of the engineering development phase of the RIGS system.

7. RECOMMENDATIONS

The results of the present program provide the necessary justification for initiating engineering development of the RIGS system for application to the Apollo SPS tankage. The major objectives of the engineering development phase will be to:

- Demonstrate that the RIGS system meets all specified performance requirements
- Determine the service life and performance of the gauging system and components
- Verify and refine the design, fabrication, and testing procedures for a flightweight system

The engineering development phase should include the following tasks:

Phase I. Engineering Model

- 1) Interface Definition. Prepare detailed interface specifications for the SPS tankage. Specify system weight, power, performance, and duty cycle requirements and define environmental requirements such as vibration, shock, and operating temperature range. Include detailed interface drawings of the gauge mounting locations in the SPS tankage.
- 2) Sensor/Driver Assembly (SDA) Component Design and Test. Optimize all components of the SDA for system weight, performance, and reliability. Evaluate alternate design approaches for key components such as the dynamic pressure sensor, resonant element, and the compliant diaphragm which is used to isolate the resonant element from the propellant. Fabricate and test the driver assembly to verify predicted performance.
- 3) Control/Display Electronics (CDE) Design and Test. Analyze the relative merits of analog and digital display techniques. Design, fabricate, and test all components using analog equipment to simulate the gauge output, including noise, prior to incorporating the data processor into the complete gauging system.
- 4) Integrated Engineering Model Test. Integrate the SDA and CDE and test the system using boilerplate tankage and simulated propellants.

Phase II. Prototype Model

- 1) System Analysis. Revise the reliability and error models of the system to reflect the results of the actual test data. Perform analyses of system behavior under zero gravity for the range of anticipated SPS duty cycles.
- 2) Design and Fabrication of Prototype Components. Based on the results of the engineering model tests, design and fabricate the SDA and CDE components for the prototype system.
- 3) SDA and CDE Performance Evaluation. Conduct tests on the SDA subsystem using a full-size SPS mockup and simulated propellants. Similarly evaluate the CDE using simulated inputs. Evaluate off-design conditions of temperature and pressure to determine their effect on performance.
- 4) Component Service Life Tests. Perform life tests on all components using actual propellants and simulating actual flight conditions.
- 5) Prototype System Demonstration Testing. Incorporate the prototype versions of the SDA and data processor into a full-sized SPS-type tank. Perform tests to demonstrate that the RIGS system meets all specified performance requirements. Conduct performance and life tests for the range of anticipated tank conditions and duty cycles.
- 6) Flightweight System Design. Execute a complete flightweight design of the RIGS system.

APPENDIX A

RHO PROPELLANT GAUGE

1. INTRODUCTION

As a result of the Phase I study, a second system for gauging under zero gravity was also considered extremely promising. This system, called the RHO gauge (or ρV gauge), employs the direct measurement of ullage gas density and composition along with pressurant tank gas density to perform a gas balance and determine the propellant volume. Exploratory development of this system is currently under way at TRW Systems under AEC-DID sponsorship. A brief description of this system and a summary of the experimental results to date are given below.

2. PRINCIPLE OF OPERATION

As described in the Phase I report, the quantity of propellant remaining in a propellant tank can be determined by performing a material balance on the pressurant gas, assuming a single pressurant tank for each propellant tank, and neglecting leakage. Knowing the density of the helium in the propellant tank, and both the volume and the density of the helium in the pressurant tank, the gas volume and corresponding propellant volume may be obtained. A number of systems have been proposed using the helium mass balance approach. The simplest of these is the pressure, volume, temperature (PVT) system in which both the temperature and pressure in the pressurant and propellant tanks are measured. An error analysis has shown, however, that system accuracies are limited to 4 to 8 percent and that pressure and temperature measurements are inadequate to perform the gauging under typical space conditions with the high vapor pressure oxidizer N_2O_4 .

One simple improvement on the PVT system uses a beta-ray attenuation technique to directly determine the helium density in the pressurant tank. This technique is called the ρV gauge, and is sufficiently accurate that the gas density in the pressurant tank is no longer a major source of error. The remaining large error source is the density of the helium gas in the propellant tank. Accurate determination of the partial density of the helium in this tank is required to complete the mass balance of the

pressurant gas. A technique using both beta and X-ray sources, called the RHO gauge system, is capable of measuring the helium density in the propellant tank to a high degree of accuracy. The technique exploits the fact that whereas beta attenuation is dependent on only the bulk density of the gas mixture, the attenuation of the low energy photons, or X-rays, is predominated by the photoelectric effect and is roughly proportional to the 5th power of the atomic number (Z) of the absorber. The strong dependence of photon attenuation on Z results in the propellant or oxidizer being the controlling factor for X-ray attenuation. Thus, the combined beta and X-ray attenuation measurements permit an accurate determination of the partial density of helium in the propellant tank. A schematic of the RHO gauge is shown in Figure A-1.

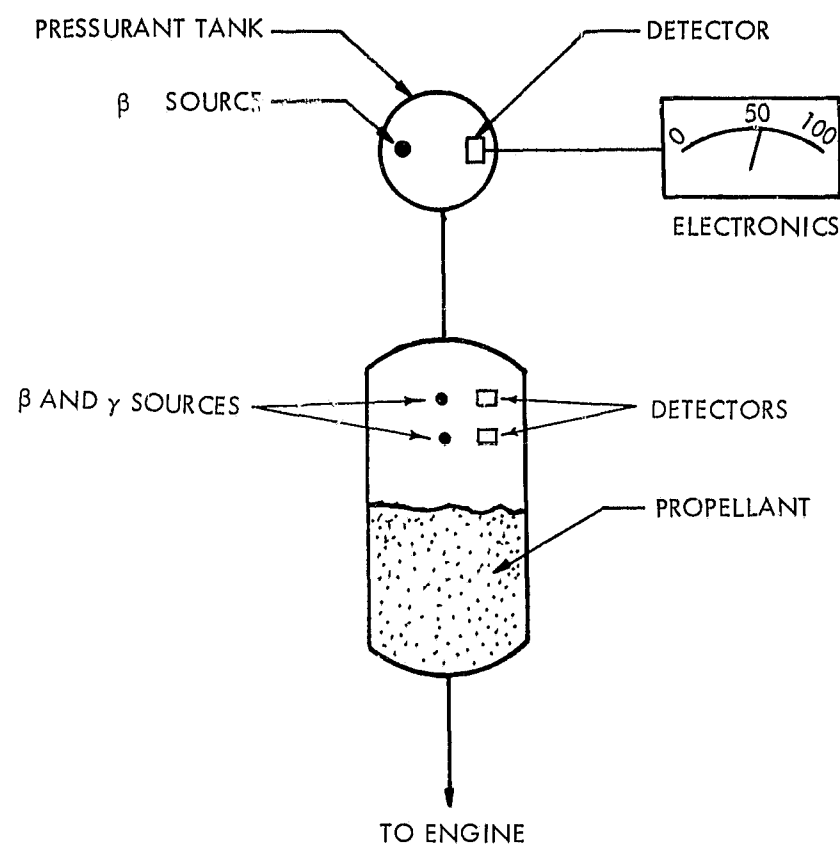


Figure A-1. Schematic Diagram of RHO Gauge

This concept is currently being evaluated experimentally by TRW Systems for the Atomic Energy Commission, Division of Isotopes Development, under contract AT (04-3)-539. The three objectives of the program are:

- Feasibility demonstration of the X-ray attenuation technique for measuring gas composition.

- Laboratory demonstration of a beta attenuation device to measure gas density to within 0.1 percent
- Demonstration of the ρV gauge system to measure propellant quantity within 1-1/2 percent

This appendix includes data of the X-ray attenuation feasibility experiments and results of the measurements of gas density by beta attenuation.

3. MEASUREMENTS OF GAS COMPOSITION

3.1 Analysis

The fraction of low energy photons (X-rays) transmitted by a gas mixture can be calculated from the equation:

$$\tau = \exp - \left\{ \left[\left(\frac{\mu}{\rho} \right)_1 \rho_1 + \left(\frac{\mu}{\rho} \right)_2 \rho_2 \right] x \right\}$$

where:

τ = transmission factor

μ = absorption coefficient, cm^{-1}

ρ = density, gm/cm^3

x = thickness of material, cm

Subscripts 1 and 2 denote the pressurant gas and propellant vapor, respectively.

Figure A-2 shows the theoretical mass attenuation coefficients (μ/ρ) for H, He, O, N, and C for low energy X-rays. Figure A-3 shows the theoretical mass attenuation coefficients for He, N_2O_4 , and Aerozine-50. The graphs show that for photon energies less than 20 kev, the μ/ρ values for the propellants are much greater than those for the helium pressurant gas. In a typical propellant tank, pressure is regulated at 200 psia, and the propellant vapor partial pressure may rise to as high as 30 psi. If the photon energy is 5.9 kev (iron-55), for example, μ/ρ is only 0.45 for helium compared to 13 for Aerozine-50 and 20 for N_2O_4 . Furthermore, if x is assumed to be 1 cm, the fraction of photons transmitted by pure helium at 170 psia is 0.99 and that by 30 psia N_2O_4 is 0.194.

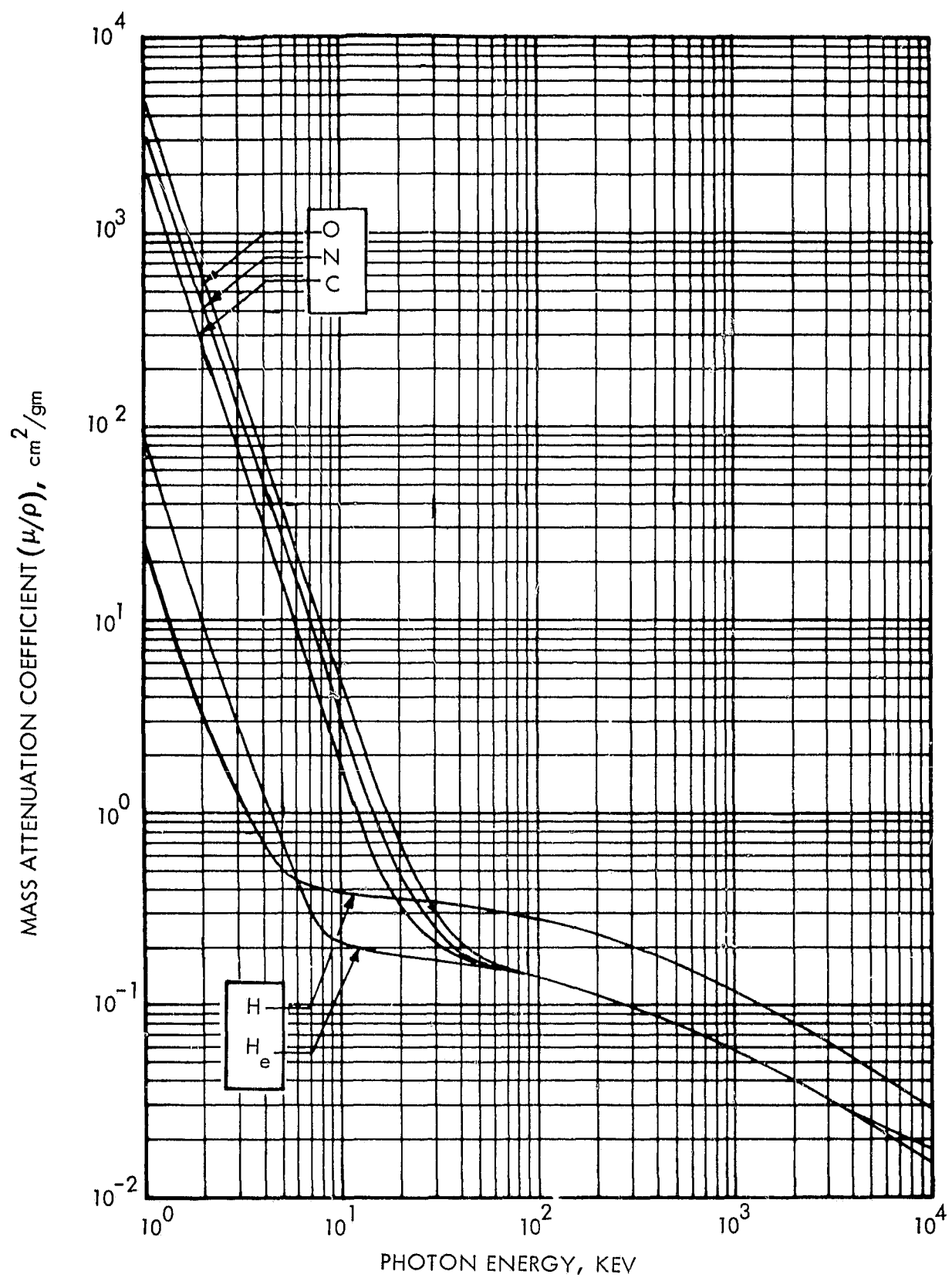


Figure A-2. Mass Attenuation Coefficients for the Elements—H, He, O, N, and C

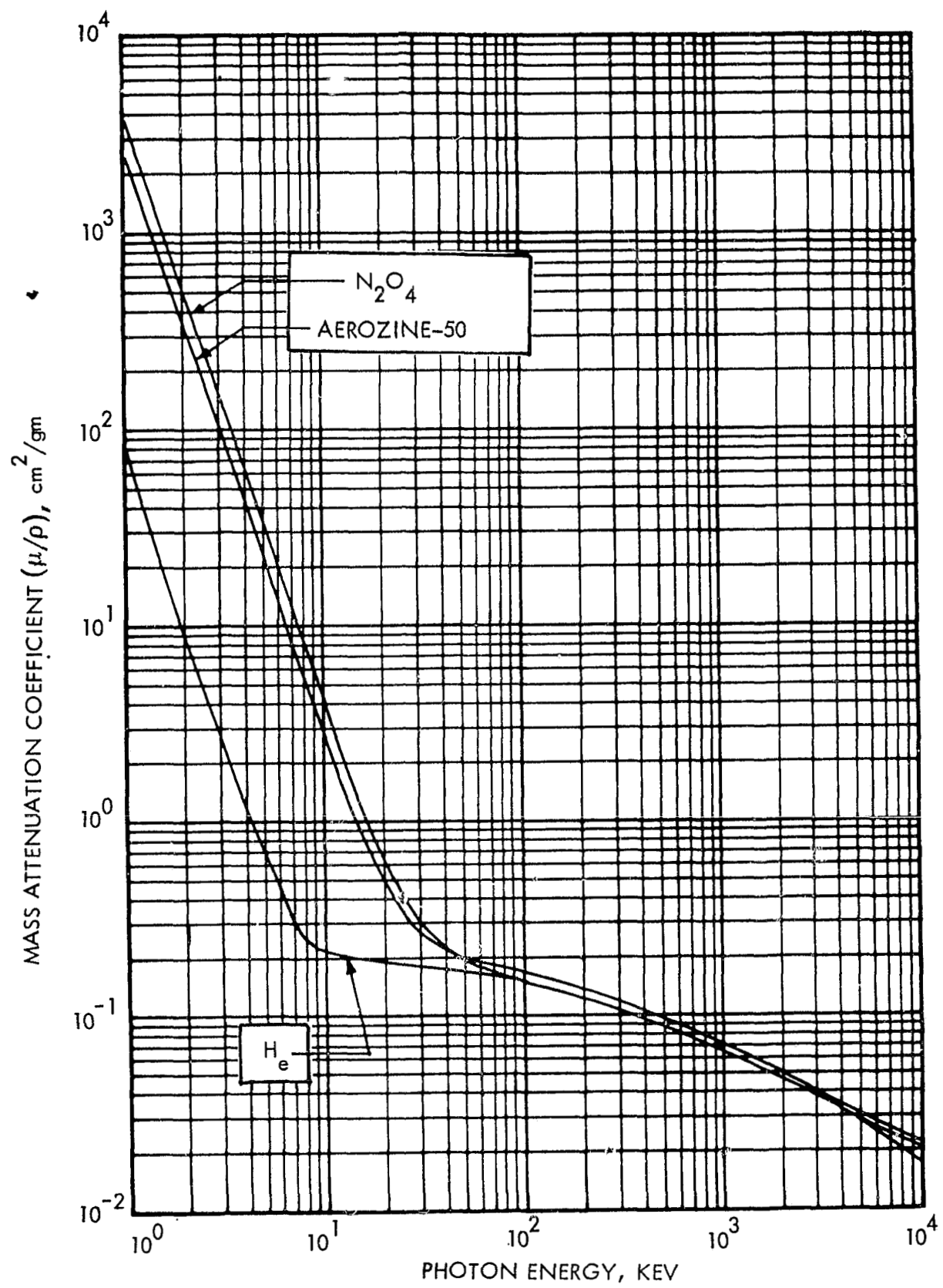


Figure A-3. Mass Attenuation Coefficients for He, N_2O_4 , and Aerozine-50

These figures illustrate that X-ray absorption is essentially due to the propellant vapor and that the total attenuation can be used as an accurate indication of the quantity of propellant vapor present. Helium absorption has a negligible effect on the measurement of propellant vapor partial density.

3.2 Source and Detector Selection

X-ray emissions can be obtained from radioisotopes which emit X-rays either directly or as the result of beta-particle excitation, or alternately from X-ray generating machines. Of the candidate radioisotope sources, beta-excited sources are less desirable than radioisotopes which emit X-rays directly. Iron-55, a radioisotope that emits a 5.9 kev X-ray was selected as the source since it is readily available and its energy is high enough to be detected without great difficulty and yet low enough that it can be used to measure the absorption in the mass thickness range of interest.

System considerations and preliminary tests led to the selection of a specially designed NaI scintillation detector. A suitable proportional counter would probably have performed equally well but did not lend itself readily to the available instrumentation.

3.3 Experimental Hardware

A schematic representation of the test setup and a photograph of the experimental hardware employed in these tests are shown in Figures A-4 and A-5, respectively. An X-ray source was mounted at one end of the pressure vessel and the NaI scintillation detector viewed the radiation through a supported mylar pressure window at the other end of the chamber. A split-ring collimator provided a parallel radiation beam and reduced forward scatter to the detector. Pressure and temperature transducers were used to determine the gas density within the pressure vessel, and a pulse height analyzer (PHA) was used to measure the intensity of the X-rays transmitted through the different absorber gases.

3.4 Gas Composition Test Results

To demonstrate the X-ray attenuation technique for determining gas composition, mixtures of helium and nitrogen were used. Helium was

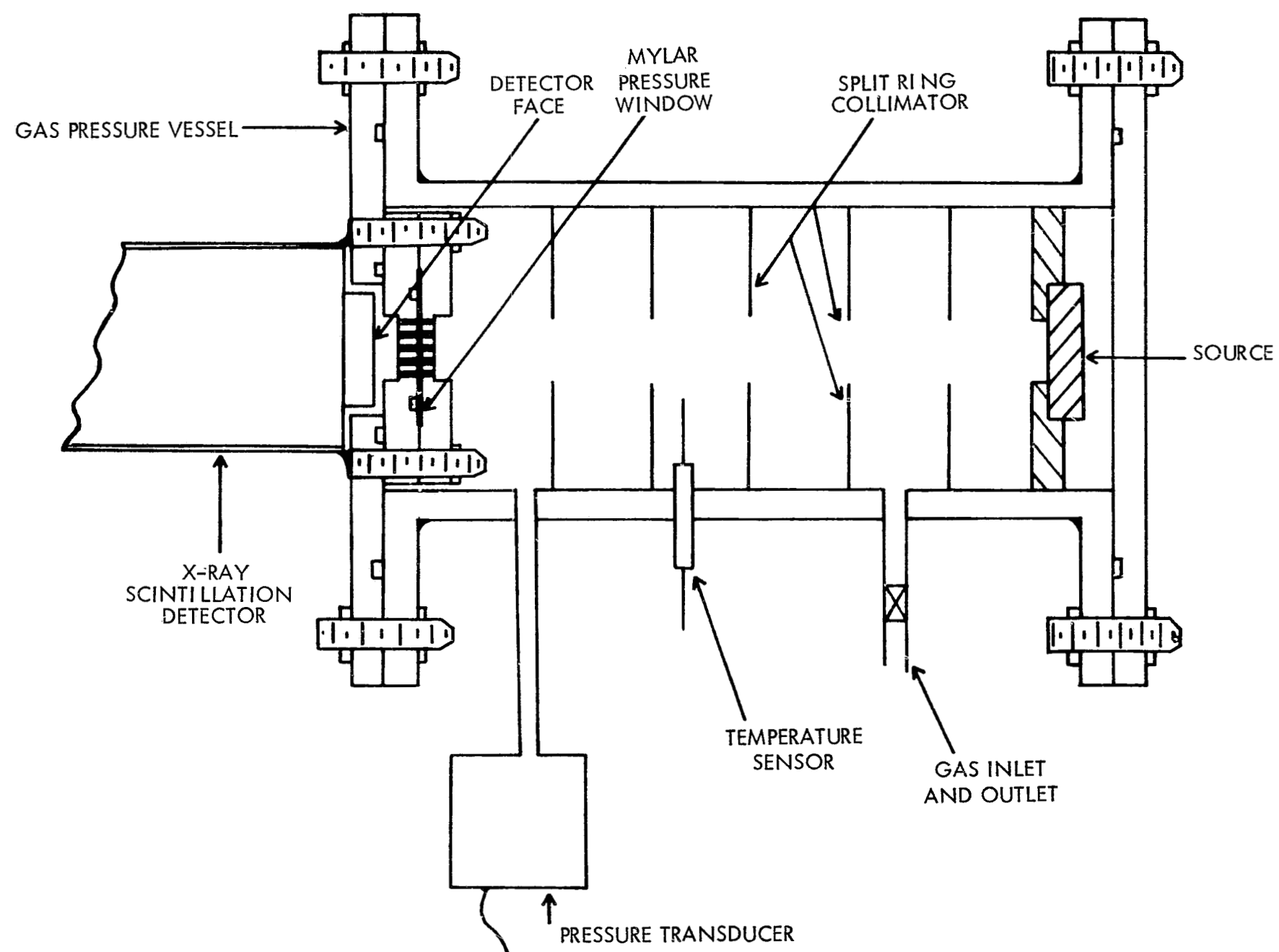


Figure A-4. Gas Composition Test Hardware

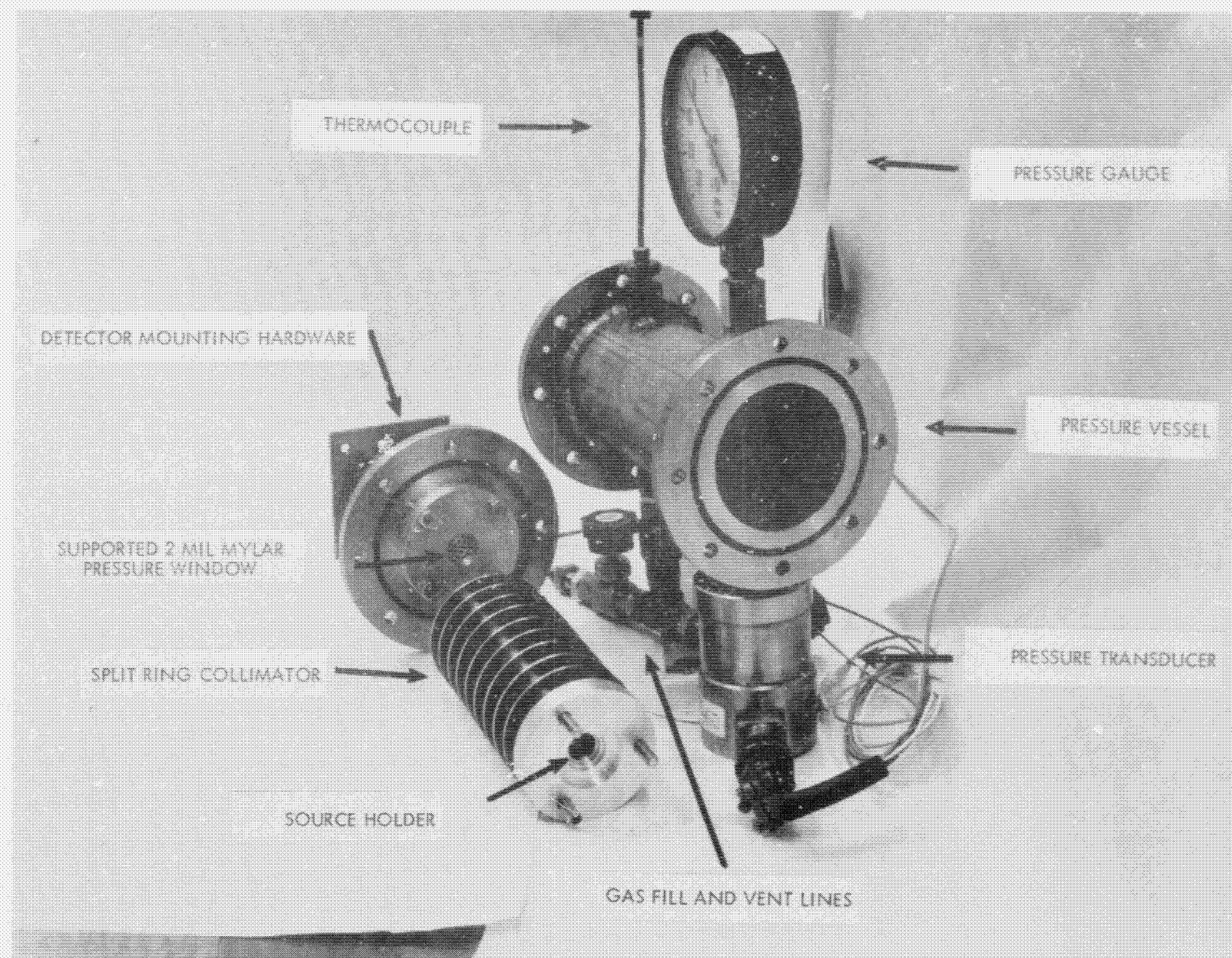


Figure A-5. X-Ray Attenuation Hardware

selected because it is a common pressurant gas and nitrogen was selected because its X-ray absorption characteristics are much like those of the common rocket propellants N_2O_4 and N_2H_4 (hydrazine).

Tests were performed by first measuring X-ray transmission through a vessel pressurized to 93 psia with helium. Then the tank was vented down to 85 psia and refilled to 93 psia with nitrogen; an absorption measurement was taken. This process was repeated several times until the gas mixture was approximately 50 percent nitrogen and 50 percent helium. The data from these tests are shown in Figure A-6. The data fall on a straight line since X-ray attenuation is an exponential function of gas density. The two points at zero partial nitrogen pressure were obtained through a vacuum and through 93 psia helium (no nitrogen).

In another test, a mixture of oxygen and nitrogen was used to simulate N_2O_4 . The mixture was 35 percent nitrogen and 65 percent oxygen by volume and the total pressure was 84 psia. A method similar to the one employed in the previously discussed test was used to obtain several partial pressures of the mixture. The data from this test are shown in Figure A-7.

These tests show that accurate measurements of gas composition are feasible by use of the X-ray absorption technique, and that practical measurements of partial pressure can be made in a helium-propellant vapor mixture by neglecting helium absorption. The analysis in Section 3.1 shows that this assumption can also be made at typical propellant tank pressures of 200 psia.

4. GAS DENSITY MEASUREMENTS

4.1 Analysis

The fraction of beta particles transmitted by a particular material can be closely approximated by the equation:

$$\tau = e^{-(\mu/\rho) \rho x}$$

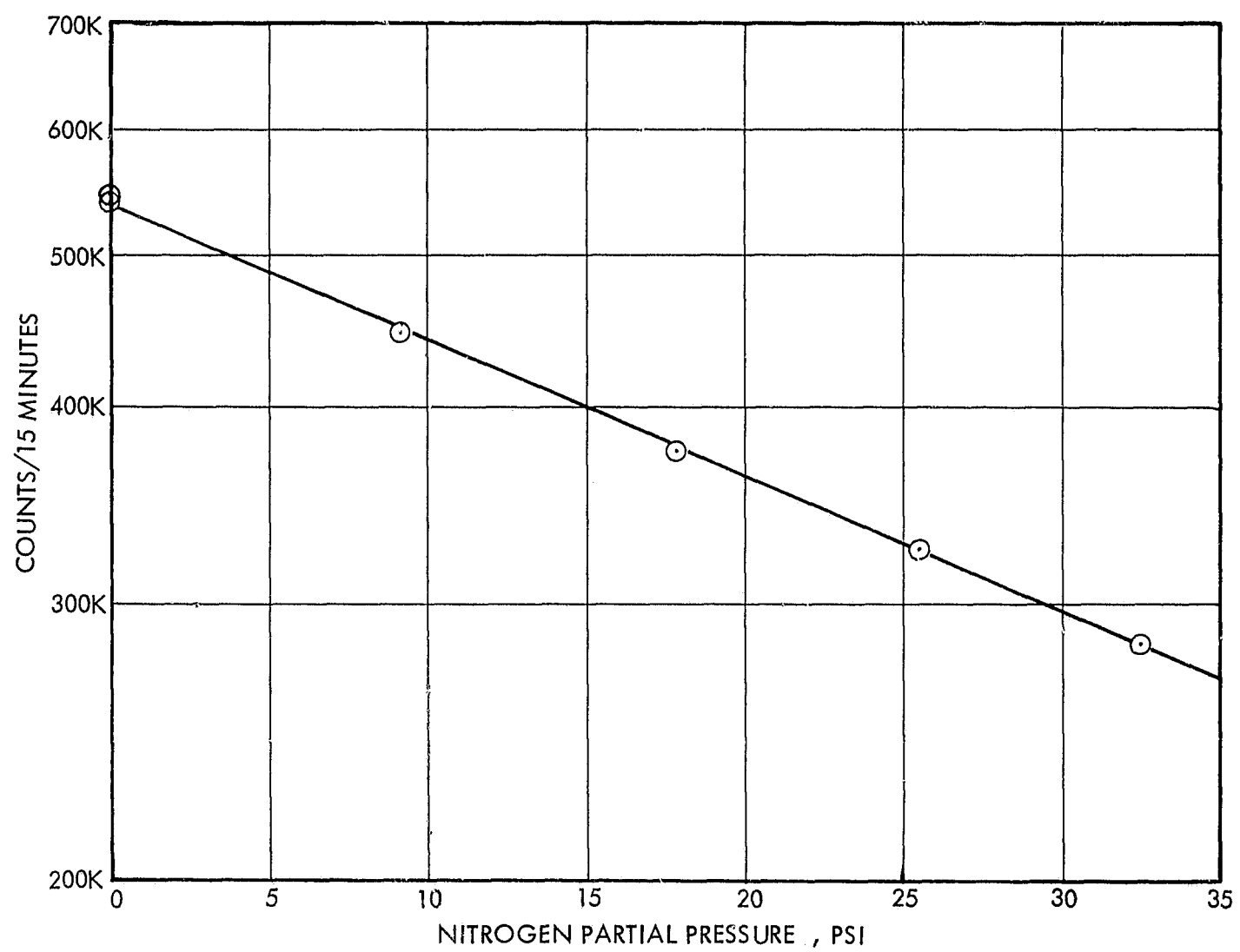


Figure A-6. Measurement of Nitrogen Partial Pressure in a Helium-Nitrogen Gas Mixture (Total Pressure: 93 psia)

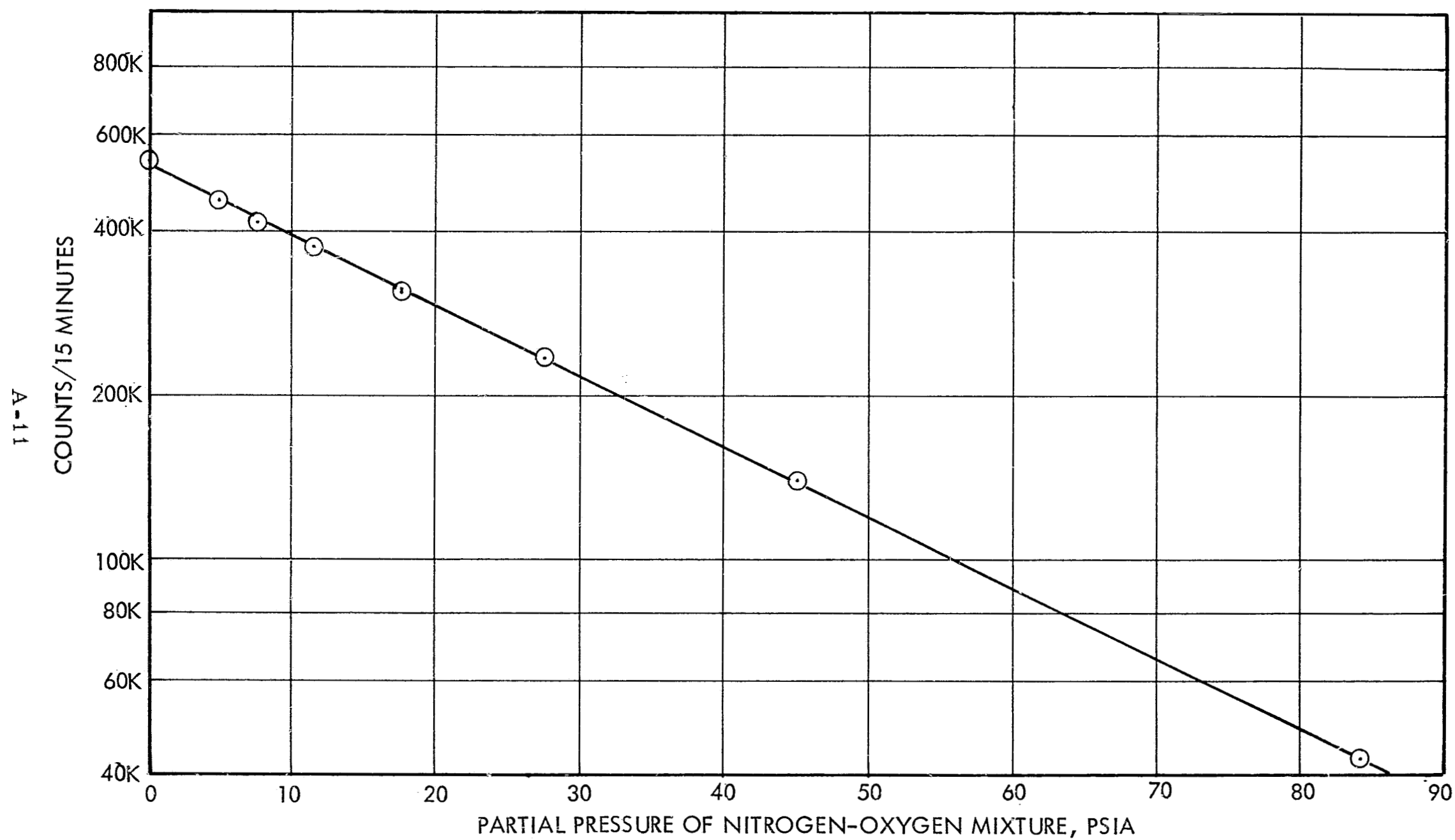


Figure A-7. Measurement of Nitrogen-Oxygen Partial Pressure in γ -Helium,
Nitrogen-Oxygen Gas Mixture (Total Pressure: 84 psia)

where:

τ = transmission factor

μ = absorption coefficient, cm^{-1}

ρ = bulk density, gm/cm^3

x = thickness of material, cm

It has been found experimentally that the mass absorption coefficient, μ/ρ , is determined by E_{max} , the maximum beta particle energy associated with the decay, and by the ratio of the atomic number and weight, Z/A :

$$\frac{\mu}{\rho} = \frac{35Z}{E_{\text{max}}^{1.14} A}$$

Since μ/ρ and the distance, x , are fixed quantities for a given measurement system, the bulk gas density can be determined directly by measuring the beta particle transmission. Thus, after calibration of the system, the detected count rate can be used as a direct measure of gas density.

4.2 Source and Detector Selection

In order to meet the required accuracy of the gauge and produce a low external radiation field, only C^{14} , Cl^{36} , and Tc^{99} were considered as beta-emitter source candidates.

Since the beta detector may be used to measure gas density in either the propellant or the pressurant tank, it must be capable of withstanding pressures on the order of 3000 psi without compromising detection efficiency. Semiconductor detectors were selected because they have this capability, consume small amounts of power, and are compact.

4.3 Experimental Hardware

Argon gas at pressures from approximately 30 to 300 psia was used to simulate helium gas in the pressurant tank at pressures from 300 to 3000 psia. This substitution was made to reduce the working pressure so that available pressure vessels could be used.

The experimental system used in these tests is shown schematically in Figure A-8. The pressure transducer, a Winsco Data Sensors Model PB 923A, was calibrated to measure pressure within 0.05 percent. The platinum resistance thermometer, a Rosemont Engineering Model 414L3BFA, and linear bridge system were calibrated to measure temperature within 0.025 percent. These instruments were used to accurately measure the gas density in the pressure vessel and were used in the calibration of the radioisotope technique.

4.4 Gas Density Test Results

Measurements were initiated with several source-to-detector distances to calibrate the experimental hardware and to determine the experimental relationship between density and count rate. Figures A-9 and A-10 show data taken with 20 μCi of Cl^{36} and a source-to-detector distance of 0.364 cm and 3.00 cm, respectively. To achieve maximum system sensitivity, the slope of the curve of counts versus density should be as steep as possible. Measured gas density was reproducible and fell within 0.14 percent of the least-squares, polynomial curve-fit. Increasing the counting time at each data point will improve the accuracy even further.

The objective of these tests is to measure gas density to within 0.1 percent, but other errors such as electronic errors (± 0.2 percent), propellant density measurement errors (± 0.4 percent), and errors due to dissolved helium (± 0.2 percent) also contribute to the overall gauging error. Based on these individual contributing errors, an overall gauging error of less than 1 percent can be achieved.

5. EXTERNAL RADIATION FIELDS

Results of analyses indicated that all the isotopes considered give rise to external radiation fields which are extremely small. The highest radiation level was obtained for Cl^{36} at a separation distance of 5 cm and was on the order of normal radiation background on earth (0.01 to 0.04 mr/hour). All other cases considered gave rise to appreciably smaller fields.

The analyses indicated that the external radiation field produced by the X-ray source in the propellant tank would be much smaller than the field produced by the beta sources in the propellant and ullage tanks.

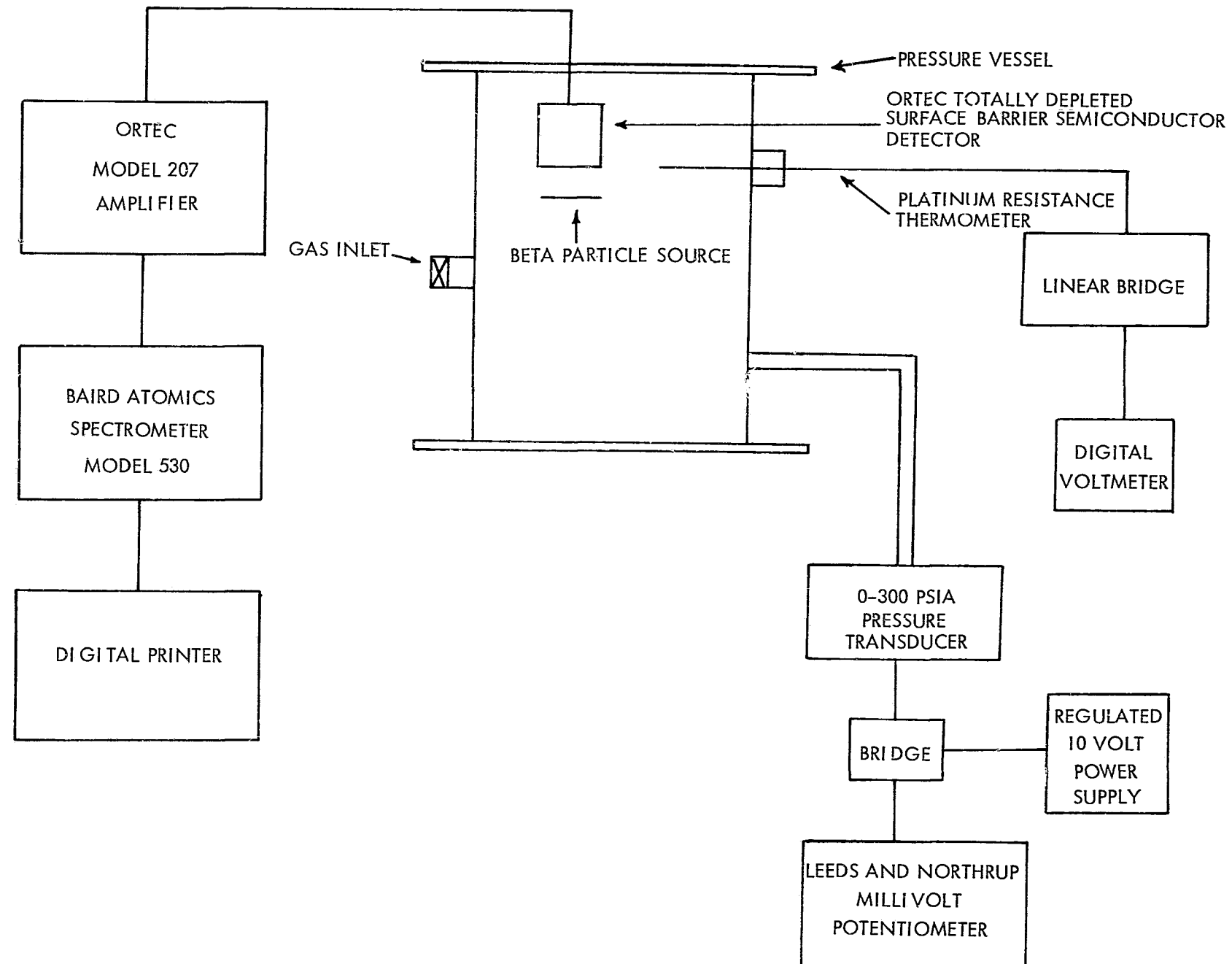


Figure A-8. Experimental System for Measuring Gas Density

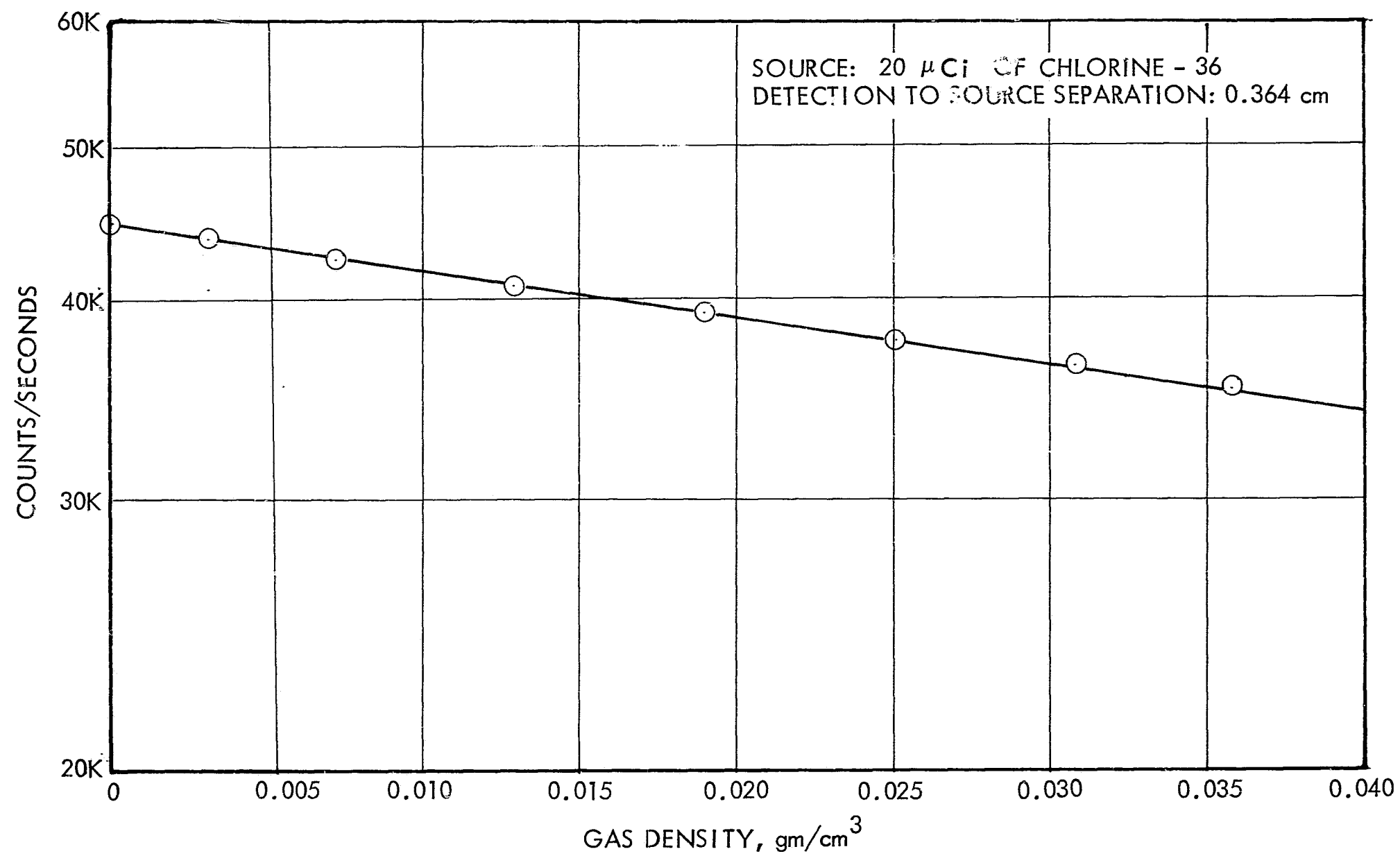


Figure A-9. Beta Particle Attenuation Measurements
of Argon Density

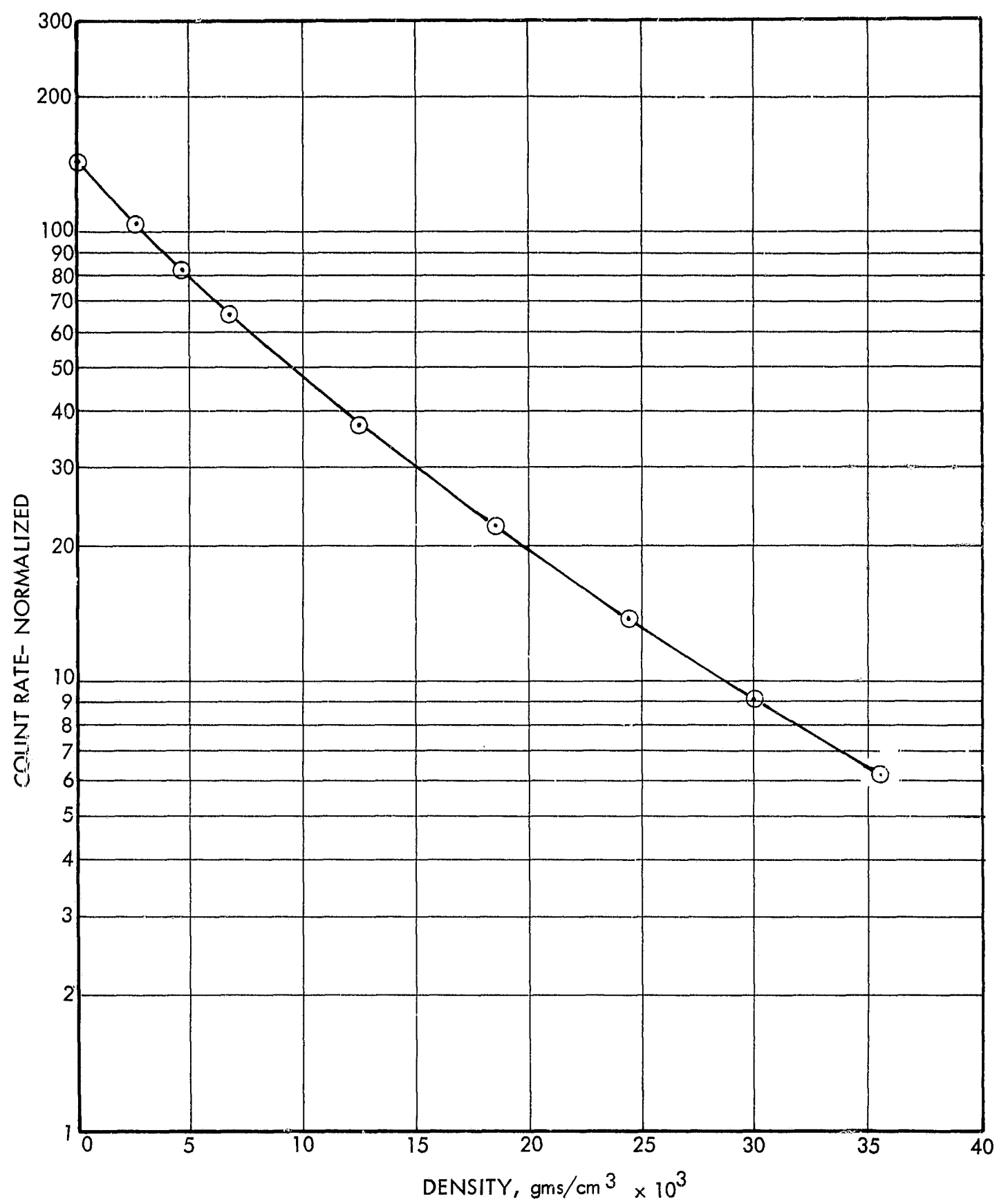


Figure A-10. Count Rate vs Argon Gas Density for
Detector to Source Distance of 3 cm

The external radiation field at the tank surface was estimated assuming that all beta particles were absorbed within the tank and that all external radiation was produced by bremsstrahlung resulting from the beta particle absorption. Since the intensity and energy of the bremsstrahlung radiation is directly proportional to the atomic number of the beta absorber, it was assumed that all of the betas were absorbed by the stainless steel source/detector container. This is a conservative assumption because part of the betas are actually absorbed by the helium pressurant gas, propellant vapor, and titanium tank walls, all of which have lower atomic numbers.

Bremsstrahlung source-to-tank wall distances (detector casing to wall distance) of 5.0, 10.0, and 20.0 cm were assumed to estimate the photon attenuation through the helium pressurant gas. The 20.0 cm value represents the distance for a typical reaction control system tank with the bremsstrahlung source at the tank center, whereas the 5.0 cm value is for a source in a separate measuring vessel or very close to the tank wall. The helium gas pressure was assumed to be 300 psia, which again is a conservative case, since pressurant tanks commonly have initial pressures as high as 3000 psia and would attenuate more of the radiation.

As mentioned above, the radiation field calculated for this case was on the order of normal background on earth. Therefore, the external radiation field resulting from the gauge will not present a safety hazard to personnel or sensitive onboard radiation detection equipment.

6. CONCLUSIONS

The operating principles of the RHO gauge have been successfully demonstrated. The X-ray attenuation technique was shown to be capable of measuring the partial pressure of a simulated oxidizer in the presence of helium gas to an accuracy of better than ± 1 percent. Beta attenuation measurement of the gas density was demonstrated to an accuracy of ± 0.14 percent. Based upon these results, the actual helium density in the propellant tank can be determined to an accuracy of ± 0.5 percent resulting in a potential gauging accuracy of better than ± 1.0 percent.

Although these results are quite promising, additional effort is required to determine the true potential of the RHO gauge in an actual propellant system.